Cardiovascular Magnetic Resonance Deformation Imaging By Feature Tracking For Assessment Of Left And Right Ventricular Structure And Function

Augustine, Daniel

Cardiovascular Magnetic Resonance Deformation Imaging By Feature Tracking For Assessment Of Left And Right Ventricular Structure And Function

Daniel Augustine BSc (Hons), MBBS, MRCP (UK)

Thesis Submitted For The Degree Of Doctor Of Medicine (Research)

April 2014

Table Of Contents

Acknowledgements

I would like to thank a number of people without whom this thesis would not have been written. Firstly I would like to thank my principle supervisors Professor Paul Leeson and Professor Steffen Petersen. I will always be grateful for their guidance, advice, support and encouragement at all the critical stages of this work. A special thanks also to Professor Harald Becher for his support and advice during my time at the University Of Oxford Cardiovascular Clinical Research Facility (CCRF). I would also like to thank my colleagues in the CCRF, the University of Oxford Centre for Clinical Magnetic Resonance Research and Professor Alison Noble and her team at the University Of Oxford Institute Of Biomedical Engineering.

I am indebted to the Engineering and Physical Sciences Research Council, the British Heart Foundation and the National Institute for Health Research Oxford Biomedical Research Centre for funding this work.

Declaration

The work in this thesis is my own. The research studies were approved by the local ethics committee and informed consent for participation obtained from all subjects. The subjects used were recruited as normal controls as part of two other research studies lead by Dr Lewandowski and Dr Lazdam. Both Drs Lewandoski and Lazdam have given permission for me to analyse the CMR images acquired as part of their studies. Dr Bull provided the images for analysis for patients with diastolic dysfunction in chapter 5. I undertook all echocardiography and analyzed all of the CMR scans and echocardiograms, interpreted the data, carried out the statistics and wrote the script.

Papers And Abstracts

Papers

Chapter 3

Augustine D, Lewandowski AJ, Rai A, Lazdam M, Francis J, Becher H, Petersen S, Myerson S, Neubauer S and Leeson P. Global and regional left ventricular myocardial deformation measures by magnetic resonance feature tracking in healthy volunteers: comparison with tagging and relevance of gender. J Cardiovasc Magn Reson, 2013. 15: p. 8.

Lewandowski, AJ, **Augustine D**, Lamata P, Davis EF, Lazdam M, Francis J, McCormick K, Wilkinson AR, Singhal A, Lucas A, Smith NP, Neubauer S and Leeson P. Preterm Heart in Adult Life: Cardiovascular Magnetic Resonance Reveals Distinct Differences in Left Ventricular Mass, Geometry, and Function. Circulation, 2013. 127(2)u: p. 197-206.

Chapter 7

Lewandowski, AJ, Bradlow WM, **Augustine D**, Davis EF, Francis J, Singhal A, Lucas A, Neubauer S, McCormick K and Leeson P Right Ventricular Systolic Dysfunction in Young Adults Born Preterm.Circulation, 2013. 128(7): p. 713-720.

Abstracts

European Society Of Cardiology 2012 (Munich)

Augustine D, Lewandowski AJ, Rai A, Lazdam M, Francis J, Becher H, Petersen S, Myerson S, Neubauer S & Leeson P. LV mass, volumes and ejection fraction estimation with magnetic resonance feature tracking: a comparison with traditional short axis LV CMR contouring.

Society of Cardiovascular Magnetic Resonance Imaging Conference 2012 (Orlando, US)

Augustine D, Suttie J, Cox P, Lewandowski A, Holloway C, Petersen S, Myerson S, Neubauer S & Leeson P.CMR right ventricular strain assessment using feature tracking cine images: agreement with echocardiography.

EuroEcho 2011 (Budapest, Hungary)

Augustine D, Basagiannis C, Cox P, Suttie J, Lewandowski A, Lazdam M, Rai A, Holloway C, Becher H & Leeson P.Left Ventricular 3D speckle tracking echocardiography with CMR correlation: agreement between vendor dependent and vendor independent software.

European Society Of Cardiology 2011 (Paris, Framce)

Augsutine D, Basagiannis C, Cox P, Suttie J, Lewandowski A, Lazdam M, Davis E, Holloway C, Becher H & Leeson P.Assessment of left ventricular 3D speckle tracking echocardiography using vendor dependent and vendor independent software with CMR correlation.

3D fusion echocardiography improves transoesophageal left ventricular assessment. **Augustine D**, Rajpoot K, Biasagianis C, Pavolopoulous H, Jin X, Myerson S, Newton J, Noble A, Becher H & Leeson P.

Other papers published related to study groups

Augustine, D., L.V. Ayers, E. Lima, L. Newton, A.J.J. Lewandowski, E.F. Davis, B. Ferry, and P. Leeson, Dynamic Release and Clearance of Circulating Microparticles During Cardiac Stress. Circulation Research, 2014 Jan 3; 114(1):109-13

Abstract

Cardiac magnetic resonance (CMR) imaging is the gold standard imaging technique for assessment of ventricular dimensions and function. CMR also allows assessment of ventricular deformation but this requires additional imaging sequences and time consuming post processing which has limited its widespread use.

A novel CMR analysis software package, 'feature tracking' (Tom Tec, Germany) can measure ventricular deformation directly from cine CMR images. This thesis seeks to further our understanding of the feasibility of feature tracking to assess myocardial deformation and volumetric measures. Chapter 3 validates normal ranges for deformation parameters and compares values against traditional tagging measures. The work identifies global circumferential strain measures as being the most reproducible.

In chapters 4 and 5, feature tracking values for left and right ventricular strain are compared with echocardiography derived speckle tracking indices of deformation. For left ventricular (LV) parameters, circumferential and longitudinal strain are most consistent and for the right ventricular (RV) measures, assessment of free wall strain using feature tracking shows promise and with modifications in algorithms is likely to further improve in the future.

Chapter 6 assesses the ability of feature tracking to measure diastolic function. The results show that radial diastolic velocities and longitudinal diastolic strain rates can predict diastolic dysfunction (as diagnosed by echocardiography) with acceptable levels of sensitivity and specificity, particularly when used in combination.

The use of feature tracking to provide automated measures of ventricular volumes, mass and ejection fraction is assessed in chapter 7. Feature tracking in this context shows acceptable correlation but poor absolute agreement with manual contouring and further adjustments to algorithms is necessary to improve its accuracy.

This work offers insights into the use of feature tracking for the assessment of ventricular deformation parameters. It is a technique with advantages over CMR tagging methods and given the speed of post processing has the potential to become the CMR preferred assessment for strain quantification in the future.

Abbreviations

%	Percent
2D	Two dimensional
2DE	Two dimensional echocardiography
3D	Three dimensional
3DE	Three dimensional echocardiography
A	Mitral valve inflow peak late velocity
a’	Late diastolic velocity by tissue Doppler either at the basal LV septum or lateral wall
AUC	Area under the receiver operator curve
BP	Blood pressure
BPM	Beats per minute
CI	95% confidence interval
Circ	Circumferential
CM	Centimetres
CMR	Cardiac magnetic resonance
CT	Computed tomography
CV	Coefficient of variation
DBP	Diastolic blood pressure
Deg	Degrees
DT	Deceleration time
E	Mitral valve inflow peak early velocity
e’	Early diastolic velocity by tissue Doppler either at the basal LV septum or lateral wall
ECG	Electrocardiogram
EDV	End diastolic volume
EF	Ejection fraction
EF Cor	Corrected ejection fraction
ESV	End systolic volume
ESV Cor	Corrected end systolic volume
FPS	Frames per second
FT	Feature tracking
G	Grams
HARP	Harmonic phase
HDL	High density lipoprotein
HLA	Horizontal long axis
ICC	Intra class correlation coefficient
Kg	Kilogrammes
LA	Left atrium
Long	Longitudinal
LDL	Low density lipoprotein
LOA	Limits of agreement
LV	Left ventricle
LVOT	Left ventricular outflow tract
M	Metre
Min	Minute
Mm	Millimetre

mmHg	Millimetre mercury
Mmol/L	Millimoles per litre
ms	Milliseconds
n	Number
N/A	Not applicable
RA	Right atrium
Rad	Radial
ROC	Receiver operator curve
RV	Right ventricle
S	Seconds
SBP	Systolic blood pressure
SD	Standard deviation
SR	Strain rate
SSFP	Steady state free precession
TAPSE	tricuspid annular plane systolic excursion
TDI	Tissue Doppler imaging
TE	Echo time
TR	Repetition time
VPS	Volume rate per second (3D) images
VLA	Vertical long axis
yrs	Years

List Of Figures And Tables

Chapter 1: Introduction

1.1 The non invasive assessment of cardiac function

The non invasive assessment of ventricular function is critical in clinical practice and is an important marker of prognosis and response to treatment. The accurate, serially reproducible, non-invasive methods for assessing cardiac function are essential for the management of patients [1]. Historically this has been achieved initially with the use of equilibrium radionuclide angiography and echocardiography. More recently the emergence and utilisation of cardiac magnetic resonance has added a further dimension to the assessment of ventricular function.

Initially radionuclide angiography was widely used for the assessment of cardiac function due to its non invasive properties and the advantage of not relying on assumptions of LV geometry. However it's limitations including the use of radiopharmaceutical agents as well as its lower resolution for assessing regional ventricular function together with the emergence of echocardiography and cardiac magnetic resonance imaging has restricted its ongoing use.

Echocardiography has the advantage of complete safety and portability and both echocardiography and CMR imaging provide immediate provision of clinically interpretable images and have improved ability when compared with radionuclide imaging to assess valvular function, hemodynamics, cardiac mass, regional wall motion abnormality and diastolic function.

1.2 Left ventricular systolic function assessment

1.2.1 Echocardiography

1.2.1.1 Two dimensional LV systolic function

The LV ejection fraction is one of the most commonly used echocardiographic methods to quantify LV systolic function. This represents the fraction of blood within the LV which is ejected in one cardiac cycle. As it is difficult to quantify a 3- dimensional (3D) structure using 2 dimensional (2D) imaging, the techniques developed with 2D echocardiography rely on measuring the ventricle in standard planes. 2D echocardiographic assessment of ejection fraction can be assessed using linear (Teicholz method or fractional shortening) or volumetric methods. It is widely accepted that there are limitations to both methods. Linear methods especially are based on assumptions that become invalid in patients with abnormally shaped ventricles [2]. The 2D volumetric Simpson's method for the assessment of LV ejection fraction is based on the principle of slicing the LV from apex down to the mitral valve into a series of discs. The volume of each disc is then calculated (using the diameter and thickness of each slice). It is assumed that the LV is circular at each level. Accuracy is improved by using diameters in two perpendicular planes (apical four and two chamber) so that the disc surface area is more precisely defined. These volumes can be estimated at end systole and end diastole and the machine or off line analysis software packages can process these values to give an estimation of ejection fraction.

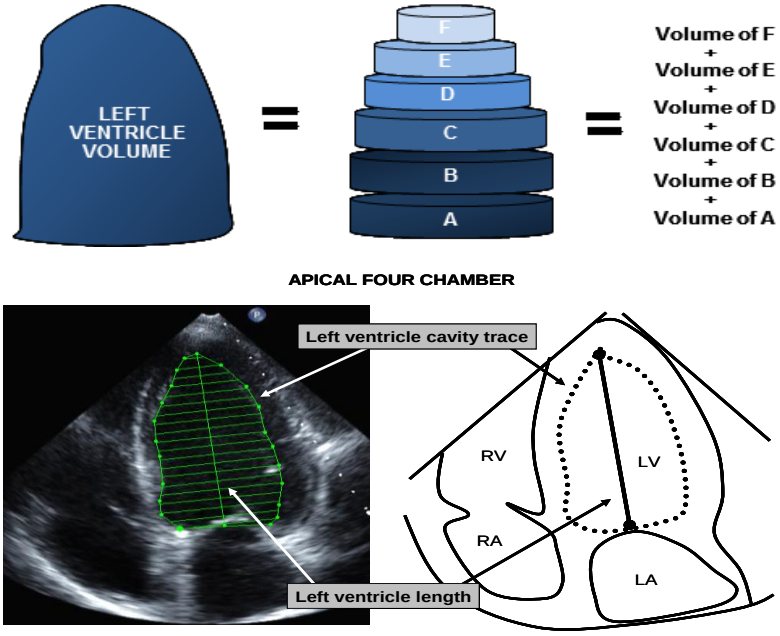

Figure 1.1: Biplane Simpson's method for the estimation of ejection fraction.
Regional wall motion abnormalities most commonly occur due to coronary artery disease. Echocardiographic assessment of these is usually by eye and are dependent on operator experience although can be semi quantified with wall motion scores. Figure from Echocardiography (Leeson P, Augustine D, Mitchell A & Becher H. Oxford University Press, 2012)[3].

1.2.1.2 Three dimensional LV systolic function

The 2D echocardiographic assessment of ejection fraction has inherent limitations as it makes geometric assumptions of the LV. This consideration is especially important for repeat imaging, for which exact plane duplication is almost impossible. 3D echocardiography is an advance on the Simpson's method as it allows contouring of the cavity within the 3D space of the echocardiographic volume acquisition. Therefore, there is no need to assume that the short axis view of the ventricle follows the shape of a circle (or oval) and sum together a '*stack of discs*'. Instead you can contour the actual shape of the ventricle in all dimensions. Commercially available scanners contain software tools which allow the assessment of LV volumes and ejection fraction.

Full volume datasets allow the generation of a 3D data set with the final image of the heart created by acquiring several sub volumes (usually 1-7 depending on vendor) over the corresponding number of sequential cardiac cycles. The greater the number of sub volumes used, the higher the frame rate and temporal resolution. The spatial resolution of images for current 3D transducers is around 0.5-1mm in the axial (y) dimension, 1.5-2.0mm in the lateral (x) dimension and 2.5-3.0mm in the elevation (z) dimension.

Since the potential of 3D echocardiography imaging to overcome many of the limitations of 2D echocardiography, ultrasound imaging has gone through multiple phases of development and most recently real time 3D echocardiography allowing single beat acquisition of datasets without the need for off line reconstruction is available.

With newer technology allowing increased volume rates and reduced time for complete cardiac volumes acquisition the estimation of 3D LV ejection fraction is comparable to that of cardiac magnetic resonance [4-5].

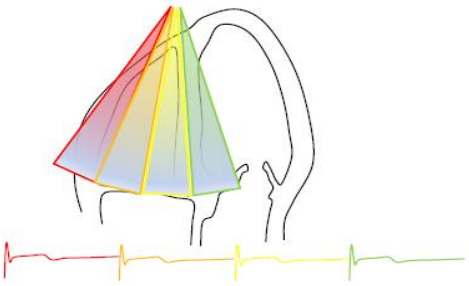

Figure 1.2: Diagrammatic representation of 3D subvolume acquisition. The first subvolume (red) is taken during the first cardiac cycle (red), the second subvolume (orange) is taken during the second cardiac cycle (orange) and so on. All subvolumes are merged together to create the final dataset. Figure from Echocardiography (Leeson P, Augustine D, Mitchell A & Becher H. Oxford University Press, 2012)[3].

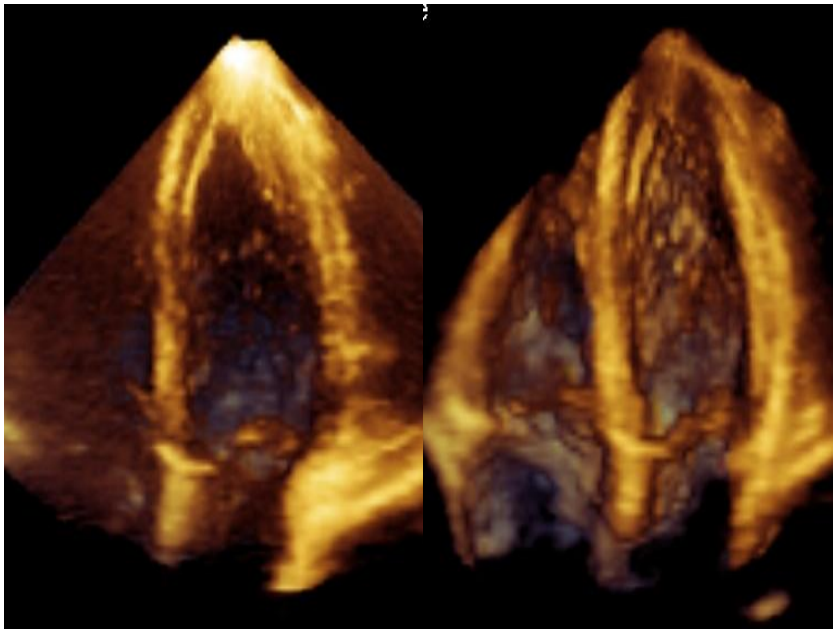

Figure 1.3: 2 beat and 7 beat 3D full volume acquisition. 2 beat 3D LV full volume acquisition (left) is composed of 2 subvolumes acquired over 2 consecutive cardiac cycles has a lower frame rate and temporal resolution than a 7 beat 3D LV full volume acquisition. Figure from Echocardiography (Leeson P, Augustine D, Mitchell A & Becher H. Oxford University Press, 2012)[3].

1.2.1.3 Tissue Doppler assessment of systolic function

Tissue Doppler echocardiography has become an established component of the diagnostic ultrasound examination permitting the assessment of myocardial motion using Doppler ultrasound imaging [6]. Whilst the ejection fraction reflects the sum contribution of several regions it does not provide information on regional function and is unable to provide information on the underlying myocardial mechanical activity. Whereas conventional Doppler techniques assess the velocity of blood flow by measuring high- frequency, low

amplitude signals from small fast-moving blood cell, tissue Doppler imaging, TDI, uses the same Doppler principles to quantify the higher amplitude, lower velocity signals of myocardial tissue motion. With this information, TDI depicts myocardial motion at a specific location in the heart. The high velocity signals from the blood are filtered out and amplification scales suitably adjusted so that Doppler signals from tissue motion can be recorded. The tissue velocity indicates the rate at which a particular point in the myocardium moves towards or away from the transducer.

The accuracy of TDI is angle dependent and only measures the vector of motion that is parallel to the direction of the ultrasound beam. The use of TDI has been validated and examined in a variety of settings [7-8].

Figure 1.4: Example of pulsed wave tissue Doppler imaging placed at the basal LV septum. Figure from Echocardiography (Leeson P, Augustine D, Mitchell A & Becher H. Oxford University Press, 2012) [3]

1.2.2 Cardiac magnetic resonance

Cardiovascular magnetic resonance imaging (CMR) is an increasingly available diagnostic method offering good spatial resolution (0.5mm) and acceptable temporal resolution. Each image slice obtained consists of several sequential cardiac phases throughout systole and diastole. From these, the LV ejection fraction can be accurately measured by applying Simpson's rule as for echocardiography. In this way, CMR imaging provides anatomic image quality avoiding the need for any geometric assumptions – an advantage over the LV systolic function assessment using 2D echocardiography with Simpson's method.

1.3 Right ventricular systolic function assessment

1.3.1 Echocardiography

1.3.1.1 Two dimensional RV systolic function

RV dysfunction is associated with excess morbidity and mortality and the non invasive assessment of RV function is vital in assessing prognosis and as a marker of response to therapy. Echocardiographically, the LV has been studied in much greater detail than the RV. This has partly been due to the complex geometry of the RV which has limited its assessment.

Whilst 2D systolic function can be evaluated qualitatively by studying the movement of the RV free wall and assigning a label of normal or impaired to RV systolic function, more robust objective methods of quantification are of common practice. A number of measures of RV systolic function have evolved whose purpose is to try to avoid the difficulties of using volumetric techniques established in the LV for the geometrically complex RV. 2D markers

of RV systolic function include the tricuspid annular plane systolic excursion (TAPSE), the peak systolic RV basal free wall TDI and ejection fraction / fractional area of change.

TAPSE is a measurement of how much the lateral side of the tricuspid annulus moves towards the apex during systole, thus reflecting RV longitudinal function. Similar to TAPSE, the peak systolic RV basal free wall TDI assesses the movement of the RV free wall but uses TDI. It is widely accepted that RV ejection fraction can be difficult to assess accurately on 2D images because of the complex RV geometry although one surrogate used to try to do this is the RV fractional area of change. Here, the end diastolic and end systolic areas are contoured with the difference between the two measures being reported as a percentage.

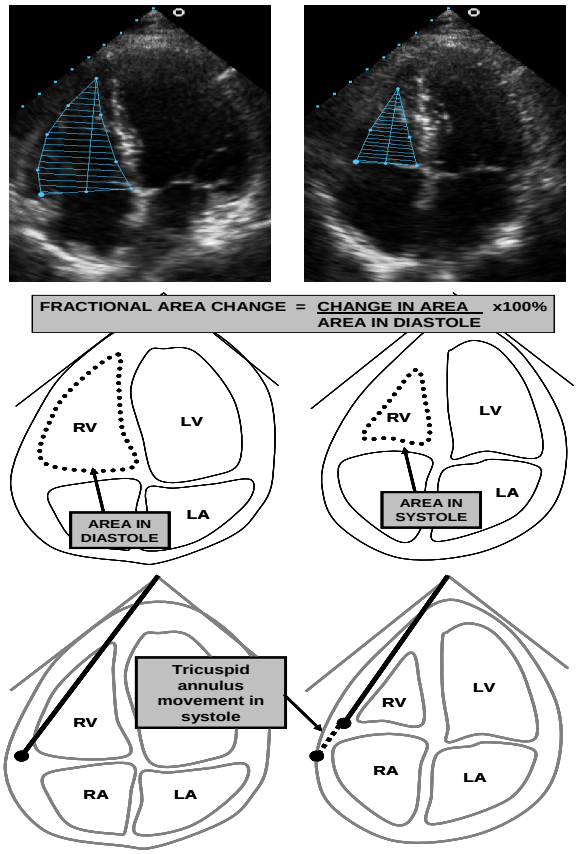

Figure 1.5: Right ventricle fractional area change (above) or tricuspid annular plane systolic excursion (below). RA, right atrium; LA, left atrium, %, percentage. Figure from Echocardiography (Leeson P, Augustine D, Mitchell A & Becher H. Oxford University Press, 2012)[3].

1.3.1.2 Three dimensional RV systolic function

Three dimensional RV volume and ejection fraction assessment is now possible. As with 3D LV assessment this has the advantage of contouring the actual shape of the ventricle in all dimensions although it has been noted that a number of factors including the irregular RV boundaries and increased trabeculations could lead to inaccuracies in the assessment of RV volumes and ejection fraction. 3D acquired cardiac data has been subject to testing against CMR, the current gold standard and computed tomography (CT). These studies have shown that RV 3D volumes, ejection fraction and stroke volume all compare favourable in both adults and children [9-11] and in patients with pulmonary hypertension [12]. 3D echocardiographic studies using software designed specifically for volumetric analysis of the RV has reported high levels of agreement with CMR or small underestimation in RV volumes [10, 13].

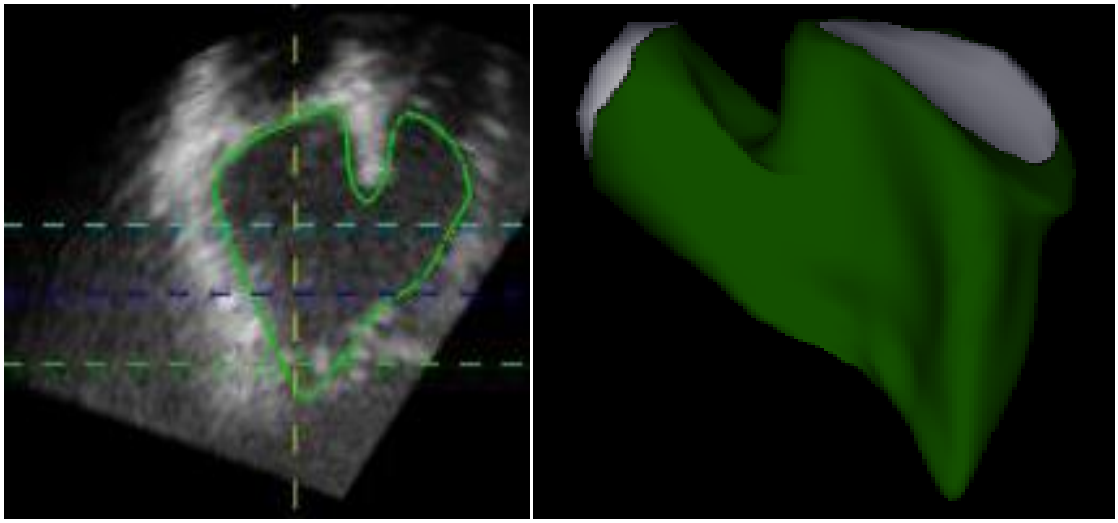

Figure 1.6: 3D RV contouring. RV contouring left (sagittal plane) and 3D echocardiographic RV reconstruction. Figure from Echocardiography (Leeson P, Augustine D, Mitchell A & Becher H. Oxford University Press, 2012)[3].

1.3.2 Cardiac magnetic resonance

RV systolic function is prognostically important although its assessment by echocardiography can be compromised due to its complex anatomy as well as suboptimal images due to adverse body habitus. For these reasons and because of the good spatial and temporal resolution that CMR offers, CMR assessment of RV ejection fraction remains widely accepted the gold standard non invasive method of assessment [14-16]. CMR derived volumes have shown good correlation with in vivo studies [17] as well as good accuracy and reproducibility for RV measurements [18-19].

1.4 Diastolic function

The assessment of LV diastolic function is as important as the assessment of LV systolic function. In diastolic dysfunction there is an abnormal cardiac relaxation, stiffness or filling as opposed to impaired cardiac contractile function seen with systolic dysfunction. The diagnosis of diastolic dysfunction or heart failure with a preserved ejection fraction accounts for around 50% of patients assessed with a new diagnosis of heart failure [20]. Impaired LV diastolic function often precedes systolic dysfunction in heart failure and is associated with increased mortality [21].

1.4.1 Echocardiography

Echocardiography is the most practical routine clinical approach for assessing diastolic dysfunction given its versatility. Echocardiographic diagnosis of diastolic dysfunction is one of the criteria needed to fulfil its diagnosis [20]. Specific echocardiographic markers of diastolic dysfunction include transmitral Doppler inflow velocity patterns, pulmonary venous Doppler flow patterns, tissue Doppler velocities and left atrial size.

Transmitral Doppler flow is acquired by placing a 1-2mm pulsed wave Doppler sample volume at the level of the tips of the mitral valve leaflets usually in the apical four chamber view. Assessment of the early (E) and late (A) filling, and deceleration time (DT) are integral in the assessment of the three major patterns of abnormal mitral inflow [22]: impaired relaxation; pseudonormal and restrictive filling. Echocardiography is well suited to making this distinction in grading diastolic dysfunction due to its excellent temporal resolution. Progressively worse diastolic dysfunction , culminating in restrictive filling has been shown to be associated with an increased mortality in patients with heart failure and in a post myocardial infarction setting [23] [24].

As previously mentioned, TDI enables measurement of high amplitude, low frequency Doppler shifts caused by myocardial motion allowing measurements of global and segmental function. For global function assessment, the Doppler region of interest is placed at the lateral and septal borders of the mitral valve annulus. During systole it moves toward the apex and during diastole it returns towards the base in early (e') and late (a') diastole. Early diastolic velocity is related to LV relaxation and decreases with age [25]. The E/e' ratio can be used for assessment of LV filling pressures as described in different clinical settings [26-27].

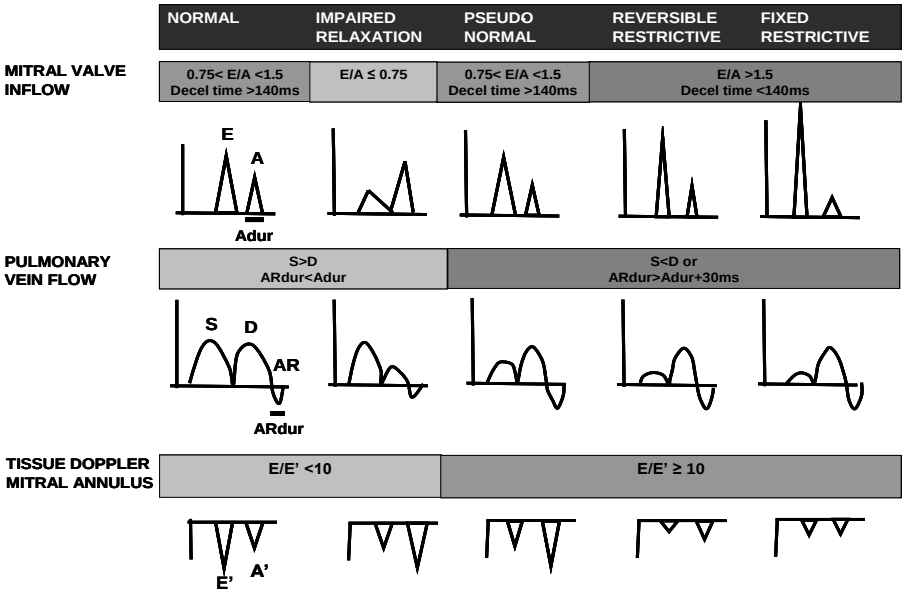

Figure 1.7: Doppler patterns for mitral valve, pulmonary vein and mitral annulus to characterize diastolic function. Figure from Echocardiography (Leeson P, Augustine D, Mitchell A & Becher H. Oxford University Press, 2012) [3].

1.4.2 Cardiac magnetic resonance

Echocardiography is widely accepted as the principle non invasive method for assessing diastolic dysfunction. However, CMR offers an alternative method for the assessment of diastolic dysfunction. CMR in general achieves superior image quality and has sufficient temporal and spatial resolution to allow reproducible assessment of cardiac volumes [28],including LA volumes. The accurate assessment of LV volumes achieved by CMR enables the estimation of LV time-volume relation to quantitatively evaluate LV filling pressures [29]. As with echocardiography, CMR is also able to evaluate transmitral flow using velocity or phase encoded magnetic resonance imaging. This allows the generation of a time-velocity curve representing one average cardiac cycle. A typical time-velocity curve would have a temporal resolution of 20-30 milliseconds (ms) and allows estimation of early, late velocities

and approximation of DT. Whilst acceptable correlation between echo Doppler studies and CMR has been reported , the cut off values used in echo cannot simply be translated to those CMR indices based on time flow rate curves [30]. Whilst these CMR parameters provide an insight into diastolic function, further improvements especially to achieve better temporal resolution and to reduce the scan time for velocity encoded MRI will advance the CMR assessment of diastolic function in the future.

1.5 Myocardial deformation imaging

The term “strain” refers to an objects’ fractional or percentage change from its original, unstressed, dimension and reflects the deformation of a structure. When applied to myocardium, this deformation or strain directly describes the contraction / relaxation pattern.

At rest, an object that has an initial length (L_0) can be stretched or compressed to a new length (L). This change in length is usually represented as a percentage, with a negative score indictating a shortening in length. Should L equal L_0 then strain remains zero. The strain rate provides the velocity at which deformation occurs and requires a high temporal resolution (>100Hz) which avoids underestimation due to under sampling [31]. Therefore, despite two objects displaying the same percentage of deformation, the speed at which this occurs can vary.

Although ejection fraction is simple and intuitive, as well as being supported by a wealth of prognostic information, it has important limitations including image quality dependence, geometric assumptions, load dependence and insensitivity to early disease (which is

characterized by disturbances of longitudinal function). Global strain measurement avoids inaccuracy due to inaccurate border tracing, but is dependent on image quality.

The two echocardiographic methods used for the approximation of myocardial strain are TDI which derives strain from strain rate, a gradient of adjacent velocities over a sampling distance and speckle tracking - which derives strain from excursion of the speckles.

1.5.1 Speckle tracking echocardiography

The measurement of myocardial strain has allowed the analysis of wall motion and deformation [32]. Prior to the advent of speckle tracking echocardiography, TDI enabled the quantification of tissue velocities at specific myocardial points as identified by the operator. The myocardial fiber orientation of the LV is complex. The major limitation of the Doppler based approach is the angle dependency required during image acquisition [6, 33] which allows longitudinal strain values to be estimated much more easily than circumferential or radial strain. This has been overcome by the introduction of speckle tracking echocardiography where speckles generated by reflected ultrasound signal form a pattern. Different regions of myocardium will have a unique speckle pattern which will move from one frame to the next. These speckles can be tracked using dedicated speckle tracking software which use algorithms to track the movement of speckles and allow this movement to be quantified via a number of parameters (such as longitudinal strain, circumferential strain, radial strain, twist/ torsion, displacement, strain rates, area tracking).

Strain is a mechanical characteristic that describes the deformation of objects. There are several different ways to measure strain. In its simplest (1-D) form, ε describes the deformation of an object relative to its original length using the following formula:

$$\frac{L - L_0}{L_0}$$

At rest, an object that has an initial length (L_0) can be stretched or compressed to a new length (L). The results of this are traditionally expressed as a percentage, with a negative score dictating a shortening in length. Should L equal L_0 then ε remains zero.

When the length of the object is not only known before and after deformation but also during the deformation process then the instantaneous strain can be defined:

$$\frac{L(t) - L(t_0)}{L(t_0)}$$

with L(t) the length of the object at time instance t and $L(t_0)$ its initial length. The instantaneous deformation is expressed relative to the initial length. This is the Langrangian strain. Other measures for strain include natural strain (also termed logarithmic strain) which uses the natural logarithm function ln. Natural strain has the same properties as conventional strain regarding the sign: it is positive for lengthening, negative for shortening and zero for no change in length. The actual strain, however, is slightly different for each method. When compared to that of conventional strain, the natural strain amplitude is smaller for positive strains and larger for negative strains (e.g. a conventional strain of 20% corresponds to a natural strain of 18.2%).

Longitudinal strain is measured from the LV apical views whereas radial and circumferential strains are taken from LV short axis views.Longitudinal strain is the motion from base to apex. During systole the contraction in this plane leads to fibre shortening, represented as a

negative percentage value (i.e. the more negative the value – the greater the deformation which has occurred). Radial strain is the amount of thickening of the myocardium which occurs. During systole myocardial contraction leads to fibre thickening in the radial plane. This is represented as a positive percentage value (i.e. the more positive the value – the greater the deformation which has occurred). Circumferential strain is the change in radius in the short axis. During systole myocardial contraction leads to fibre shortening. This is represented as a negative percentage value (i.e. the more negative the value – the greater the deformation which has occurred).

During the cardiac cycle the left ventricle also undergoes a twisting motion. During systole the apex rotates counterclockwise whilst the base rotates in a clockwise fashion. These movements can also be estimated by speckle tracking and is known as rotation or torsion. Rotation is the angular displacement of a myocardial segment in the short axis view. Torsion (or twist) is the net difference between apical short axis and basal short axis rotation.

1.5.1.1 Practical considerations when using speckle tracking

Unlike TDI, speckle tracking is an angle independent technique and so the transducer can be placed off axis to obtain the optimal image. Optimal image quality and especially clear delineation of the endocardial border is necessary for reliable tracking. The optimal frame rate for acquisition of images is around 50-90 frames per second (FPS), much lower than frame rates needed for TDI (>120 FPS). TDI estimates the velocity relative to the transducer of tissues and can be calculated in each pixel. As a result the higher frame rates used when compared to speckle tracking allow the velocities to be tracked throughout the cardiac cycle. With speckle tracking, in patients with tachycardia or during rapid events in the cardiac cycle, these lower frame rates mean that there may be under sampling, with peak

strain and strain rate values being lower than the true value. Higher frame rates will reduce the problem of under sampling but at the expense of spatial resolution. These lower frame rates are thus used to ensure optimal spatial resolution but care must be taken not to lower the frame rate too much otherwise the speckle will not be able to be tracked from frame to frame highlighting the necessity of a good balance between temporal and spatial resolution. Another advantage speckle tracking echocardiography has over tissue Doppler imaging is that it is not influenced by the passive traction of scar tissue to adjacent myocardium (the tethering effect) [34].

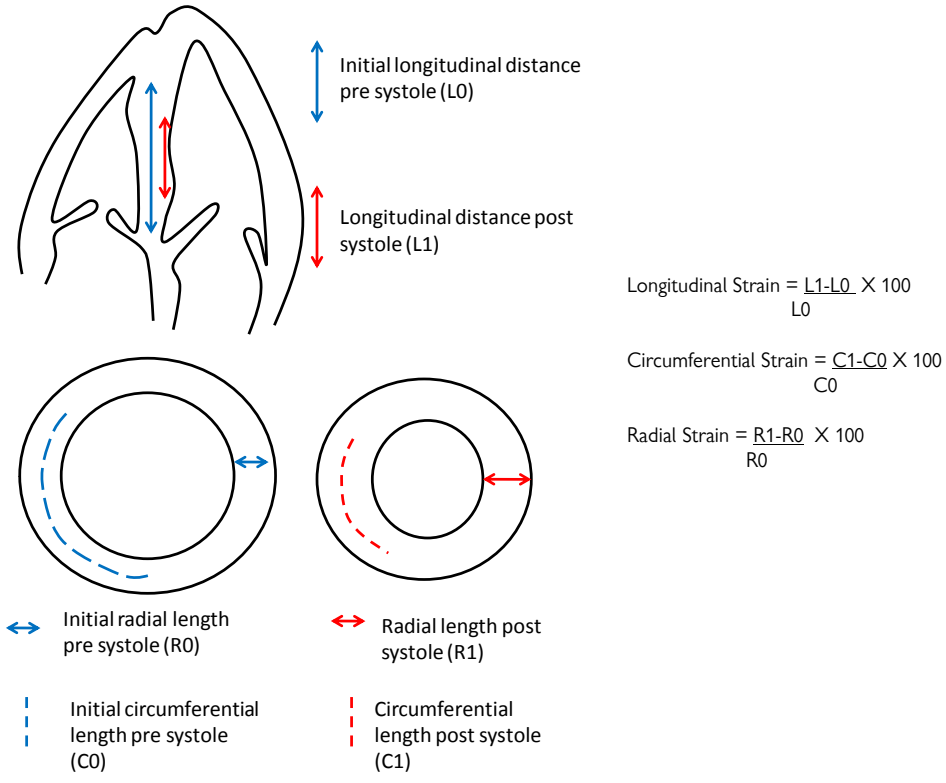

Figure 1.8: Representation of longitudinal, circumferential and radial strain. Figure from Echocardiography (Leeson P, Augustine D, Mitchell A & Becher H. Oxford University Press, 2012) [3].

1.5.1.2 Speckle tracking assessment of 2D and 3D LV systolic function

The advent of speckle tracking echocardiography has allowed myocardial deformation to be estimated in the longitudinal, circumferential and radial planes. 2D speckle tracking has been used for the analysis of left ventricular function in a number of pathologies including the assessment of coronary artery disease [35-37], valvular heart disease [38] and cardiomyopathies [39-40].

In reality speckles move through 3D space rather than remaining within the 2D sector. Newer technology is now available allowing the measurement of 3D speckle tracking strain. This has the advantage over 2D speckle tracking of being able to track the speckle throughout a cardiac volume irrelevant of their direction thus reducing the amount of speckle not being tracked due to out of plane motion as seen in 2D speckle tracking. 3D speckle tracking also allows the quantification of strain from the same cardiac volume rather than needing the acquisition of several (usually 6) 2D images from both short axis and apical views, thus reducing the concerns over heart rate variability affecting image analysis and also allowing quicker acquisition time. 3D speckle tracking has been used in the assessment of ventricular function in several situations including the estimation of LV ejection fraction and volumes [41] and dyssynchrony [42].

Whilst there have been a number of papers using both 2D and 3D speckle tracking, it still remains largely a research tool with no universally accepted standard reference ranges.

Vendor variability has been shown to exist between different machine vendors in 2D (in vendor dependent software) [43-44] echocardiography and for certain strain parameters in 3D echocardiography (with vendor independent software) [45].

The lack of a universally accepted reference range may be due to several factors including differences between different echocardiography machines in the generation of speckles, algorithm differences between software analysis packages, differences in frame rates between studies for image acquisition or even differences in heart rate of patient groups used.

1.5.1.3 Speckle tracking assessment of RV systolic function

Currently, RV systolic function assessment is limited to a visual assessment: area tracing, or measurements made at the basal position of the myocardium, used as a surrogate indicator of global function. Historically used for the assessment of LV deformation, speckle tracking echocardiography has more recently been applied to the assessment of RV systolic function by using algorithms and speckle overlays designed for the LV. Despite the lack of RV specific algorithms, STE has been applied to the right ventricle (RV) for the assessment of both regional and global systolic function, in a number of pathological conditions and in situations of RV conditioning, with promising results [46-52].

1.5.1 4 Speckle tracking assessment of diastolic function

Speckle tracking echocardiography has also been used for the assessment of diastolic function. Whilst similar advantages and limitations for its use exist as with speckle measures of systolic deformation parameters, increasing studies have highlighted its potential use with the assessment of diastolic function. Speckle tracking untwist [53] as well as diastolic strain rates [54] have been shown to be altered in those with diastolic dysfunction.

1.5.2 CMR assessment of myocardial deformation

CMR using a 'tagging' technique has been used to measure myocardial deformation [55-57]. Here, magnetization saturation bands in a grid format are placed onto the myocardium typically at the start of the cardiac cycle upon detection of the QRS complex. These tags are then able to track the myocardial motion during the cardiac cycle, reflecting underlying myocardial deformation. Image processing is then often performed using harmonic phase (HARP) analysis [57] to obtain similar deformation parameters to those seen with speckle tracking echocardiography [58-59].

1.5.2.1 Myocardial deformation analysis: comparison of echocardiography and CMR

The echocardiographic assessment of myocardial deformation parameters has advantages over CMR assessment, which include improved temporal resolution, its portability, quicker imaging time and cost effectiveness. The fading of CMR tagging grids during the cardiac cycle also favors the use of echocardiography in the assessment of diastolic deformation parameters. However, in favor of CMR in the assessment of myocardial deformation are the excellent spatial resolution and the excellent image quality, not always seen with echocardiography.

Myocardial strain derived from 2D speckle tracking echocardiography has been validated using CMR strain derived by tagging [55] although more recent studies have shown that correlations between the two imaging modalities for systolic deformation analysis is modest [59-60].

1.5.2.2 Deformation assessment using CMR feature tracking

A new software system, 'feature tracking' (2D cardiac performance analysis, Tom Tec, Germany) can measure ventricular deformation directly from steady state free precession (SSFP) cine CMR images, without the need for specialised tagged images. At the onset of this project there were relatively few publications using feature tracking. Since then, the results presented in this thesis by me and others have provided a body of work to establish the feasibility and normal ranges for feature tracking.

Feature tracking has potential advantages of reducing the overall scan time as well as allowing retrospective analysis of images to obtain deformation parameters without the need for additional imaging sequences. A wide range of deformation parameters can be calculated including strain, strain rate, rotation as well as displacement and tissue velocity values.

The technology used for feature tracking is similar in concept to speckle tracking echocardiography. It requires the operator to manually insert individual points to delineate the endocardial ± epicardial border over a single frame. A computed line through these individual points traces the border. This trace is then followed in time by tracking features that are in close proximity around this point in subsequent frames. These tracking features, can include the cavity boundary, anatomical elements or tissue patterns, related to the myocardial contour [61]. The movement of features from frame-to-frame are used to quantify myocardial deformation over the cardiac cycle.

CMR feature tracking software has been used to assess LV systolic deformation parameters in patients with arrhythmias [62], ventricular hypertrophy [63],cardiomyopathies [64-65],

dyssynchrony [66-67], pre and post dobutamine [68] and patients with congenital heart disease [69-71]. Studies have also used this software to identify RV strain [70, 72] and more recently both RV and LV strain in young adults born pre term [73-74].

Despite increasing numbers of studies using feature tracking software, currently no standardised normal values exist for systolic strain parameters [62]. To date peer reviewed published studies assessing feature tracking LV systolic deformation normal values have in general used relatively small numbers as part of control groups, varying between 10 – 42 people [68-70, 75-78] with the largest of these study populations (n=42) measuring circumferential strain only [76].

The software also offers the opportunity for the estimation of ventricular ejection fraction, mass and volumes and the potential to analyse diastolic deformation parameters also exists, although to date these parameters have not been assessed in peer reviewed published studies.

The increasing number of reports using feature tracking CMR technology highlights it's potential although more detailed studies to identify normal ranges as well as comparison with existing CMR (tagging) and echocardiographic (speckle tracking) strain modalities would be of use to assess whether strain measurements using different imaging modalities are truly interchangeable, irrespective of vendor or analysis technique.

1.6. Study aims

This study reviews the use of CMR feature tracking including its feasibility, reproducibility and comparison with other imaging modalities to provide assessment of myocardial deformation. Specifically, this study aims to:

1. Define normal feature tracking LV systolic deformation values and to assess their reproducibility.
2. Assess the ability of feature tracking to estimate ventricular volumes, mass and ejection fraction.
3. Assess the feasibility of feature tracking to measure diastolic function and to compare this with standard echocardiographic assessment.
4. To compare LV and RV feature tracking strain values with CMR tagging and speckle tracking echocardiography.

Chapter 2: Methods

2.1 Patient group

Over the course of the two year study period the feasibility and comparison with echocardiography of myocardial strain from CMR cine images using feature tracking was assessed. This was performed in normal healthy volunteers (chapters 3, 4, 5 and 7) as well as those with diastolic dysfunction (chapter 6).

In total, CMR images from two hundred and forty eight healthy volunteers, recruited by advertisement as controls for research studies over a two year period, were analysed. None of the healthy volunteers had documented cardiovascular risk factors, cardiac disease or other medical problems relevant to cardiac function, Table 2.1. The research studies were approved by the local ethics committee and informed consent for participation obtained from all subjects.

Table 2.1: Study population demographics.

Patient Characteristics (N=248)	
Age, yrs	29.0±7.1
Male, n (%)	99 (40%)
Body Mass Index, kg/m^2	24.1±4.3
Haemodynamics	
Systolic arterial BP, mmHg	115±12
Diastolic arterial BP, mmHg	69±6
Blood Profile	
Total Cholesterol (mmol/L)	4.7±1.0
LDL (mmol/L)	2.3±1.0
HDL (mmol/L)	1.9±0.8
Glucose(mmol/L)	4.9±0.5

2.1.1 Patient group chapter 3

In chapter 3 we define normal ranges for the various deformation parameters available using feature tracking software. This cohort consisted of 145 of the healthy volunteers. Prior to the onset of this work, the use of myocardial strain assessment from CMR cine images was in its infancy with no normal values existing. However, this number of participants is greater than current published studies assessing the use of myocardial strain from cardiac magnetic resonance tissue tagging in healthy normal subjects [79-82].

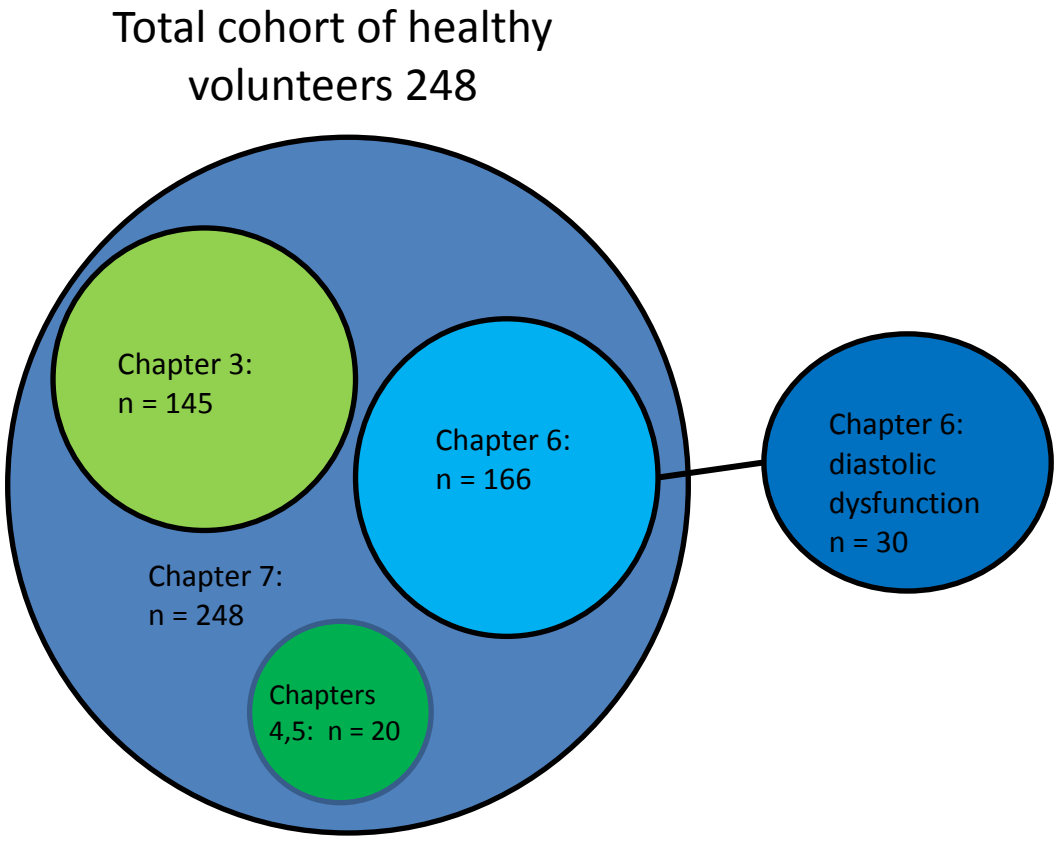

Figure 2.1: Study Cohort

2.1.2 Patient group chapter 4 and 5

In chapters 4 and 5 LV and RV myocardial strain (n= 20) was assessed and compared using a variety of techniques (CMR feature tracking, CMR tagging, 2D echocardiography and 3D echocardiography).

2.1.3 Patient group chapter 6

In chapter 6 the use of feature tracking to assess diastolic function from cine CMR images and a comparison with standard echocardiography techniques is made. For this, 30 participants with diastolic dysfunction and 30 age and sex matched controls were used. The group with diastolic dysfunction (defined using international guidelines [26], see section 2.4.4) was used from a cohort of patients with asymptomatic moderate - severe aortic stenosis. The specificity and sensitivity of the feature tracking parameters to identify diastolic dysfunction was calculated and finally from the cohort of healthy volunteers (n=166), normal ranges for diastolic feature tracking parameters were identified.

2.1.4 Patient group chapter 7

In chapter 7, analysis of CMR scans from 248 healthy volunteers was used to assess the feasibility of using feature tracking software to estimate LV and RV mass, volumes and ejection fraction.

2.2 Clinical assessment

During this thesis, two main cohorts of participants were used: healthy volunteers (n= 248) and those with diastolic dysfunction (n = 39).

As part of the research studies from where the cohort for this work was obtained, on the day of CMR scanning, all subjects underwent a clinical assessment. This included recording a full medical history and documenting:

- The presence or absence of exclusion criteria
- The presence or absence of cardiovascular symptoms
- The past medical history (with particular attention paid to any past cardiovascular history)
- Drug history, including allergies
- Alcohol and smoking history
- Family history, with particular reference to cardiovascular problems

A full physical cardiovascular examination was also performed and the following recorded:

- Height and weight using calibrated scales
- Blood pressure measurements using a manual sphygmomanometer
- Pulse rate, volume, regularity
- The presence/absence of added heart or chest sounds and ankle oedema
- Abnormalities of the abdominal, neurological or respiratory system

The following investigations were performed:

- 12 lead electrocardiogram, (ECG)
- CMR scan
- Echocardiography where appropriate.

2.3 Cardiac magnetic resonance

This study assesses the use of myocardial strain derived from CMR acquisitions and using either feature tracking or myocardial tagging techniques. This study also assesses the

feasibility of feature tracking for the assessment of ventricular volumes, mass and ejection fraction. The main potential advantages of using CMR for these purposes is that image quality is not limited and therefore can be used for measures of LV mass, volumes and function.

2.3.1 CMR cine acquisition protocol

In chapters 3,6 and 7 CMR images were recorded using a Siemens 1.5T Sonata scanner with a 16 channel receiver coil without the use of contrast following the same standardisation protocol for all acquisitions. Image acquisition was prospectively ECG gated with a precordial three lead ECG and acquired during end-expiratory breath holding. SSFP cine sequences were used to acquire localisation images followed by a SSFP ventricular short axis stack to obtain coverage of the entire LV and horizontal long axis, vertical long axis and LV outflow tract views (LVOT) cine images. Image acquisition parameters were echo time (TE) of 1.5ms, a repetition time (TR) of 3.0ms, temporal resolution 39.0±2.8ms and a flip angle of 60º, field of view 360mm, slice thickness 8mm, acquisition window 800 msec. Slice positions were chosen from the images obtained for the left ventricular short axis SSFP stack. The nearest slice to the base in which a complete circle of myocardium was visible throughout the cardiac cycle was selected as the basal slice. The mid-ventricular and apical slices were then selected with sequential 2cm gaps towards to the apex.

In Chapters 4 and 5, CMR imaging was acquired at 3-Tesla (Trio, Siemens Healthcare, Erlangen, Germany). Here, image acquisition parameters were TE of 1.5ms, a TR of 3.0ms, temporal resolution 37.8ms and a flip angle of 60º, field of view 360mm, slice thickness 8mm, acquisition window 800 msec.

2.3.2 CMR tagging acquisition protocol

When necessary, a gradient echo-based tagging pulse sequence was performed in the long axis (HLA, VLA and 3 chamber view) and in the basal, mid ventricular and apical short axis slices with a segmented K-space, multi-shot sequence (repetition time 25ms, echo time 7.4ms and flip angle 25º). Slice positions were chosen from the images obtained for the LV short axis SSFP stack. The nearest slice to the base in which a complete circle of myocardium was visible throughout the cardiac cycle was selected as the basal slice. The mid-ventricular and apical slices were then selected with sequential 2cm gaps towards the apex [83].

2.3.3 CMR ventricular volumes, ejection fraction and mass by manual contouring

CMR has demonstrated excellent accuracy and reproducibility for the estimation of ventricular volumes and left ventricular mass [84-85] based on the contoured disc summation method, which is widely accepted as the gold standard technique.

CMR mass, volumetric and ejection fraction analysis was performed off line using commercially available analysis software (Argus, Siemens). Imaging was triggered on the R wave. As images were triggered on the R wave mostly the first phase of each slice corresponded to end diastole, however end diastole was always selected to be the frame or phase with the largest LV cavity. The systolic frame for contouring was determined by visual assessment, using the frame where the LV cavity was at its smallest. At end diastole the LV endocardial and epicardial contours were manually traced and at end systole the endocardial border was traced (Figure 2.2C). Epicardial fat was excluded from the epicardial contour [86] and the papillary muscle was excluded from the LV cavity and included in the LV mass.

2.3.4 CMR ventricular volumes, ejection fraction and mass by feature tracking

Diogenes feature tracking software (2D cardiac performance analysis TomTec, Germany) was used for analysis. Following uploading of the HLA image, the brightness was optimised to ensure optimal endocardial / blood pool discrimination to aid visual assessment when marking the endocardium. Points were placed along both the LV endocardial and epicardial border at end diastole (Figure 2.2A) as well as the RV endocardial border. The software then automatically delineated borders through the marked points and searches for similar features in subsequent frames (Figure 2.2B). From applying the algorithm to the end diastolic frame it is possible to produce values for LV mass, ejection fraction as well as left and right ventricular end diastolic and end systolic volumes. Given that the feature tracking algorithm is different to contour tracking software we also evaluated results for end systolic volumes by applying the algorithm to the end systolic frame and examining the effect this had on the end systolic volume (the corrected end systolic volume, ESV Cor). Using the ESV Cor and the initial end diastolic volume (EDV) value it was also possible to estimate a corrected ejection fraction (EF Cor (%)): 100*(EDV-ESV Cor)/ EDV.

A **B** **C**

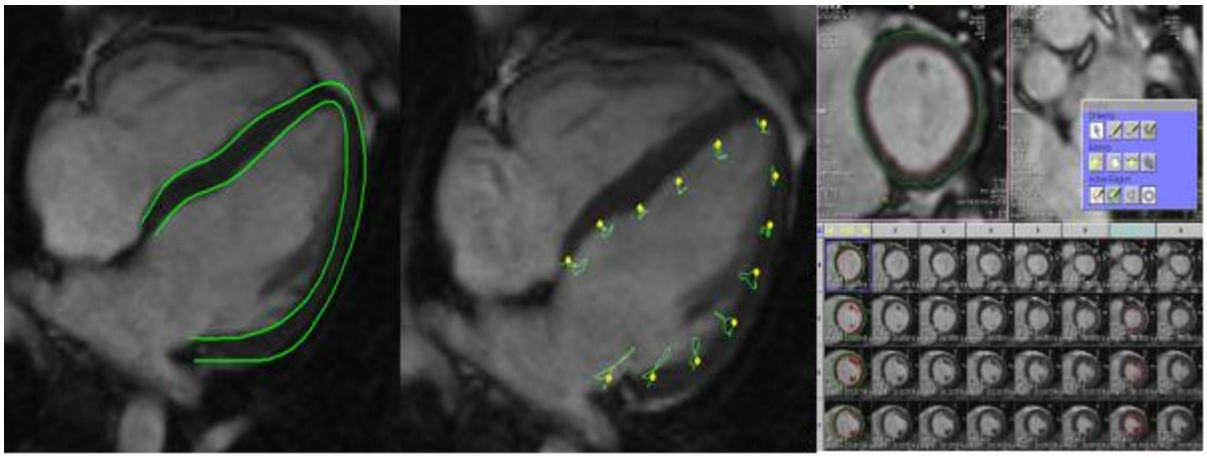

Figure 2.2: Contouring using feature tracking and CMR Argus.
A: Endocardial and epicardial contouring using feature tracking
B: Representation of the regions of features (green circles) followed by the contoured point (yellow).
C: Manual end systole and end diastole contouring using CMR Argus.

2.3.5 CMR feature tracking assessment for strain parameters

2D Cardiac Performance Analysis Software (TomTec, Germany) was used to obtain strain quantification directly from cine images, Figure 2.3. The same experienced operator performed all measures following a standard protocol taught by the software manufacturer. Following uploading of the image the brightness is optimised to ensure optimal endocardial / blood pool discrimination. Points are placed along the endocardial border (for determination of longitudinal and circumferential deformation parameters) and both the epicardial and endocardial borders (for determination of the radial deformation parameters). The software then automatically delineates the endocardial border through the marked points and searches for similar features in subsequent frames. In a proportion of subjects it was visually apparent the software failed to track myocardial motion in certain segments. Poor tracking was considered to be present when the movement of the points

along a portion of the border deviated from the movement of the endocardium by greater than 50% of the myocardial width. A record was kept of which segments failed to track and these segments were excluded from subsequent analysis. For systolic strain parameters, longitudinal strain, strain rates, velocities and displacement were obtained from the long axis views. Circumferential and radial strain, strain rates, velocities as well as basal and apical rotation and rotation rates were measured from the short axis SSFP views.

For diastolic strain parameters longitudinal and radial measured parameters included global and regional (basal, mid and apical) diastolic strain rates as well as early and late diastolic velocities to allow estimation of the ratio of early to late velocities. In addition global and regional circumferential diastolic strain rates were recorded as well as basal and apical untwist rates. Longitudinal values were obtained from the long axis views. Radial and circumferential values were obtained from the short axis views.

Short axis slice position was selected in the same way as for tagging image acquisition and, therefore, corresponding slices were used in those who had both sets of measures.

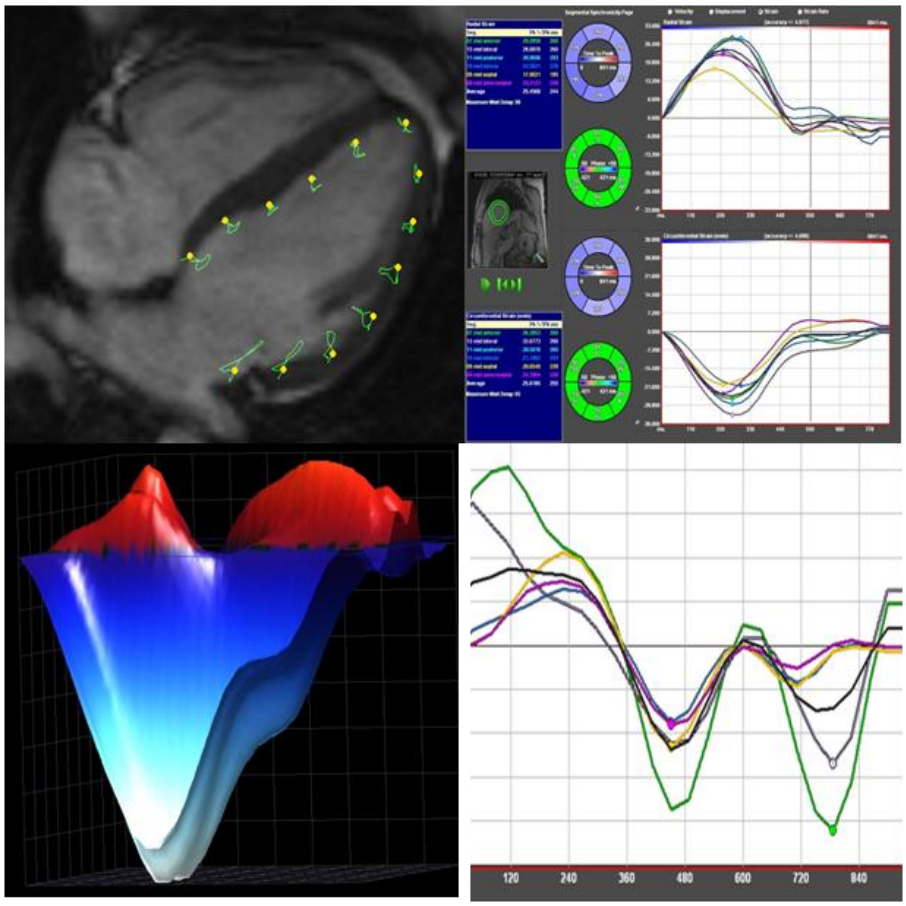

Figure 2.3: CMR strain analysis using feature tracking. Top row: Left, representation of the regions of features (green circles) followed by the contoured point (yellow). Right, short axis radial and circumferential strain curves; Bottom row: Left, 3D longitudinal strain curve. Right, feature tracking radial velocity curves demonstrating early and late diastolic velocities.

2.3.6 CMR tagging assessment for strain parameters

In those subjects who had undergone tagging studies semi-automated analysis of the tagged cine images was performed using CIM software (CIMTag2D v.7, Auckland MRI Research Group, New Zealand). CimTag2D is a manual corrected tracking procedure where a grid was aligned automatically to the myocardial tagging planes at end diastole. End systole is determined visually, and tags are adjusted at each frame through the cardiac cycle, Figure

2.4. Errors in the tracking are corrected by visual feedback by the user, previously validated against displacement encoding using stimulated echoes (DENSE) and deformable gel phantoms [87]. Circumferential, longitudinal and radial myocardial strains and strain rates were calculated by the software from the motion of the intersected tag lines. Global values were recorded. Regional values were calculated at basal, mid and apical levels.

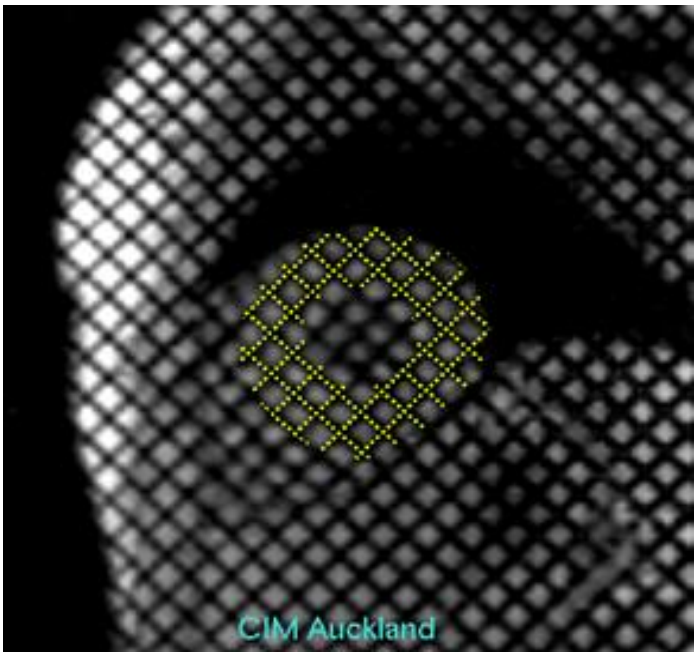

Figure 2.4: CMR Tagging. CimTag2D software tracks tagging which has been applied to short axis LV for measurement of circumferential and radial strain.

2.4 Echocardiography

Echocardiography has the advantage of having superior temporal resolution when compared with cardiac magnetic resonance imaging. This makes it an excellent modality for the assessment of both systolic strain parameters by speckle tracking and also in the assessment of diastolic dysfunction.

2.4.1 2D and 3D speckle tracking echocardiography acquisition protocols

Selected participants underwent echocardiograms to allow strain parameters to be processed. Two different ultrasound systems were used (iE33 system with X5-1 transducer for both 2D and 3D images (Philips Medical Systems, Zoetermeer, The Netherlands) and Toshiba Artida 4D system with PST 30BT probe for 2D and PST-25SX probe for 3D images. Three apical 2D views (4 chamber, 3 chamber and 2 chamber) and three short axis views (basal, mid and apical) were acquired. For the analysis of RV free wall longitudinal strain the 2D apical 4 chamber view was recorded with careful optimisation of the tilt and sector width to focus on the RV.

3D images were acquired using full volume datasets based on 4 subvolumes over 4 consecutive cardiac cycles. 3D volumes were checked for the presence of stitching artefacts and if present the volume was discarded and re acquired. Gain settings, sector widths and frame rates were optimised prior to image acquisitions, which were taken at end expiration.

2.4.2 2D Speckle tracking echocardiography post processing

2D images were analysed by software from the same vendor as the ultrasound acquisition systems (Philips QLab 8.1 and Toshiba WMT) and also by vendor-independent software (TomTec). Figure 2.5 depicts the analysis process, which is based on tracing or manually delineating the endocardial border. The software then performs automatic segmentation, which can be manually adjusted to ensure optimal endocardial overlay. Global circumferential and radial LV strain was estimated by averaging peak strains from all segments in the short axis planes and longitudinal strain from apical views.

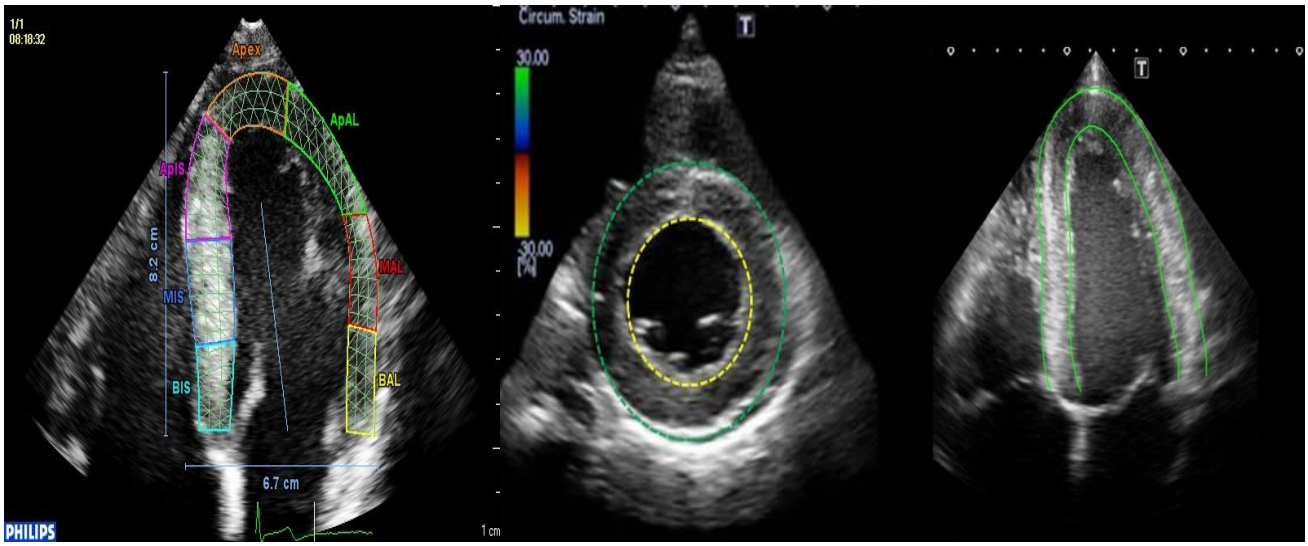

Figure 2.5: 2D Speckle tracking post processing. Left: Apical 4 chamber contouring using QLAB 8.1 CMQ – the operator is asked to mark the left, right mitral annulus and the apex before the software delineates the myocardial borders. Middle: Short axis basal level contouring using Toshiba Artida – the operator is asked to identify 3 anatomical points corresponding to 4, 8 and 12 o'clock, the software then automatically delineates the endocardial (yellow dashed line) and epicardial (green dashed line) borders. Right: Apical 4 chamber contouring using TomTec cardiac performance analysis – the operator manually marks the endocardium and contour is formed.

2.4.3 3D Speckle tracking echocardiography post processing

3D images were analysed by vendor independent software (TomTec). In addition, Toshiba images were analysed by Toshiba software (there is no dedicated Philips 3D software). Apical four chamber, two chamber and short axis views reconstructed from the 3D acquisition are automatically segmented and then manually adjusted to minimise foreshortening. Anatomical landmarks, according to software requirements, were identified to allow semi-automatic endocardial contouring (see Figure 2.6), which could then be manually adjusted, if required. Peak segmental strain values were averaged to give the overall global peak circumferential, radial and longitudinal strain.

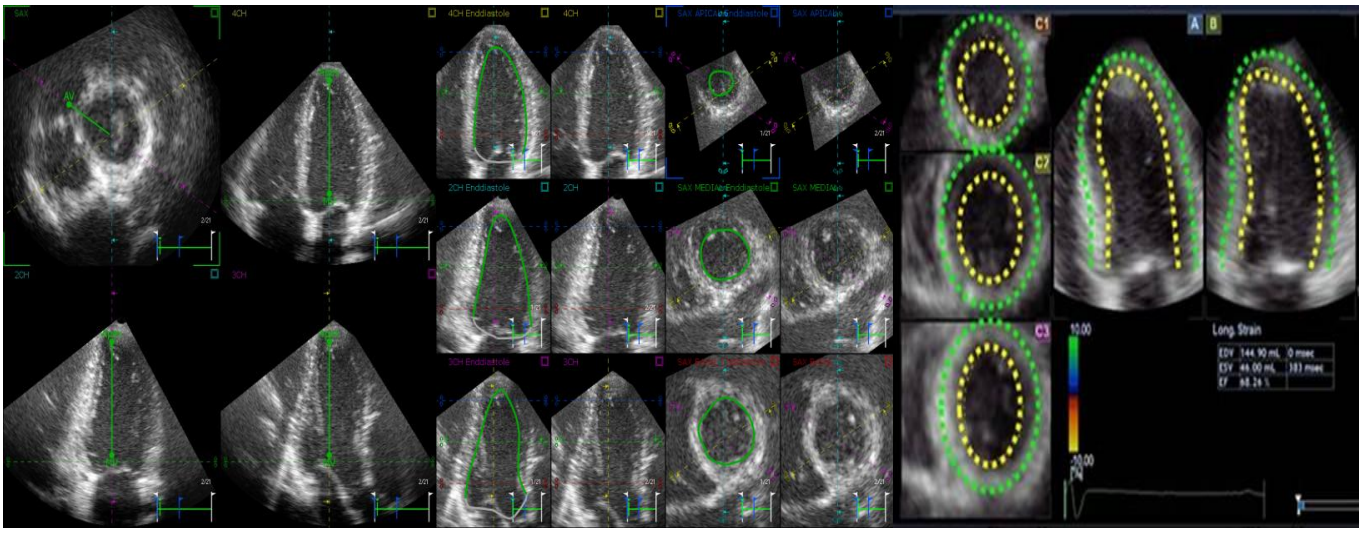

Figure 2.6: Contouring of 3D echocardiographic images. Left: 3D volume analysed in TomTec LV analysis 3 – the operator is asked to identify the aortic valve position (AV) and the centre of the mitral valve and the apex in the three apical views. The software package automatically contours the endocardium in the end diastolic frame and depicts the apical and short axis contours (middle). Right: 3D LV volume contouring on Toshiba 3D WMT – the volume is shown in 5 views (two apical long axis and 3 short axis views). The left, right mitral hinge point and the apex are marked allowing contouring.

2.4.4 Diastolic function assessment

2D echocardiography was performed using either a Phillips iE33 system with X5-1 transducer (Philips Medical Systems, Zoetermeer, The Netherlands) or Toshiba Artida 4D system with PST 30BT probe. Images to assess ventricular diastolic function were performed according to the American and European Societies of Echocardiography guidelines [26]. Measurements used to assess diastolic function included measurement of left atrial volume [88]; pulsed Doppler to record transmitral inflow in the apical four chamber view [89] and tissue Doppler velocities at the septal and lateral annular sites [90].

LV diastolic post processing was performed using Toshiba Artida Analysis [91] and Phillips Xcelera (for images acquired using Phillips iE33). Left atrial volume was assessed by the biplane method of discs (using an average of apical four and two chamber views). Mitral

inflow measurements included peak early (E) and peak late (A) velocities, E/A ratio and the deceleration time of E, Figure 2.7. The early diastolic (e') velocity by tissue Doppler at the septal and lateral annular sites was measured and the E/e' ratio calculated, see below Figure 2.7.

Figure 2.7: Assessment of diastolic function. Top row left atrial volume assessment; bottom left mitral inflow measurements; bottom right tissue Doppler recording at the lateral annular site.

LV diastolic function was graded according to the American and European Societies of Echocardiography guidelines [23], see Figure 2.8 below.

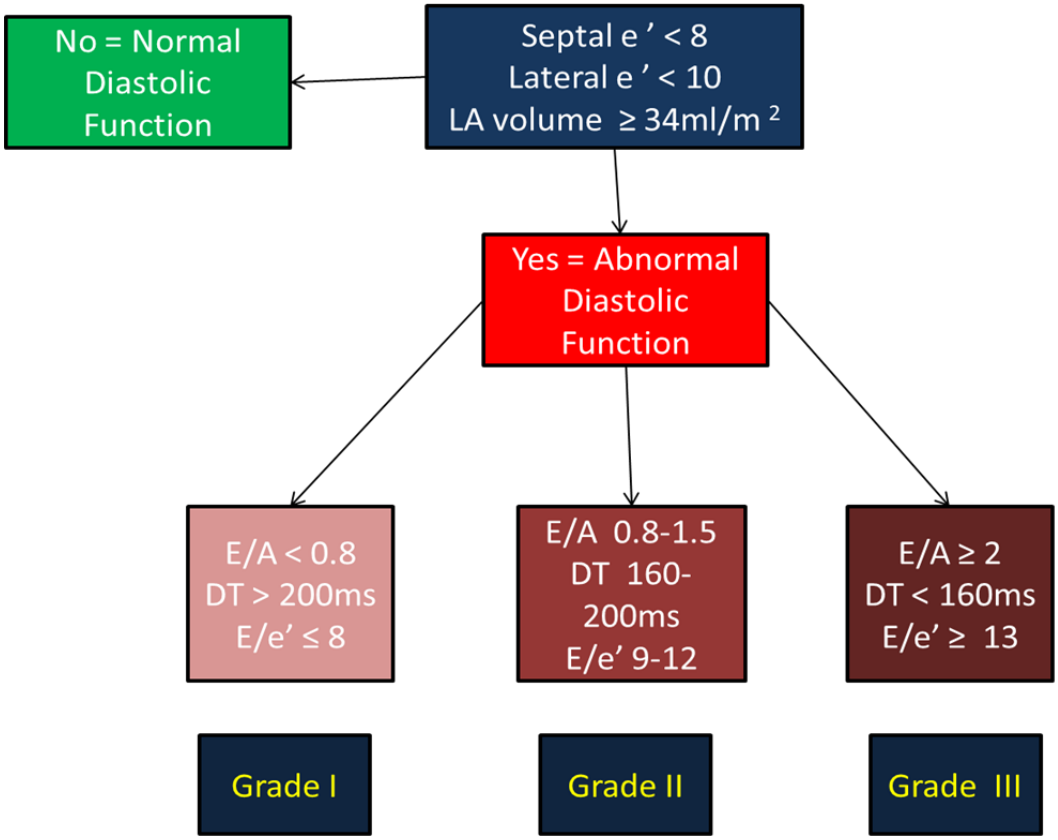

Figure 2.8: Echocardiographic grading of diastolic dysfunction. e', early diastolic velocity by tissue Doppler ; LA, left atrium; E, early mitral inflow velocity; A, late mitral inflow velocity; DT, deceleration time.

Chapter 3: Left Ventricular Myocardial Deformation Measures By Magnetic Resonance Feature Tracking: Normal Values and Comparison with Tagging

3.1 Introduction

LV myocardial systolic strain and deformation parameters alter early in disease pathogenesis [92-93] and vary with cardiac pathologies [38-39]. These parameters can be measured with CMR using a 'tagging' technique, in which magnetization saturation bands in a grid format are placed onto the myocardium at the start of the cardiac cycle. Image processing is then often performed using HARP imaging [57]. However, this can be difficult as tagged images have lower temporal resolution and the tag overlay fades through the cardiac cycle. A new software system, 'feature tracking' (2D Cardiac Performance Analysis, Tom Tec, Germany) can measure LV deformation directly from SSFP cine CMR images, without the need for specialised tagged images. The software tracks features, such as the cavity boundary or tissue patterns, related to the endocardial contour. The movement of features from frame-to-frame are used to quantify myocardial deformation over the cardiac cycle. Feature tracking has been used to quantify myocardial strain at a global level and within individual short axis slices in several studies [68, 76, 94]. However, clinical scenarios such as stress imaging or dyssynchrony evaluation need to measure strain regionally or even at a segmental level, and determine whether measured deformation parameters differ from normal values. The aims of this chapter were to:

1. Perform feature tracking analysis on cine CMR images obtained in a large number of normal subjects to determine ranges for deformation parameters including strain, displacement, velocity and twist at a regional and segmental level.

2. To evaluate reproducibility of the different measures and whether normal values vary by myocardial region and between genders.

3. To compare values to those obtained by traditional tagging techniques.

3.2 Methods

One hundred and forty five healthy volunteers were recruited as described in Chapter 2. Anthropometric measurements (height and weight), blood pressure and fasting blood tests (lipid profiles and glucose) had been obtained at the time of the CMR scan. All subjects underwent the same standardised CMR scan (Chapter 2.3.1). Twenty of the cohort also had CMR tagging images acquired (Chapter 2.3.2). LV systolic strain parameters were obtained using feature tracking for analysis of cine SSFP images (Chapter 2.3.5) and CIM software for tagged images (Chapter 2.3.6). Using basal, mid and apical levels from the short axis stack, circumferential and radial strain parameters as well as torsion were derived. From the HLA view, longitudinal LV strain was determined. In 12 subjects feature tracking measures were repeated after an interval of 3 weeks by both the first observer and a second experienced observer to assess inter and intra-observer agreement for measures.

3.3 Statistical analysis

Summary variables for subject characteristics and normal ranges of deformation parameters are presented as mean ± standard deviation. Inter and intra observer variability was assessed using the coefficient of variation (CV). Comparison of demographic, clinical and myocardial deformation data between genders was performed by independent student t test for normally distributed variables and Wilcoxon test for non-normally distributed variables. Distribution of the variables was assessed using the Kolomogrov Smirnov test. Comparisons of myocardial deformation parameters between myocardial regions was performed by ANOVA with a repeated measure design using a Greenhouse-Geisser correction followed by paired Student t-test to define the differences. Comparison of feature tracking derived values with tagging results was assessed using Bland Altman [95]

analysis. Initially the presence of proportional bias was assessed by performing linear regression. If the slope of the regression differed significantly from zero then the data was log transformed prior to performing the Bland Altman analysis to obtain the bias and limits of agreement which were then back transformed to give representative results. All computations were performed using SPSS 18 (SPSS Inc., Chicago, IL, USA).

3.4 Results

3.4.1 Study population and strain analysis

Baseline characteristics of the 145 subjects in the study cohort are demonstrated in Table 3.1. All subjects had analysable scans and of the 5200 segments assessed, 520 could not be tracked adequately by the software (10%). This was predominantly a problem with the segmental analysis of radial and longitudinal directed deformations, affecting 291 and 211 segments, respectively. Only 18 segments were considered unsuitable for analysis of circumferential strain. Inter and intra-observer agreements for feature tracking analysis are shown in Table 3.2. For global and regional strain measurements, the best observer agreement tended to be with circumferential strain at both global (CV 2.8-4.9%) and regional (CV range between 3.2% and 9.2%) levels with the poorest agreement for radial strain (global CV 22.9-32.3%; regional CVs range from 13.5 to 48.5%). Regional reproducibility was best at the mid and basal ventricular levels (with an inter-observer CV for mid circumferential strain of 4.5%) and worst at the apex.

Table 3.1: Baseline characteristics

Characteristic	Overall
Male (Total number)	54
Female (Total number)	91
Age (Years)	29.7±7.6
Weight (kg)	70.7± 13.6
Height (cm)	171.2± 9.1
Body mass index (Kg/m^2)	24.1± 4.4
Fasting total cholesterol (mmol/l)	4.5± 1.1
Fasting glucose (mmol/l)	4.8± 0.5
Systolic blood pressure (mmHg)	116.3± 11.9
Diastolic blood pressure (mmHg)	70.6± 8.2
Heart rate (beats/min)	66.9± 9.3
Data are presented as mean ± SD	

Table 3.2: Feature tracking, interobserver and intraobserver coefficient of variation (%).

	Global		Basal		Mid		Apical	
	FT Interobserver Agreement	FT Intraobserver Agreement	FT Interobserver Agreement	FT Intraobserver Agreement	FT Interobserver Agreement	FT Intraobserver Agreement	FT Interobserver Agreement	FT Intraobserver Agreement
Longitudinal Strain	10.9	12.3	10.8	17.7	17.5	17.7	31.3	42.7
Longitudinal Strain Rate	16.2	16.0	34.3	19.2	21.1	17.8	25.6	23.2
Radial Strain	32.3	22.9	13.5	48.5	26.3	14.8	29.1	23.9
Radial Strain Rate	14.9	15.6	15.8	14.1	27.2	11.3	31.3	30.2
Circumferential Strain	4.9	2.8	3.2	6.0	4.5	6.4	9.2	6.0
Circumferential Strain rate	7.9	6.3	15.9	6.3	6.9	18.3	17.3	9.1
Longitudinal Velocity	13.2	22.2	24.3	23.3	33.7	32.2	65.5	31.2
Longitudinal Displacement	18.6	31.8	25.6	18.1	37.2	34.9	43.9	75.6
Radial Velocity	2.4	6.2	5.2	5.1	5.0	4.5	6.2	7.3
Radial Displacement	2.7	4.3	7.5	4.3	6.4	4.5	7.5	5.7

3.4.2 Global and regional feature tracking strain deformation values.

Ranges for deformation parameters derived by feature tracking at a global and regional level are shown in Table 3.3. The results at the segmental level are shown in Table 3.4. Interestingly, all longitudinal, circumferential and radial parameters were higher at the basal compared to the apical level ($p<0.05$) although the magnitude of difference for circumferential strain did not meet significance ($p=0.09$). Absolute rotation and rotation rate were also higher at the base compared with the apex ($p<0.05$). Table 3.5 presents recorded values for global deformation parameters by gender with groups matched to ensure similar age distributions. There were no significant differences between genders in circumferential strain or strain rate. However, longitudinal strain values were higher in females, whereas, radial values were higher in males for strain (0.23± 0.04 vs. 0.22± 0.06, $p=0.02$), strain rate (1.16± 0.17s^{-1} vs. 1.13± 0.49s^{-1}, $p=0.03$), velocities (2.60±0.29cm/s vs. 2.29±0.28, $p<0.001$) and displacement (5.24±0.60 vs. 4.76±0.69, $p<0.001$).

Table 3.3: Normal values for systolic deformation parameters obtained using feature tracking

	Longitudinal				Radial				Circumferential				
Level	Strain	Strain Rate (s^{-1})	Velocity (cm/s)	Displacement (mm)	Strain	Strain Rate (s^{-1})	Velocity (cm/s)	Displacement (mm)	Strain	Strain Rate (s^{-1})	Rotation (deg)	Rotation Rate (deg/s)	Torsion (deg)
Global	-0.19 ±0.03	-1.08 ±0.24	2.60 ±0.55	5.04 ±1.14	0.25 ±0.06	1.25 ±0.4	2.5 ±0.36	5.1 ±.073	-0.21 ±0.03	1.21 ±0.18	N/A	N/A	15.52 ±7.55
Basal	-0.21 ±0.05	-1.21 ±0.36	3.38 ±0.72	6.61 ±1.83	0.26 ±0.08		2.84 ±0.53	6.02 ±1.08	-0.22 ±0.04	-1.33 ±0.28	-8.44 ±6.06	-59.79 ±33.44	N/A
Mid	-0.19 ±0.04	-1.08 ±0.27	2.65 ±0.69	6.37 ±10.15	0.24 ±0.08	1.25 ±0.36	2.48 ±0.41	4.89 ±0.82	-0.18 ±0.03	-1.05 ±.018	N/A	N/A	N/A
Apical	-0.16 ±0.05	-0.98 ±0.34	1.7 ±0.74	2.74 ±1.15	0.23 ±0.09	1.18 ±0.43	2.19 ±0.41	4.38 ±0.82	-0.21 ±0.38	-1.26 ±0.25	7.36 ±5.38	52.90 ±28.78	N/A

Data are presented as mean ± SD. Strain values represented as a fraction written in decimal form.

Table 3.4: Normal segmental values for systolic deformation parameters obtained using feature tracking

	Longitudinal				Radial				Circumferential	
Level	Strain	Strain Rate (s^{-1})	Vel (cm/s)	Displacement [21]	Strain	Strain Rate (s^{-1})	Vel (cm/s)	Displacement [21]	Strain	Strain Rate (s^{-1})
Basal										
Anterior	-0.21 ±0.10	-1.08±0.88	4.13±1.83	8.15 ±4.54	0.39 ±0.21	1.73 ±0.81	3.12 ±0.99	6.69 ±2.08	-0.22 ±0.08	-1.06 ±2.77
Lateral	-0.20 ±0.11	-1.61±3.82	3.29±1.55	5.85 ±3.25	0.35 ±0.17	1.93 ±0.35	2.88 ±0.75	5.89 ±1.70	-0.26 ±0.10	-1.59 ±0.69
Posterior	-0.24 ±0.11	-1.49±0.69	3.72±1.75	7.01 ±3.00	0.26 ±0.14	1.18 ±0.56	3.01 ±0.81	6.24 ±1.69	-0.23 ±0.08	-1.41 ±0.58
Inferior	-0.16 ±0.09	-0.87±0.58	2.64±1.15	5.16 ±2.86	0.17 ±0.11	0.93 ±0.49	3.03 ±0.9	6.51 ±1.91	-0.20 ±0.09	-1.21 ±0.57
Septum	-0.15 ±0.08	-1.08±0.59	3.55±1.73	5.86 ±3.31	0.12 ±0.08	0.81 ±0.49	2.38 ±0.75	5.04 ±1.57	-0.22 ±0.09	-1.26 ±0.62
Anterior Septum	-0.24 ±0.12	-1.5±0.77	3.29±1.81	7.30 ±3.89	0.22 ±0.12	1.13 ±0.69	2.6 ±0.8	5.67 ±1.65	-0.20 ±0.07	-1.20 ±0.57
Mid										
Anterior	-0.23 ±0.08	-1.21 ±0.61	3.36±1.72	6.05 ±3.17	0.33 ±0.18	1.61±0.74	2.45 ±0.58	4.92 ±1.15	-0.18 ±0.06	-1.05 ±0.38
Lateral	-0.22 ±0.11	-1.36±0.74	2.98±1.58	4.17 ±2.9	0.32 ±0.14	1.69 ±0.8	2.6 ±0.56	5.05 ±1.12	-0.19 ±0.06	-1.09 ±0.45
Posterior	-0.18 ±0.09	-1.14±0.67	2.59±1.33	4.68± 2.58	0.26 ±0.13	1.25 ±0.5	2.56 ±0.65	4.95 ±1.3	-0.18 ±0.06	-1.10 ±0.37
Inferior	-0.13 ±0.07	-0.73±0.42	2.64±1.15	4.86 ±2.58	0.16 ±0.09	0.89 ±0.44	2.50 ±0.60	4.9 ±1.22	-0.17 ±0.06	-1.05 ±0.37
Septum	-0.15 ±0.08	-0.91±0.51	2.97±1.57	4.14 ±2.26	0.13 ±0.08	0.85 ±0.46	2.38 ±0.6	4.67 ±1.22	-0.18 ±0.06	-1.04 ±0.37
Anterior Septum	-0.19 ±0.12	-1.22±0.83	2.49±1.37	4.79 ±2.1	0.22 ±0.13	1.25 ±0.64	2.41 ±0.59	4.83 ±1.14	-0.17 ±0.06	-0.93 ±0.38
Apical										
Anterior	-0.18 ±0.07	-1.11 ±0.60	1.49 ±0.77	2.66 ±1.39	0.29 ±0.14	1.42 ±0.61	2.09 ±0.51	4.20 ±0.98	-0.20 ±0.05	-1.12 ±0.34
Lateral	-0.13 ±0.07	-0.83 ±0.43	3.07±2.33	2.37 ±2.03	0.24 ±0.14	1.28 ±0.60	2.27 ±0.54	4.48 ±1.06	-0.22 ±0.05	-1.31±0.43
Inferior	-0.16 ±0.07	-0.9 ±0.44	1.53±0.88	3.19 ±1.81	0.14 ±0.12	0.90 ±0.55	2.30 ±0.53	4.60 ±0.91	-0.23±0.07	-1.38 ±0.47
Septum	-0.13±0.07	-0.88± 0.46	1.95± 1.24	2.33 ±1.43	0.18±0.10	1.07 ±0.57	2.09 ±0.51	4.22 ±1.05	-0.21 ±0.07	-1.21 ±0.48

Data are presented as mean ± SD. Strain values represented as a fraction written in decimal form.

3.4.3 Feature tracking and tagging comparison

Analysis of a complete data set using feature tracking was quicker than by tagging (8.8 ± 4.7 minutes vs. 15.4±4.9 minutes, $p<0.05$). The plots of Figure 3.1 show evidence of differences between the feature tracking and tagging methods of strain measurement, particularly for measurements of longitudinal and radial strain. Comparing the longitudinal measures of strain, about half of the points showed >25% differences of global values, greater deformation being associated with greater overestimation of the negative strain by feature tracking relative to tagging. Comparing radial measures of strain, more than half of the points showed between 50 and 100% differences, with all points except one showing overestimation of strain by feature tracking relative to tagging, and a trend suggestive of greater overestimation when there is greater strain.

Figure 3.1: Modified Bland Altman plots showing agreement between feature tracking and CMR tagging for global strain parameters

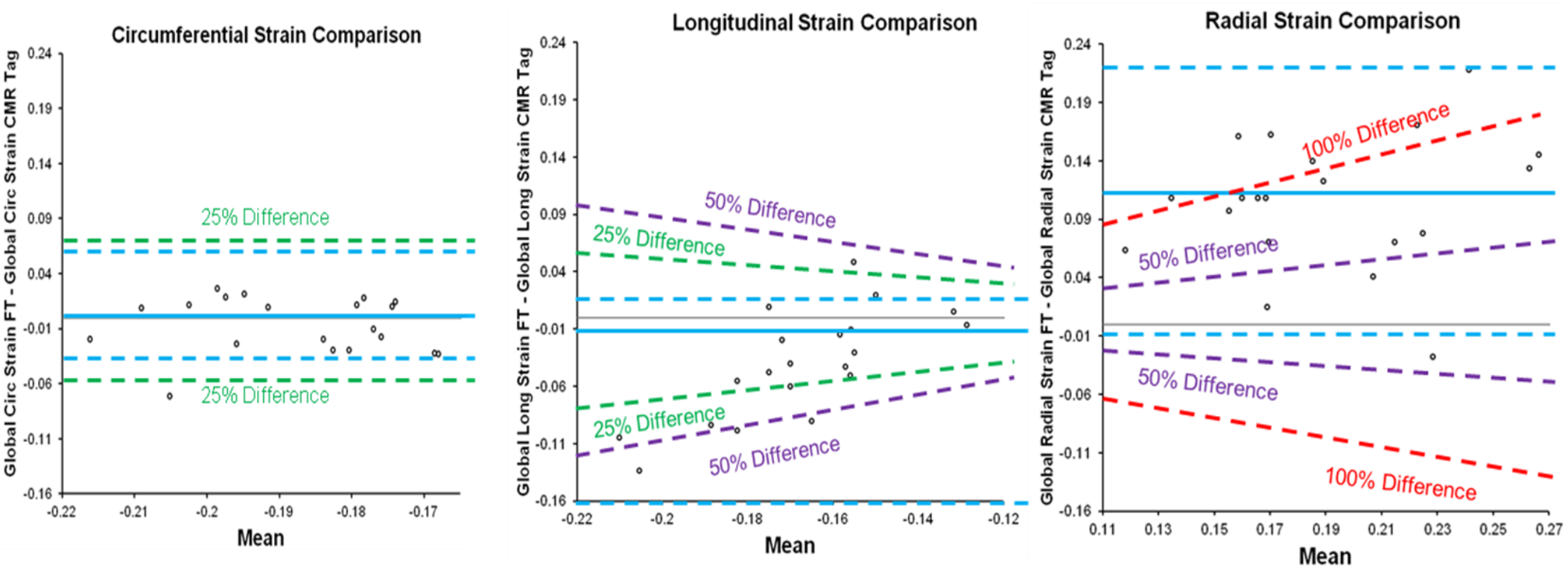

Circumferential strain (left); longitudinal strain; radial strain. The bias (blue solid line) and limits of agreement (blue dashed line) are shown. The oblique dashed lines demonstrate 25 (green), 50 (purple) and 100% (red) difference levels.

Absolute values for tagging derived strain for each gender are presented in Table 3.5. The different patterns in regional strain between genders was similar to those described for feature tracking. However, absolute values of reported strain differed, in particular for radial strain in females. This is demonstrated in the Bland Altman analysis which is presented in Table 3.6 for both global and regional parameters. For global strain parameters the narrowest limits of agreement were seen for circumferential strain (-0.06 to 0.04) with wide limits of agreement for radial strain (-0.01 to 0.23). A similar pattern was seen when comparing strain rates estimated by feature tracking and those by tagging with the lowest bias and narrowest limits of agreement being seen with circumferential strain rate ($-0.21s^{-1}$, -0.53 to 0.11) and the poorest agreement with radial strain rate ($0.26s^{-1}$, -0.34 to 0.86). Larger biases and limits of agreement were seen when comparing feature tracking with tagging at a regional level compared with a global level although again, the agreement for radial strain was poorest.

Table 3.5: Deformation results from feature tracking and tagging according to gender.

	CMR FT			CMR Tagging		
	Male (n = 54)	Female (n = 62)	P Value	Male (n = 7)	Female (n = 13)	P Value
Age (years)	27.46±5.06	26.59±4.64	0.29	26.76±1.53	27.57±1.51	0.35
Systolic BP (mmHg)	115.61±10.61	112.96±10.74	0.24	110.31±5.87	116.42±12.67	0.35
Diastolic BP (mmHg)	68.15±7.45	69.98±6.99	0.25	66.61±6.65	69.42±4.31	0.35
BMI (Kg/m^2)	23.99±3.06	23.11±4.03	0.02	23.89±3.20	21.26±2.11	0.06
LV Mass Index (g/m^2)	63.83±5.07	49.27±7.93	**<0.001**	57.45±9.16	42.34±5.99	**0.002**
EF CMR (%)	63.88±5.07	64.35±5.23	0.62	63.76±4.56	65.42±4.57	0.28
Longitudinal Strain	-0.17±0.04	-0.18±0.04	0.04	-0.14±0.01	-0.16±0.01	**0.005**
Longitudinal Strain Rate (s^{-1})	-0.98±0.28	-1.13±0.31	0.02	-0.69±0.66	-0.81±0.12	0.09
Circumferential Strain	-0.20±0.02	-0.21±0.03	0.86	-0.19±0.02	-0.19±0.02	0.08
Circumferential Strain Rate(s^{-1})	-1.19±0.16	-1.16±0.15	0.31	-0.84±-0.10	-0.91±0.64	0.12
Radial Strain	0.23±0.04	0.22±0.06	0.02	0.15±0.04	0.10±0.02	**0.003**
Radial Strain Rate(s^{-1})	1.16±0.17	1.13±0.49	0.03	0.98±0.31	0.65±0.89	**0.014**
Radial Velocity (cm/s)	2.60±0.29	2.29±0.28	**<0.001**			
Radial Displacement (mm)	5.24±0.60	4.76±0.69	**<0.001**			
Longitudinal Velocity (cm/s)	3.04±0.91	3.14±1.06	0.64			
Longitudinal Displacement (mm)	4.51±1.91	4.90±1.98	0.28			

Data are presented as mean ± SD. Strain values represented as a fraction written in decimal form.

Table 3.6: Bland Altman analysis for comparison between CMR tagging and feature tracking

	CMR Tagging vs. FT agreement							
	Global		Basal		Mid		Apical	
Variable	Bias	LOA	Bias	LOA	Bias	LOA	Bias	LOA
Longitudinal Strain	-0.01	-0.16 to 0.03	-0.06	-0.19 to 0.06	-0.05	-0.21 to 0.11	0.04	-0.12 to 0.20
Longitudinal Strain Rate (s^{-1})	-0.22	-0.82 to 0.37	0.01	-0.16 to 0.19	0.03	-0.05 to 0.12	-0.02	-0.12 to 0.07
Radial Strain	0.11	-0.01 to 0.23	0.12	0.03 to 0.23	0.12	-0.05 to 0.30	0.08	-0.13 to 0.30
Radial Strain Rate(s^{-1})	0.26	-0.34 to 0.86	0.20	-0.71 to 1.11	0.41	-0.32 to 1.16	0.17	-0.83 to 1.16
Circumferential Strain	-0.007	-0.06 to 0.04	-0.05	-0.14 to 0.04	0.02	-0.04 to 0.07	0.009	-0.05 to 0.07
Circumferential Strain rate (s^{-1})	-0.21	-0.53 to 0.11	-0.44	-1.09 to 0.21	-0.07	-0.42 to 0.27	-0.12	-0.50 to 0.25
Strain values represented as a fraction in decimal form.								

3.5 Discussion

This study reports ranges for all LV myocardial systolic strain parameters as well as myocardial displacement and velocities using feature tracking down to a segmental level in a large group of healthy subjects. The study has identified both regional variation, with higher strain at the base than apex, as well as gender differences.

The introduction of feature tracking software has allowed estimation of strain parameters directly from cine images. The ability to calculate myocardial segmental velocities and displacement in addition to strain parameters using the same software is more time efficient during both image acquisition and post processing. The technique avoids the additional time needed for either tissue phase mapping or tagging and raises the possibility of retrospective analysis of existing CMR datasets. We found the software could be easily applied to existing SSFP cine sequences and was able to analyse 90% of imaged segments. This compares favourably to echocardiographic studies of regional speckle tracking analysis in which strain typically can only be measured in around 80% of segments [44, 96-97]; presumably due to difficulties in obtaining adequate echocardiographic windows with poorer delineation of the endocardial and epicardial borders compared with CMR.

Nevertheless, as others have reported [68, 70, 77], we found observer reproducibility to vary considerably between the three main deformation directions with global strain values acceptable for circumferential assessment (inter-observer CV 4.9%) but poor for radial strain (CV 32.3%). There was also deterioration in reproducibility from a global to regional level with poor reproducibility for apical measures. This pattern is similar to that previously reported for reproducibility using the tagging technique in which CVs for circumferential strain range from 8.3% to 10.8% and for radial strain from 9.0% to 59.2% [98]. It has been

proposed that the poor reproducibility for radial parameters may be due to the geometry of the heart with analysis in a plane of movement with the smallest potential diameter for tracking. In addition, with tagging the tag lines may occasionally delete part of the endocardial contour thus potentially impacting on the estimation of radial movement between the endocardium to the epicardium. Our results suggest both tagging and feature tracking are similarly limited in the radial direction. This poor reproducibility may explain why we found significant variation in absolute deformation values recorded in the radial direction with tagging and feature tracking. This was particularly evident in females for whom mean radial strain by feature tracking was 0.22±0.06 compared to 0.10±0.02 by tagging. Alternatively, as there was a systematic bias, with larger values derived from feature tracking, this difference may be a real effect and relate to how strain is measured by the two techniques.

Tagging measures myocardial strain from the changing in-plane separations of tags that mark the intersections of orthogonally orientated tagging planes. They are therefore relatively unaffected by a through-plane component of motion. In contrast, feature tracking analyses motion in a 2D plane within a myocardial band defined by the endocardial border. The algorithms used by TomTec to track features are based on an adaptation of particle velocimetry algorithms in common use in multiple technologies including speckle tracking. They use voxel patterns within the image identified during initial contour application and subsequent searching between frames based on a hierarchical protocol that allows for reducing region of interest to improve accuracy, recognition of variation in motion between base and apex and rules regarding endocardial and epicardial boundaries [99]. Interestingly, the variation between feature tracking and tagging measures of longitudinal strain appears

to vary with magnitude of strain so that the difference in measures is greater with larger strain values.

Changes in the voxel pattern during the cardiac cycle within the myocardium may have an impact on consistency of feature tracking and account for some variation in strain measures, particularly in the radial direction. For instance, it is possible the compaction and exclusion of blood from interstices in trabeculated myocardium at end systole may alter voxel appearances in this region sufficiently to make accurate tracking difficult. The higher degree of trabeculations seen at the LV apical level when compared with the basal level may account, in part, for the increased variability in measurements seen regionally.

These significant differences in the approach of feature tracking prompted our study to define feature tracking-specific ranges for strain [68, 76, 94, 100]. Normal ranges of strain and velocities have already been described using various other imaging modalities including tagging [96-97, 101-103] and significant variations noted. In the future, development of standardised reference ranges may allow convergence of technologies and ranges. However, significant further work is needed including with feature tracking, for example, it is not known what effect contrast agents have on strain results and future validation of segmental strain values is necessary.

Our results did find some consistent findings between techniques in our study population. For instance, deformation values varied between genders and myocardial regions when assessed by both feature tracking and tagging [104-105]. Multi-modality imaging studies describing normal strain values have tended to vary in their findings with respect to differences between the base and apex [79] with some reports of lower strain values towards the apex [106]. However, the velocity values we obtained in this study are similar to

previous reports both in terms of normal ranges and the finding of a reduction of myocardial velocities at the apex compared to the LV base [107]. Circumferential measures, particularly at a global or mid-ventricular level were also strikingly reproducible and comparable between techniques within our study. Furthermore, at the mid-ventricular level the circumferential strain values reported in our study are very similar to those previously reported for feature tracking by Hor et al (0.18 ± 0.03 vs. 0.19 ± 0.02) [6] and Harrild et al (0.18 ± 0.03 vs. 0.21 ± 0.04) [83]. Indeed, it has been suggested, simple measures such as relative change of boundary length may be equally robust to characterise circumferential myocardial deformation [70].

We have recorded ranges for deformation parameters, as reported by feature tracking, from a global to segmental level in healthy volunteers and show the software can be used to rapidly extract these measures from existing SSFP cine images acquired in large numbers of subjects. We find ranges vary with gender and myocardial region and that the reproducibility of feature tracking measures, as well as agreement with tagging-derived indices, appears to be best for circumferential measures and poorest for radial strain.

Chapter 4: Left Ventricular Myocardial Deformation Measures By Magnetic Resonance Feature Tracking: Comparison With 2D And 3D Echocardiography

4.1 Introduction

Changes in myocardial strain have been proposed as sensitive markers of left [32] ventricular systolic dysfunction based on the observation that strain reduces early in disease pathogenesis [93] as well as being impaired in established coronary artery disease [36-37], valvular disorders [38, 92] and cardiomyopathies [39-40].

Tissue Doppler imaging has been used to quantify myocardial deformation based on tissue velocities [6, 33] but has been superseded, first by 2D, and then 3D speckle tracking echocardiography, which quantify deformation by tracking changes in the myocardial ultrasound speckle pattern [41-42]. The speckles are tracked in multiple directions, which allow longitudinal, circumferential and radial strain to be measured. Strain quantification by CMR is also possible based on tracking of the deformation of magnetisation tag lines superimposed at end-diastole onto cine images [55-57]. More recently, software to track inherent myocardial features within standard cine sequences has become available (feature tracking) and, like 3D echocardiography, has been proposed to have advantages of simpler acquisition and quicker analysis. As a result of these developments in imaging and analysis a diverse range of strain parameters are now reported.

The aims of this chapter are to:

1. Compare the technical characteristics as well as operator variability of all the key technologies, including newer 3D echocardiography and feature tracking CMR techniques, for measurement of global parameters of left ventricular strain.

2. To identify specific parameters that appeared reproducible irrespective of technique and to demonstrate consistency of these measures both within and between modalities.

4.2 Methods

Twenty (mean age 29.1 ± 5.3 years) subjects without cardiovascular disease were recruited as described in chapter 2. Initially they all underwent the same standardised CMR protocol including acquisition of tagging sequences as described in sections 2.3.1 and 2.3.2. Within one month of the CMR they all underwent 2D and 3D echocardiography on both a Philips iE33 (Zoetermeer, The Netherlands and a Toshiba Artida 4D system echocardiography as described in 2.4.1. The study design is shown in figure 4.1. For each participant LV systolic strain parameters were derived using tagging and feature tracking cine analysis as described in Chapters 2.3.5 and 2.3.6. From the short-axis stack, peak systolic 2D circumferential and radial strains were derived. From the HLA view, 2D longitudinal LV strain was determined. The 2D echocardiograms were analysed for LV systolic strain measures using both vendor dependent software (QLAB 8.1 for images acquired using the Philips iE33 system and Toshiba WMT for images acquired using the Toshiba system) as well as vendor independent software (TomTec). The Toshiba 3D LV images were analysed to provide strain parameters again using its own vendor dependent software and also TomTec vendor independent software. As there is no vendor dependent 3D strain analysis package for the Philips iE33 system, these images were analysed using the TomTec vendor independent software. Echocardiography image analysis techniques for 2D and 3D images are described in Chapters 2.4.2 and 2.4.3.

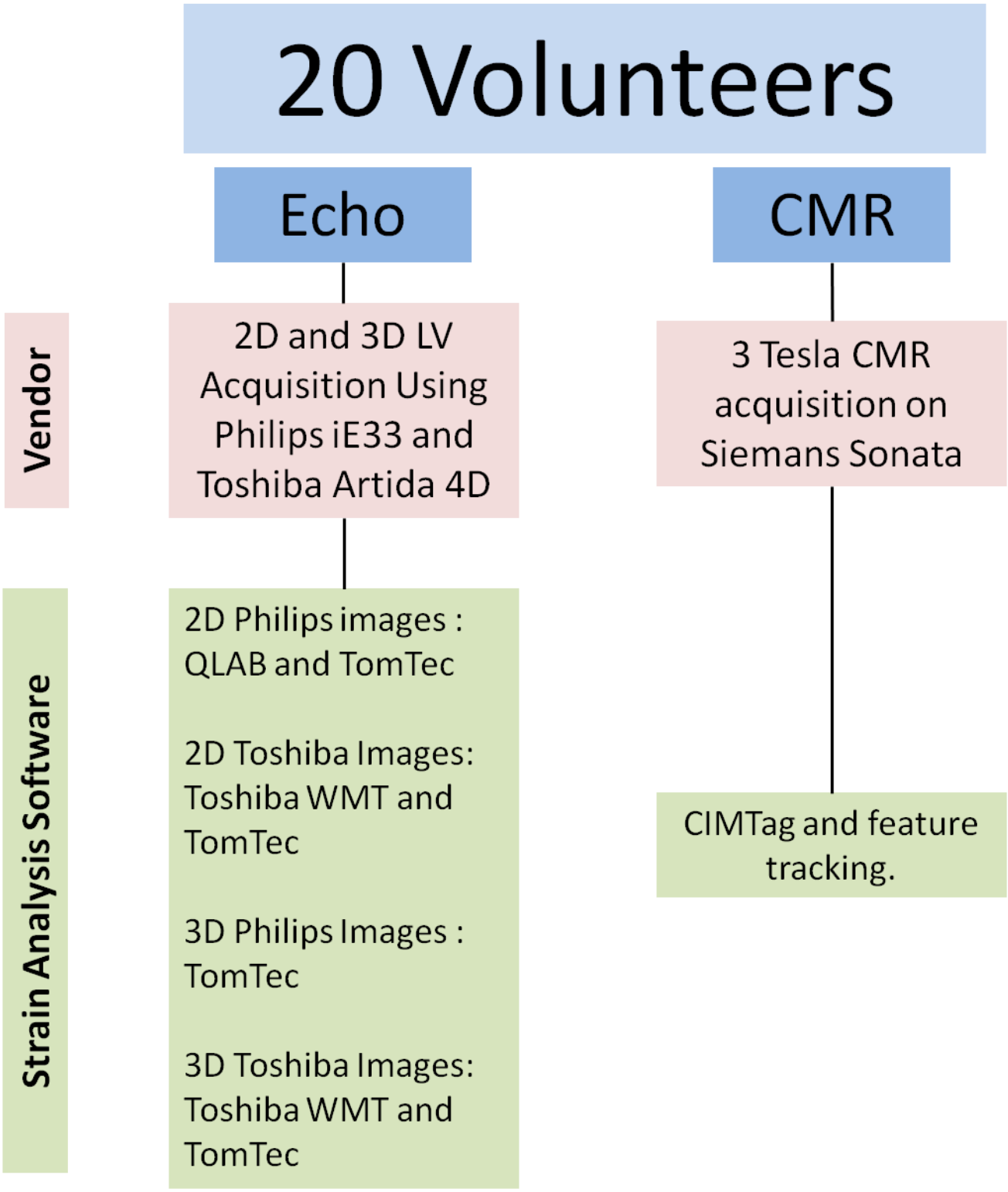

Figure 4.1: Study design

4.3 Statistical analysis

Summary variables for technical aspects of image acquisition, subject characteristics and strain in the 20 volunteers are presented as mean ± SD. Variable distribution was assessed using Kolomogrov Smirnov test. Normally distributed variables were compared by paired Student t test and non-normal variables by Wilcoxon test. Inter- and intra-observer agreement for different techniques was based on an experienced reader undertaking repeated strain analysis, blinded to the original results, in 7 of the participants. A second reader then also undertook the analysis on the same individuals. Data was reviewed based on the mean and confidence intervals of the intra-class correlation (ICC) and, specifically, the average correlation amongst all pairs for either the inter or intra-observer study [108]. An ICC value of 1 indicates perfect agreement and, for example, an ICC of 0.95 indicates the balance of the variance (1 – ICC = 5%) is attributable to error; in this study due to instrumentation or operator [109] For comparison purposes we classed ICC scores of <0.4 as poor reproducibility; 0.4-0.6 as low; 0.6-0.8 as moderate and >0.8 as good reproducibility. We then used Bland-Altman analysis [95] to compare levels of strain between and within modalities to identify parameters that were measured consistently between techniques. The calculated mean difference between two measurements was used to identify systematic bias and the consistency across measurement approaches reviewed by study of the limits of agreement, based on the 95% confidence intervals for the differences between the two measurement methods. All statistical analysis was performed using SPSS 18.0 (Chicago, Illinois) and $P < 0.05$ was deemed statistically significant.

4.4 Results

4.4.1 Technical aspects of image acquisition and analysis

No significant differences were seen in heart rates during acquisition of echocardiography and CMR images (Table 4.1). As expected, temporal resolution of 2D echocardiography (16.5±1.2ms for Philips; 15.5±1.3ms for Toshiba) was significantly better than for 3D (53.1±5.2ms for Philips; 55.4±3.2ms for Toshiba) and CMR (37.8±4.2ms); $p < 0.05$ for difference between 2D echocardiography and either 3D or CMR. However, time taken for post-processing 2D echocardiograms (15.5±1.3 minutes for QLAB 8.1; 13.2±2.2 minutes for Toshiba) was longer than for 3D (6.7±1.2 for Toshiba; 5.3±1.3 minutes for TomTec). Furthermore, vendor-independent software was quicker than software from the same vendor as the ultrasound machine for both 2D echocardiography (11.4 ± 2.2 minutes vs. 15.5 ± 1.3 minutes or 13.1 ± 2.2 minutes) and for 3D (5.3 ± 1.3 minutes vs. 6.7 ±1.2 minutes). CMR analysis took a similar length of time to 3D echocardiography with feature tracking (4.5±1.9 minutes) but was quicker than tagging (7.8±7.6 minutes).

Table 4.1: Image acquisition parameters.

	Philips 2D	Toshiba 2D	Philips 3D	Toshiba 3D	CMR Tagging	CMR FT
Heart rate (bpm)	63.2±12.1	60.8±12.1	59.6±11.6	59.1±11.8	62.1±8.8	63.6±6.1
FPS or VPS	60.8±4.4	63.7±5.9	19.1±0.4	18.0±0.21	-	-
Temporal Resolution (ms)	16.5±1.2	15.9±1.6	53.1±5.2	55.4±3.2	37.8±4.2	39.6±6.1
Image Analysis Time Vendor Dependent Software (min)	15.5±1.3	13.1±2.2	-	6.7±1.2	-	-
Image Analysis Time Vendor Independent Software (min)	11.4±2.2		5.3±1.3		7.8±7.6	4.5±1.9
Data are presented as mean ± SD.						

Mean and standard deviation for levels of strain measured by different techniques in a healthy group of young males are reported in Table 4.2.

Table 4.2: Mean and standard deviation of strain values (%) according to imaging modality and analysis approach.

Imaging/Analysis Combination	LV Circ Strain	LV Rad Strain	LV Long Strain
2DE Toshiba/Toshiba	-19.0±2.6	37.8±16.0	-14.4±1.9
2DE Philips/Philips	-18.9±2.6	29.1± 8.2	-16.5±2.5
2DE Toshiba/TomTec	-20.6±2.4	29.5± 4.7	-17.3± 2.4
2DE Philips/TomTec	-23.9±3.6	32.7±6.6	-18.2±1.8
3DE Toshiba/Toshiba	-24.7±4.1	35.5±7.9	-15.8±2.1
3DE Toshiba/TomTec	-21.8±4.5	48.8±7.7	-15.9±2.1
3DE Philips/TomTec	-21.3±3.7	48.0±5.9	-16.6±2.6
CMR Tagging	-20.6±2.0	27.3±4.6	-16.8±1.8
CMR Feature Tracking	-17.5±2.8	17.1±6.1	-15.9±2.3
Data are presented as mean ± SD.			

4.4.2 Inter- and intra-observer variability

2D and 3D Echocardiography **-** For 2D speckle tracking, better inter and intraobserver agreement was seen for left ventricular longitudinal (best interobserver ICC 0.76 & intraobserver ICC 0.57) and circumferential strain (best interobserver ICC 0.62 & intraobserver ICC 0.76) than for radial strain (best interobserver ICC 0.47 & intraobserver ICC 0.44) (Figure 4.2, top row). The mean ICC for observer agreements was no better with 3D echocardiography (Figure 4.2, bottom row). However, in general, the confidence intervals for the ICCs with 3D echocardiography were narrower than for 2D echocardiography consistent with less inter-individual variability. For example the narrowest 95%CI for intraobserver ICC for 3D longitudinal strain was between 0 and 0.93 whereas for 2D longitudinal strain it was between -0.49 and 0.8.

Figure 4.2: Intra class correlation coefficients for 2D (top row) and 3D (bottom row) LV echocardiography inter and intra observer agreement. Levels for an ICC of 0 shown in purple line. Levels for moderate reliability (ICC 0.6) shown as solid black line; levels for good reliability (ICC >0.8) shown as dashed black line.

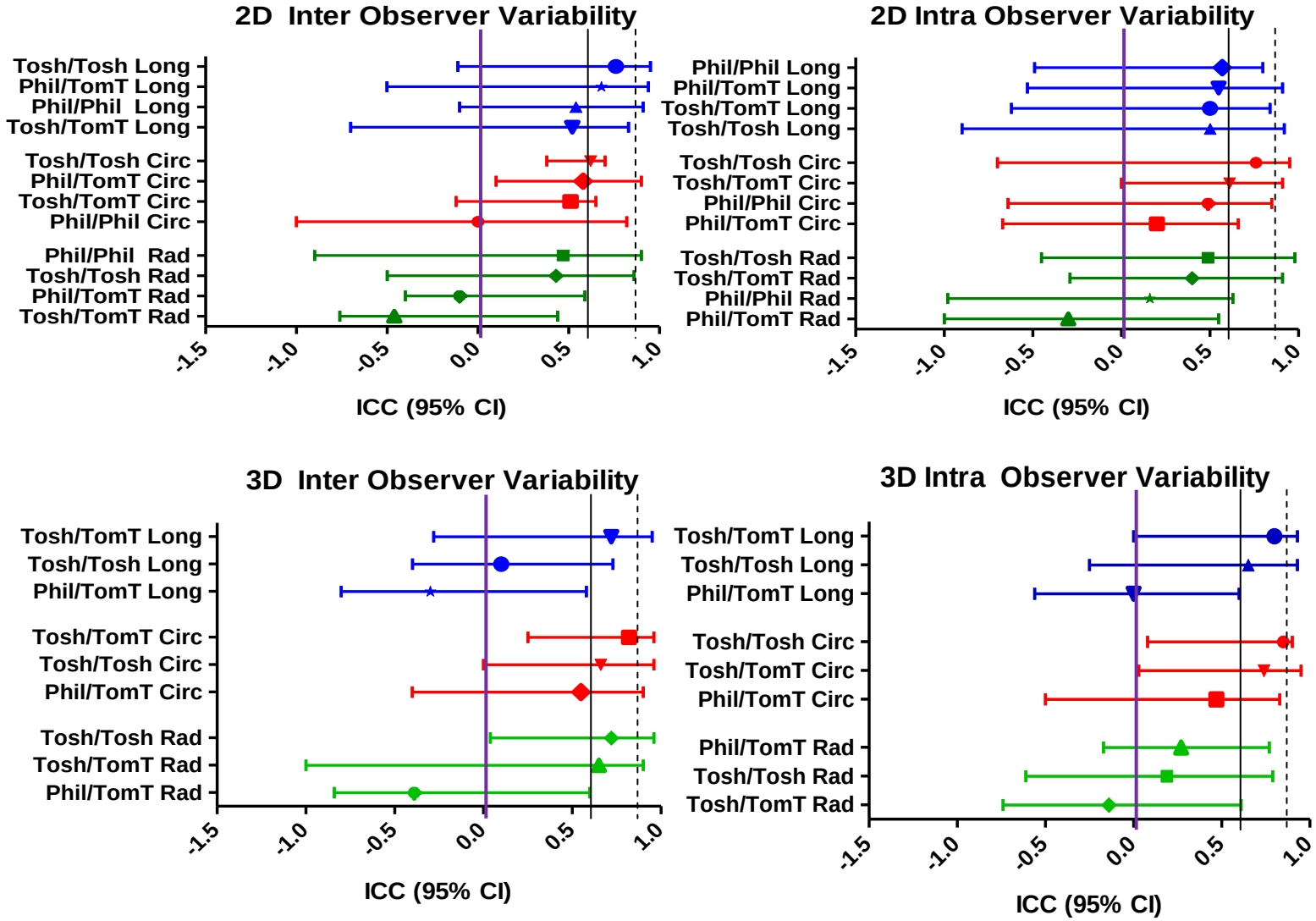

Figure 4.3: Intra class correlation coefficients for cardiovascular magnetic resonance inter and intra observer agreement. Levels for an ICC of 0 shown in purple line. Levels for moderate reliability (ICC 0.6) shown as solid black line; levels for good reliability (ICC >0.8) shown as dashed black line.

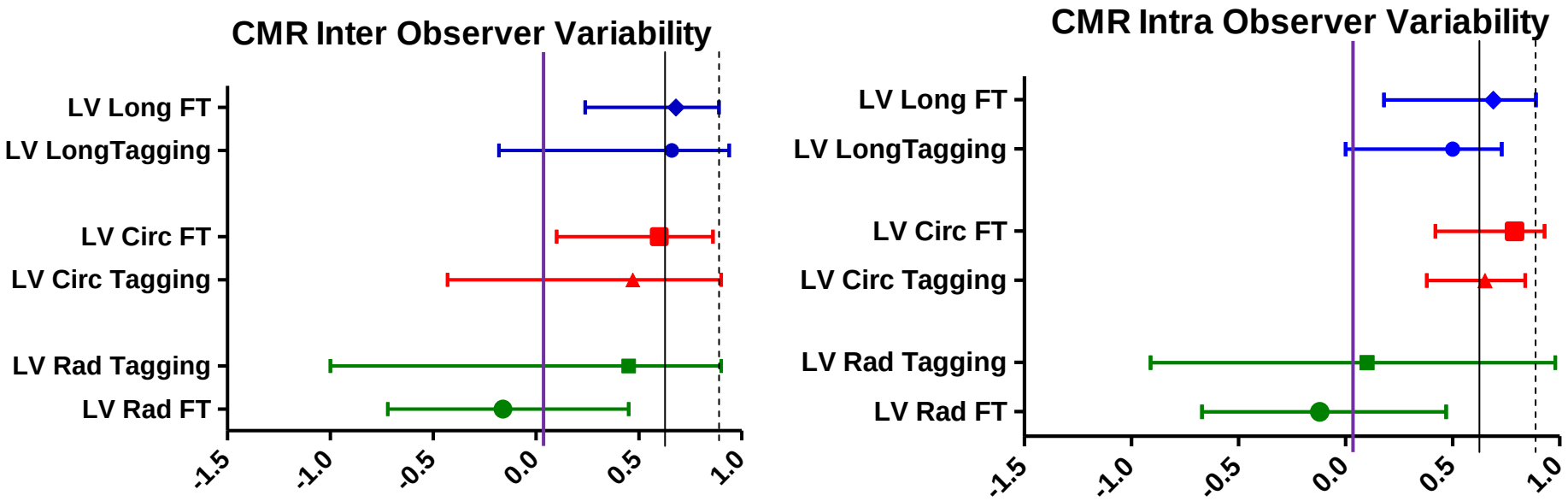

Cardiovascular Magnetic Resonance- Tagging and feature tracking-derived strain had similar inter and intra-observer correlations for left ventricular longitudinal strain (ICC for tagging=0.66 and for feature tracking=0.68) (Figure 4.3) with no consistent association for either technique for radial strain (inter-observer ICC for tagging=0.45 and for feature tracking=-0.16). Feature tracking tended to be more consistent than tagging for circumferential strain (feature tracking inter observer ICC=0.60 and tagging=0.47).

Echocardiography v Cardiovascular Magnetic Resonance – Mean ICCs were similar between echocardiography and CMR for LV strain parameters. For example the best interobserver left ventricular longitudinal strain ICC for 2D echocardiography was 0.76; for 3D echocardiography was 0.72; for CMR tagging was 0.66 and for CMR feature tracking was 0.68. However, ICC confidence intervals with CMR were in general much narrower than for either 2D or 3D echocardiography (left ventricular longitudinal strain inter-observer ICC confidence interval for CMR was 0.24 to 0.89; for 2D echo was -0.1 to 0.91 and for 3D was -0.4 to 0.73).

4.4.3 Inter- and intra-modality comparisons

2D and 3D echocardiography – For 2D echocardiography, longitudinal strain showed in general the lowest biases and narrowest limits of agreement with comparable results for circumferential but very wide bias and agreement for radial strain (Table 4.3 top section). For example in the comparison between Philips/Philips and Philips/TomTec the bias (LOA) for longitudinal strain was 0.8% (-3.7% to 5.2%) and for circumferential strain was -1.7% (-6.8% to 3.5%), whereas for radial strain was -3.2% (-17.5% to 11.1%). Of note, levels of strain were systematically 2-3% higher with vendor independent software compared to vendor-dependent analysis (Table 4.1).

For 3D echocardiography the poorest agreement irrespective of image acquisition method or analysis technique was also for radial strain (Toshiba/Toshiba vs. Toshiba/TomTec demonstrated bias/LOA of 13.4%/ -10.5% to 1 6.3%). Again, agreement for longitudinal and circumferential strain was better than that for radial strain (Table 4.3, middle section).

When 2D echocardiography was compared to 3D echocardiography (Table 4. 3, bottom section), longitudinal strain comparison showed the best agreement both in terms of smallest bias and narrowest limits of agreement and radial strain the worst. For example, 2D Philips/TomTec vs. 3D Philips/TomTec showed bias (LOA) of 0.1% (-3.8% to 7.0%) for longitudinal strain whilst radial showed bias (LOA) of 15.3% (-0.7 to 31.3%).

Table 4.3: Two and Three Dimensional Echocardiographic agreement

	Imaging / Analysis Combination	LV Circumferential Strain (%)		LV Radial Strain (%)		LV Longitudinal Strain (%)	
		Bias(CI)	LOA	Bias(CI)	LOA	Bias(CI)	LOA
2D Echo	Philips/Philips vs. Toshiba/Toshiba	-0.2 (-1.9 to 1.7)	-7.6 to 7.5	8.6 (1.6 to 15.7)	-21.6 to 38.9	2.1 (0.6 to 3.5)	-4.2 to 8.2
	Toshiba/Toshiba vs. Toshiba/TomTec	-1.6 (-3.3 to 0.2)	-8.9 to 5.8	-8.3 (-15.9 to -0.7)	-39.9 to 23.3	-2.9 (-4.2 to -1.6)	-8.4 to 2.6
	Philips/Philips vs. Philips/TomTec	-1.7 (-2.8 to -0.5)	-6.8 to 3.5	-3.2 (-6.6 to -0.2)	-17.5 to 11.1	0.8 (-0.1 to 1.8)	-3.7 to 5.2
	Philips/TomTec vs. Toshiba/TomTec	4.9 (3.1 to 6.6)	-2.4 to 12.2	5.1 (-1.5 to 11.7)	-24.3 to 34.5	3.8 (2.8 to 4.8)	-0.4 to 7.9
	Philips/Tomtec vs. Toshiba/Toshiba	-5 (-6.8 to 3.1)	-12.6 to 2.7	3.6 (-1.3 to -8.5)	-17.5 to 24.7	-1.6 (-2.7 to -0.6)	-6.3 to 2.9
3D Echo	Toshiba/Toshiba vs. Toshiba/TomTec	2.9 (0.8 to 5.0)	-6.0 to 11.9	13.4 (10.5 to 16.3)	0.9 to 25.8	-0.1 (-1.6 to 1.5)	-6.8 to 6.6
	Philips/Tomtec vs. Toshiba/Toshiba	-3.4 (-5.5 to -1.1)	-12.8 to 6.0	-12.5 (-16.1 to -8.9)	-27.6 to 2.6	0.7 (-0.8 to 2.2)	-5.6 to 6.9
	Philips/TomTec vs. Toshiba/TomTec	-0.44 (-2.6 to 1.7)	-9.8 to 8.9	0.8 (-2.5 to 4.2)	-12.8 to 14.4	0.7 (-0.8 to 2.2)	-5.7 to 7.1
2D Echo vs. 3D Echo	2D Toshiba/Toshiba vs. 3D Toshiba/Toshiba	-5.6 (-7.6 to -3.7)	-14.0 to 2.7	-2.3 (-8.6 to 4.0)	-29.7 to 25.0	-1.4 (-2.4 to -0.3)	-5.8 to 3.0
	2D Toshiba/TomTec vs. 3D Toshiba/TomTec	-1.1 (-3.3 to 0.9)	-10.5 to 8.2	19.3 (16.0 to 22.6)	4.9 to 33.7	1.4 (0.0 to 3.0)	-4.9 to 7.7
	2D Philips/TomTec vs. 3D Philips TomTec	2.5 (0.5 to 4.6)	-6.3 to 11.3	15.3(11.4 to 19.1)	-0.7 to 31.3	-0.1 (0.3 to 2.9)	-3.8 to 7.0

***Cardiovascular Magnetic Resonance*: *Tagging vs. Feature Tracking*–** As with echocardiographic comparisons, the bias (LOA) for longitudinal strain were the best 0.9% (-2.2% to 4.0%) with acceptable levels for circumferential strain 3.3% (-1.1% to 7.6%) and very wide bias and limits of agreement for radial strain -10.4% (-14.4% to -6.4%), Table 6.4 top row. Of note, longitudinal and circumferential strain values obtained by feature tracking were lower than those obtained by tagging by around 1% for longitudinal strain and 3% for circumferential (Table 4.1).

Cardiovascular magnetic resonance vs. echocardiography - Irrespective of 2D or 3D echocardiographic combination, both longitudinal and circumferential strain showed better agreement with CMR (by both tagging and feature tracking) than radial strain (Table 4.4 and Figure 4.4).

Table 4.4: Cardiac magnetic resonance strain measurements agreement with echocardiography

	Imaging / Analysis Combination	LV Circumferential Strain		LV Radial Strain		LV Longitudinal Strain	
		Bias (CI)	LOA	Bias(CI)	LOA	Bias(CI)	LOA
Tagging vs. FT	CMR Tagging vs. CMR FT	3.3 (2.2 to 4.3)	-1.1 to 7.6	-10.4 (-14.4 to -6.4)	-26.6 to 5.8	0.9 (0.2 to 1.7)	-2.2 to 4.0
2D Echo vs. CMR Tagging	Toshiba/Toshiba vs. CMR Tagging	-1.6 (-3.4 to 0.3)	-9.5 to 6.3	-10.5 (-16.5 to -4.4)	-35.7 to 14.8	-2.4 (-4.2 to 3.1)	2.1 to -4
	Philips/Philips vs. CMR Tagging	-1.7 (-2.9 to -0.4)	-6.9 to 3.6	-1.8 (-5.7 to 2.1)	-18.1 to 14.5	-0.3 (-1.6 to 0.9)	-5.5 to 4.7
	Toshiba/TomTec vs. CMR Tagging	0.01 (-1.0 to 1.0)	-4.4 to 4.4	-2 (-4.7 to 0.7)	-13.8 to 9.8	0.4 (-0.8 to 1.7)	-5.2 to 6.1
	Philips/TomTec vs. CMR Tagging	3.2 (1.5 to 4.9)	-4.1 to 10.6	-5.7 (-8.6 to -2.7)	-18.6 to 7.2	1.4 (-0.5 to 6.3)	-2.9 to 5.9
3D Echo vs. CMR Tagging	Toshiba/Toshiba vs. CMR Tagging	4.1 (2.5 to 5.9)	-3.1 to 11.3	-8.2 (-11.9 to -4.5)	-23.7 to 7.3	-1.0 (-2.5 to 0.5)	-7.0 to 5.1
	Toshiba/TomTec vs. CMR Tagging	1.2 (-1.1 to 3.5)	-8.5 to 10.9	-21.6 (-25.7 to -17.4)	-38.9 to -4.1	-0.9 (-1.9 to -0.0)	-5.0 to 3.1
	Philips/TomTec vs. CMR Tagging	0.7 (-0.9 to 2.4)	-6.1 to 7.6	-20.7 (-24.5 to -16.9)	-37.0 to -4.7	-0.3 (-1.5 to 1.1)	-5.7 to 5.2
2D Echo vs. CMR FT	Toshiba/Toshiba vs. CMR FT	1.3 (-0.9 to 3.5)	-8.2 to 10.8	-20.8 (-29.5 to 10.1)	-57.3 to 15.6	-1.4 (-2.9 to 0.1)	-8.0 to 5.2
	Philips/Philips vs. CMR FT	1.4 (0 to 2.8)	-4.6 to 7.4	-10.9 (-14.4 to 7.4)	-25.6 to 3.8	0.5 (-0.9 to 1.9)	-5.5 to 6.6
	Toshiba/TomTec vs. CMR FT	3.1 (1.7 to 4.5)	-2.8 to -9.0	-11.6 (-15.4 to 7.9)	-27.3 to 4.1	1.4 (-0.2 to 2.9)	-5.3 to 8.0
	Philips/TomTec vs. CMR FT	6.1 (4.2 to 7.9)	-2.2 to 14.3	-14.8 (-19.4 to 10.3)	-33.8 to 4.2	2.3 (1.1 to 3.5)	-2.9 to 7.6
3D Echo vs. CMR FT	Toshiba/Toshiba vs. CMR FT	6.9 (4.5 to 9.4)	-3.6 to 17.6	-18.6 (-23.8 to 13.3)	-39.3 to 2.2	-0.3 (-1.9 to 1.4)	-6.9 to 6.4
	Toshiba/TomTec vs. CMR FT	4.5 (2.2 to 6.8)	-4.7 to 13.8	-32.2 (-36.4 to -27.9)	-48.7 to -15.5	0.1 (-1.0 to 1.2)	-4.3 to 4.4
	Philips/TomTec vs. CMR FT	3.8 (2.2 to 5.5)	-2.9 to 10.5	-30.8 (-35.5 to 26.3)	-49.0 to -2.6	0.8 (-0.9 to 2.5)	-6.1 to 7.7

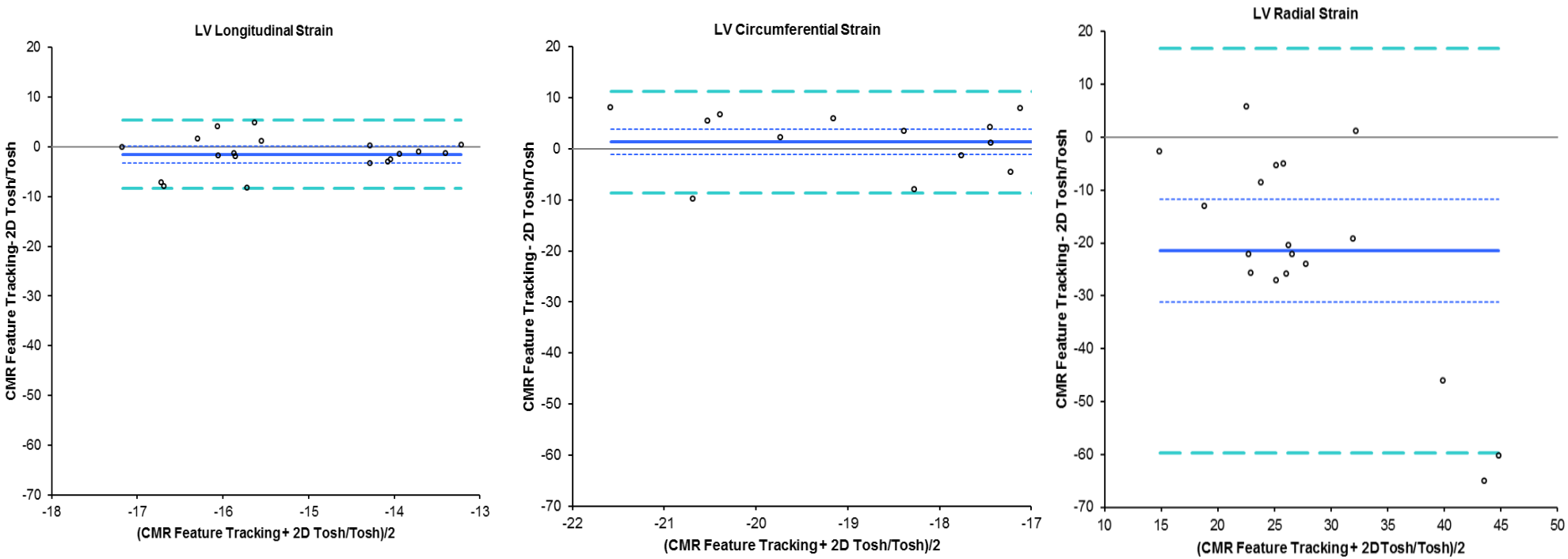

Figure 4.4: Bland Altman Graphs showing agreement between CMR feature tracking and 2D echocardiography for the measured strain parameters demonstrating bias (solid dark blue line); 95% CI for bias (dotted dark blue line) and 95% limits of agreement (dashed light blue line). Top: LV strain – longitudinal, circumferential and radial strain.

4.5 Discussion

This study demonstrates that, of the different strain parameters, left ventricular longitudinal and circumferential strain tend to have the smallest bias, narrowest limits of agreement and lowest observer variability irrespective of modality, whereas, radial strain is inconsistently measured. Of interest, the newer techniques of 3D echocardiography and feature tracking provided comparable results to established 2D echocardiography and CMR tagging, while tending to have narrower observer variability confidence intervals and shorter analysis time. Some systematic differences in reported levels of strain between approaches were found, particularly with regard to the use of vendor-dependent or independent software in echocardiography and between tagging and feature tracking CMR analysis.

Although longitudinal and circumferential left ventricular strain tended to show better agreement than radial strain irrespective of modality, the observer variability for these parameters remained modest, and for some specific imaging and analysis combinations was poor, consistent with previous findings [45, 110]. Technical differences in image acquisition or analysis approach, such as variation in image quality over the cardiac cycle or strain computation method, may affect repeated assessment of images by different observers [45]. Some of the variation between different modalities or analysis approaches could also relate to these technical differences. For example feature tracking follows voxels of the cine image whereas tagging follows a tagging overlay, which fades during the cardiac cycle. Differences in temporal resolution between 2D and 3D echocardiography as well as tagged and SSFP cine images will also influence strain measures. Furthermore, although optimal image planes were acquired, it is impossible to match them exactly between different scans. With 3D echocardiography this is less important as speckles are tracking in multiple

directions but for 2D echocardiography and cardiovascular magnetic resonance through plane movement of speckles or features makes them difficult to track. Our findings are consistent with the concept that pooled data acquired by different scanners or analysed with different software will be inherently variable, which may explain variation in previously postulated normal speckle tracking ranges [32, 96, 111-112]. This is exemplified by the differences in strain ranges related to analysis approach that we report in a healthy group of males. In multi-centre studies a standardisation in analysis techniques remains important and even greater standardisation will be required for clinical application within individual patients [97].

In summary, our results show that, levels of left ventricular longitudinal and circumferential strain are the most consistently measured strain parameters between modalities. This is likely to be explained in part by the fact that, although there was some within modality variation, these were the most reproducible measures in inter- and intra-observer comparisons. There were some systematic biases in normal ranges with certain imaging and analysis combinations, so for pooled or serial scans it is important the same scanner settings and consistent analysis software are used. Interestingly, the newer technologies of 3D speckle tracking echocardiography and cardiovascular magnetic resonance feature tracking appear to have introduced powerful additional tools for research studies. Both techniques were able to produce comparable results to established 2D echocardiography and tagging technologies with advantages of speed of application and analysis.

Chapter 5: Right Ventricular Myocardial Deformation Measures By Magnetic Resonance Feature Tracking: Comparison with Echocardiography

5.1 Introduction

Right ventricular function is an important determinant of outcome in different cardiovascular and pulmonary diseases. It is generally accepted that the assessment of RV systolic function can be challenging given the complex anatomy of the RV and currently echocardiography and CMR are the two imaging modalities most commonly used to visualize the RV allowing an assessment of function. As described earlier, myocardial strain has been shown to allow evaluation of LV systolic function and more recently has also been proposed as a sensitive marker of right ventricular systolic function in studies using both echocardiography [48-49, 52, 113-114] and using cardiac magnetic resonance [115-116].

The complex geometry of the RV in addition to the thinness of the RV free wall has meant that the measurement of myocardial RV strain has been limited to the longitudinal plane and to 2 dimensional imaging for both echocardiography and CMR.

We have shown earlier in Chapter 4 that variation in LV systolic strain assessment exists dependent on whether vendor dependent or independent software is used for echocardiography strain analysis.

The aims of this chapter were:

1. To compare the assessment of RV free wall longitudinal strain using echocardiography and CMR.
2. To identify whether RV longitudinal strain is reproducible irrespective of technique used.

3. To demonstrate consistency of RV longitudinal strain both within and between modalities.

5.2 Methods

The CMR and 2D echocardiography acquisitions described in chapter 2 were used to derive RV free wall longitudinal strain. As in chapter 4, all CMR and echocardiography images were obtained within a one month period and again 2D echocardiography was performed using both a Philips iE33 (Zoetermeer, The Netherlands) and a Toshiba Artida 4D system. These acquisitions allowed RV free wall longitudinal systolic strain to be derived using tagging and feature tracking cine analysis as described in Chapters 2.3.5 and 2.3.6. Again, the 2D echocardiograms were analysed to provide RV free wall longitudinal systolic strain measures using both vendor dependent software (QLAB 8.1 for images acquired using the Philips iE33 system and Toshiba WMT for images acquired using the Toshiba system) as well as vendor independent software (TomTec).

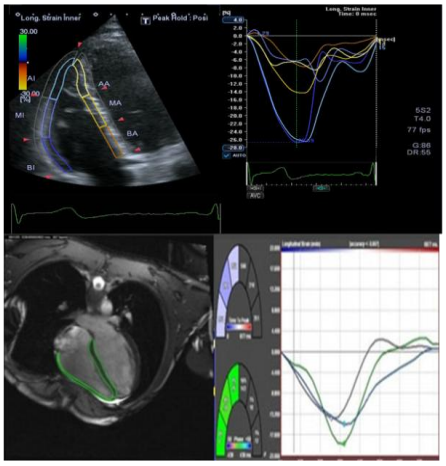

Figure 5.1: RV strain analysis by echocardiography and CMR feature tracking.

Top row echocardiography: RV 4 chamber view with tagging overlay applied and systolic strain analysis; bottom row CMR: HLA view allowing contouring of the RV using feature tracking and subsequent systolic strain analysis of the RV free wall (bottom right).

5.3 Statistical analysis

The statistical methods used were the same as described in section 4.3.

5.4 Results

5.4.1 Technical aspects of image acquisition and analysis

Mean and standard deviation for levels of RV free wall strain measured by different techniques in a healthy group of young males (n=20) are reported in Table 5.1. No significant differences were seen in heart rates during acquisition of echocardiography and CMR images (Chapter 4, Table 4.1). As expected, temporal resolution of 2D echocardiography (16.5±1.2ms for Philips; 15.5±1.3ms for Toshiba) was significantly better than for CMR (37.8±4.2ms); $p < 0.05$ for difference between 2D echocardiography and CMR.

Table 5.1: Mean and standard deviation of strain values according to imaging modality and analysis approach.

Imaging/Analysis Combination	RV Long Strain
2DE Toshiba/Toshiba	-19.9±2.6
2DE Philips/Philips	-21.1±2.6
2DE Toshiba/TomTec	-22.0 ±3.3
2DE Philips/TomTec	-23.1±3.5
CMR Tagging	-17.5±3.1
CMR Feature Tracking	-19.8±2.4
Data are presented as mean ± SD	

5.4.2 Inter- and intra-observer variability

2D Echocardiography **-** The mean inter- and intra-observer ICC range for right ventricular longitudinal strain were 0.18-0.76 and 0.34-0.70 respectively and the inter observer variability seen was generally poorer when compared with the observer variability seen for the measurement of LV longitudinal strain in Chapter 4.

Cardiovascular Magnetic Resonance- For right ventricular strain analysis, the mean inter and intra observer variability ICC was comparable with left ventricular longitudinal measures and comparable for both CMR approaches (inter observer ICC for RV tagging=0.58; LV tagging=0.66; RV feature tracking=0.64; LV feature tracking=0.68). However, the confidence intervals were broader for tagging than feature tracking (tagging=-0.25 to 0.92; feature tracking=0.2 to 0.74), Figure 7.2.

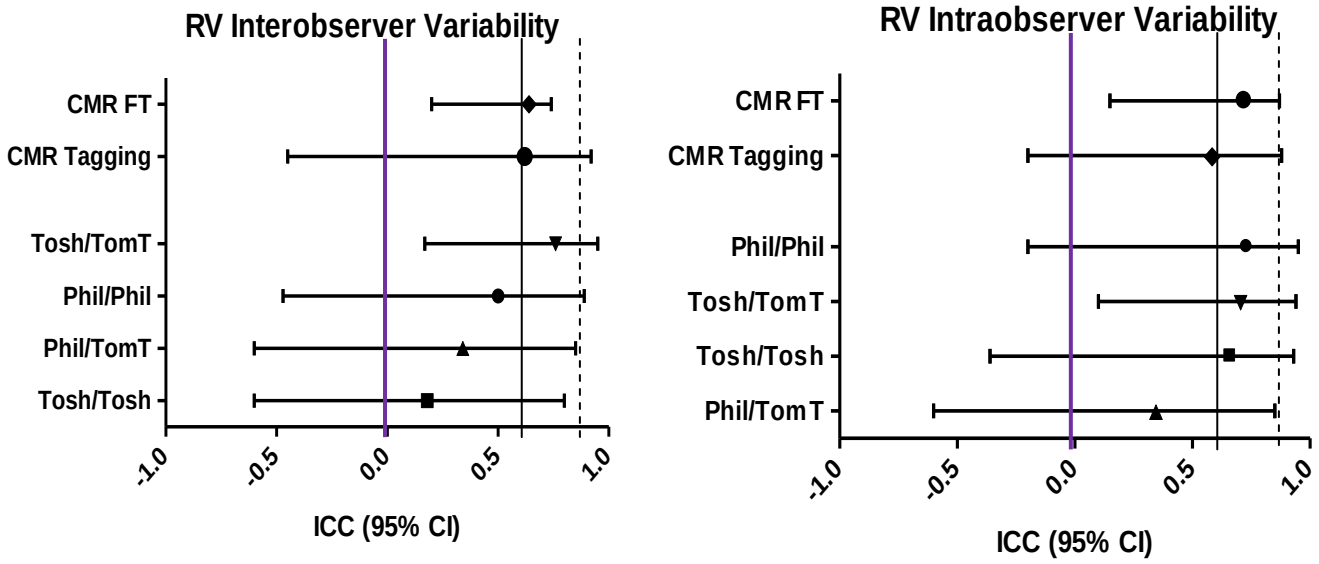

Figure 5.2: Intra class correlation coefficients for RV longitudinal strain assessment. Levels for an ICC of 0 shown in purple line. Levels for moderate reliability (ICC 0.6) shown as solid black line; levels for good reliability (ICC >0.8) shown as dashed black line.

5.4.3 Inter- and intra-modality comparisons

2D echocardiography –The biases seen for the various echocardiographic and analysis software combinations were similar to those demonstrated for 2D longitudinal left ventricular strain although the LOA were wider (Table 5.2). For example the comparison between Philips/Philips and Philips/TomTec showed bias (LOA) for LV longitudinal strain of 0.8% (-3.7% to 5.2%) and for RV 1.0% (-6.9% to 8.9%).

Table 5.2: Two dimensional echocardiographic agreement

	Imaging / Analysis Combination	RV Longitudinal Strain	
		Bias (CI)	LOA
2D Echo	Philips/Philips vs. Toshiba/Toshiba	1.1 (-0.3 to 2.6)	-4.9 to 7.2
	Toshiba/Toshiba vs. Toshiba/TomTec	-2.0 (-4.0 to -0.1)	-10.5 to 6.4
	Philips/Philips vs. Philips/TomTec	1.0 (-0.8 to 2.9)	-6.9 to 8.9
	Philips/TomTec vs. Toshiba/TomTec	3 (0.9 to 5.2)	-6.2 to 12.2
	Philips/Tomtec vs. Toshiba/Toshiba	-1.9 (-1.9 to -3.7)	-9.5 to 5.7

***Cardiovascular Magnetic Resonance*: *Tagging vs. Feature Tracking*–**For right ventricular longitudinal strain the bias was acceptable but the limits of agreement wider -2.3% (-8.3% to 3.8%) than for left ventricular measures 0.9% (-2.2% to 4.0%).

Cardiovascular magnetic resonance vs. echocardiography - Right ventricular longitudinal strain measured by tagging, but not for feature tracking, was consistently up to 5% lower than when measured by 2D echocardiography (Table 5.1). Assessment of RV strain by tagging also had wider limits of agreement with echocardiography than the comparison of echocardiography with feature tracking. For example the bias (LOA) when comparing Toshiba/Toshiba echo analysis with CMR tagging were 4.5% (-3.0% to 12.0%) and this narrowed with feature tracking to 1.7% (-4.9% to 8.4%), Table 5.3.

Table 5.3: Cardiac magnetic resonance strain measurements agreement with echocardiography

	Imaging / Analysis Combination	RV Longitudinal Strain	
		Bias(CI)	LOA
Tagging vs. FT	CMR Tagging vs. CMR FT	-2.3 (-3.8 to -0.8)	-8.3 to 3.8
2D Echo vs. CMR Tagging	Toshiba/Toshiba vs. CMR Tagging	2.4 (0.7 to 4.2)	-4.6 to 9.5
	Philips/Philips vs. CMR Tagging	3.6 (2.2 to 5.1)	-2.2 to 9.4
	Toshiba/TomTec vs. CMR Tagging	4.5 (2.7 to 6.4)	-3.0 to 12
	Philips/TomTec vs. CMR Tagging	5.6 (3.7 to 7.5)	-1.9 to 13.2
2D Echo vs. CMR FT	Toshiba/Toshiba vs. CMR FT	0.1 (-1.7 to 1.5)	-6.6 to 6.4
	Philips/Philips vs. CMR FT	1.5 (-0.2 to 3.1)	-5.2 to 8.2
	Toshiba/TomTec vs. CMR FT	1.7 (0.1 to 3.3)	-4.9 to 8.4
	Philips/TomTec vs. CMR FT	3.3 (1.1 to 5.5)	-5.7 to 12.3

5.5 Discussion

Right ventricular strain assessment by cardiovascular magnetic resonance has previously relied on tagging sequences of the RV [57]. As the RV is thin walled the size of these tags and ability to track them has been limited. The recent introduction of 'feature tracking' allows myocardial deformation parameters to be assessed directly from steady state free precession cine CMR images. We demonstrate generally narrower confidence intervals for feature tracking observer variability compared to tagging. There was also an acceptable bias for right ventricular assessment compared to 2D echocardiography, which has previously been shown to correlate significantly with right ventricular ejection fraction estimated by cardiovascular magnetic resonance [14, 117]. Further improvements in right ventricular strain measurement approaches for both echocardiography and CMR should be possible. There is no dedicated right ventricular overlay and the left ventricular overlay is currently adapted to best fit the right ventricle. The right ventricle also has a heavily trabeculated apex and a variable mechanical contribution from the septum. Therefore, better strain algorithms to account for these variations may be possible.

Chapter 6: Assessment Of Diastolic Function By Magnetic Resonance Feature Tracking: Comparison With Echocardiography

6.1 Introduction

The diagnosis of 'diastolic heart failure' or 'heart failure with a preserved ejection fraction' accounts for around 50% of patients assessed with a new diagnosis of heart failure [20]. Given that diastolic dysfunction is an independent predictor of mortality [21, 118-119], the assessment of diastolic function has become an integral part of the standard echocardiographic examination. Echocardiography is widely regarded as the gold standard technique for the non invasive assessment of diastolic function having been shown to correlate significantly with invasive parameters of left ventricular diastolic function [23, 120-121].

LV diastolic function assessment is not routinely evaluated by CMR in clinical practice particularly as some of the measures used (e.g. phase contrast techniques for the quantification of intra cardiac blood flow) can be time consuming both in terms of acquisition and post processing [122]. In addition, the assessment of diastolic function by 'tagging' techniques can be difficult as the tagging overlay fades throughout the cardiac cycle.

Feature tracking has been used to quantify left ventricular systolic strain in a number of studies [68, 76, 94, 123]. The aims of this chapter were:

1. To assess which parameters by CMR feature tracking have the best sensitivity and specificity to identify diastolic dysfunction.

2. To assess the observer variability of the different diastolic parameters obtained by feature tracking.

3. To identify normal diastolic feature tracking parameters according to age.

6.2 Methods

Volunteers were recruited as described in chapter 2. These comprised control subjects (n=166) with no history of cardiovascular disease and 30 participants with moderate-severe aortic stenosis, normal left ventricular ejection fraction and known echocardiographic diastolic dysfunction. All participants underwent the same standardised CMR scan (Chapter 2.3.1). All subjects underwent anthropometric measurements (height and weight) and blood pressure measurement recording at the time of CMR. The CMR images were analysed to identify LV mass, volumes and ejection fraction as described in chapter 2.3.3. Feature tracking analysis (as described in chapter 2.3.5) was used to identify diastolic deformation parameters. Using the short-axis stack basal, mid and apical levels, circumferential and radial strain parameters as well as torsion were derived. From the HLA view, longitudinal LV diastolic strain parameters were determined. In 10 subjects feature tracking analysis was repeated after an interval of 4 weeks by both the initial observer and a second experienced observer to assess inter and intra-observer agreement for measures.

60 subjects underwent echocardiography (30 participants with diastolic dysfunction and 30 age matched normal controls) to allow assessment and grading of diastolic function (see chapter 2.4.3).

6.2.1 Study design

The study was designed to identify which diastolic cine CMR parameters as identified by feature tracking best detect diastolic dysfunction, their observer variability and normal ranges:

- *Part 1: Identification of feature tracking parameters.* 60 of the group participants (30 normal diastolic function and 30 diastolic dysfunction) were identified. The diastolic dysfunction was graded according to severity using recent guidelines [23]: Grade I (n=13); Grade II (n=14); Grade III (n=12). The specificity and sensitivity of the feature tracking parameters to identify diastolic dysfunction was calculated.
- *Part 2: Observer reproducibility.* Inter and intra observer reproducibility was estimated for the feature tracking parameters which had been identified as having the best sensitivity and specificity for detecting diastolic dysfunction. The different observer reading was carried out one month after the initial analysis.
- *Part 3: Identification of feature tracking normal values.* From the group data, comparisons between feature tracking parameters from those with diastolic dysfunction and normal diastolic function were made and normal ranges were identified.

6.3 Statistical analysis

Summary variables for subject characteristics and ranges of results are presented as mean ± SD for continuous variables. Variables were assessed for a normal distribution using the Kolomogrov Smirnov test. Receiver-operating characteristics curves (ROC) were analysed and the area under the curve was calculated to estimate the ability of the feature tracking parameters to detect diastolic dysfunction and the respective sensitivity and specificity of these feature tracking parameters. Pearson's correlation coefficient was used for normally distributed data and Spearman for non-normally distributed data to compare feature tracking parameters with echocardiography. Variables with normal distribution were

compared using the paired Student t test and variables with non normal distribution were compared using the Wilcoxon test. Observer agreement for feature tracking (10 subjects) was assessed using Bland Altman [95] analysis and by the intra class correlation coefficient (ICC) [108], as described in section 4.3. An ICC value of 1 indicates perfect agreement and, for example, an ICC of 0.95 indicates the balance of the variance (1 – ICC = 5%) is attributable to error; in this study due to instrumentation or operator [109].

6.4 Results

6.4.1 Clinical characteristics and baseline CMR / echocardiography assessment

Table 6.1 shows the clinical characteristics and the baseline CMR (volumetric, mass and ejection fraction) and echocardiographic assessment of diastolic function. LV mass was significantly greater in the group with diastolic dysfunction when compared to the age matched controls (164.9g±39.8g vs. 101.7g±32.2g, $p<0.0005$). No significant differences were seen between the age matched control group and the diastolic dysfunction group for blood pressure, end diastolic volume, end systolic volume or ejection fraction. The echocardiographic parameters for the group with diastolic dysfunction was significantly greater than age matched controls for deceleration time and both septum and lateral E/e' values ($p<0.0005$ for all).

Table 6.1: Baseline characteristics, CMR results and echocardiographic analysis of controls, diastolic dysfunction &age matched controls.

		Normal Diastolic Function	Diastolic Dysfunction	Age matched controls	P Value
Total		166	30	30	
Male		46	23	11	
Female		96	7	19	
Age (years)	20-39	111	2	2	
	40-59	38	7	10	
	≥ 60	17	21	18	
Mean age (years)		35±9	61±14	56±11	
SBP (mmHg)		119±14	128±16	132±16	
DBP (mmHg)		71±9	76±6	79±9	
EF CMR (%)		64.73±8.32	70.3±8.4	69.6±9.6	
EDV CMR (mL)		141±32	148±34	148.0±31.1	
ESV CMR (mL)		46±13	47±25	36.28±13.1	
LVM CMR (g)		99.2 ± 29.0	164.9±39.8	101.7±32.2	<0.001
E (cm/s)			50.8±17.5	63.9±12.7	0.001
A (cm/s)			79.0±25.0	53.0±14.9	<0.001
DT (ms)			230.0±64.0	190.3±44.8	<0.001
E/A			1.08±0.36	1.17±0.23	0.26
TDI lateral e' (cm/s)			9.39±2.9	13.2±3.7	<0.001
TDI septal e' (cm/s)			5.96±1.09	9.05±2.49	<0.001
E/e' septum			13.68±3.85	7.48±1.68	<0.001
E/e' lateral wall			9.05±3.09	5.23±1.54	<0.001
LA volume (ml/m^2)			41.5±16.0	32.2±7.53	0.03

Table 6.2: Cut off values, sensitivity, specificity and area under the curve approximations for the ability of feature tracking parameters to predict diastolic parameters.

Diastolic FT Parameter	Cut Off Value For Detecting Diastolic Dysfunction	AUC	Sensitivity	Specificity	P Value For AUC
Global radial early:late velocity	2.70	0.77	67	81	<0.001
Basal radial early:late velocity	2.29	0.84	72	90	<0.001
Mid radial early:late velocity	3.11	0.74	75	66	<0.001
Apical radial early:late velocity	2.75	0.75	68	80	<0.001
Basal radial strain Rate	-1.11	0.68	68	70	0.001
Basal longitudinal strain rate (s^{-1})	0.9	0.62	59	70	0.04
Apical longitudinal strain rate (s^{-1})	1.12	0.71	77	57	<0.001
Basal circumferential strain rate (s^{-1})	1.76	0.65	79	52	0.01
Mid circumferential strain rate (s^{-1})	1.04	0.61	84	40	0.05
Apical circumferential strain rate (s^{-1})	1.52	0.64	59	65	0.01

6.4.2 Receiver operator characteristics of feature tracking parameters to predict diastolic dysfunction

The area under the ROC curve was statistically significant in 10 of the measured diastolic feature tracking parameters.

The cut off values together with the respective sensitivity, specificity, AUC and ROC curves of these parameters are shown in Table 6.2 and Figure 6.1. The sensitivity/ specificity for detecting diastolic dysfunction for individual radial parameters was 67-75%/ 66-90%; for longitudinal markers was 59-77% /57-70% and for circumferential markers was 77-84%/ 40-57% . Using a combination of parameters of basal, mid, apical and global radial early: late velocities improved the sensitivity/specificity further to 76%/87%. This was further improved when these radial parameters were used in combination with the longitudinal parameters (basal and apical strain rate), see Table 6.3.

Parameter	AUC	Sensitivity	Specificity	P Value For AUC
Mid Radial Early :Late velocity	0.74	75	66	<0.001
Apical Radial Early :Late velocity	0.75	68	80	<0.001
Global Radial Early :Late velocity	0.77	67	81	<0.001
Basal Radial Early :Late velocity	0.84	72	90	<0.001
Combined Radial Early :Late velocity	0.89	76	87	<0.001
Combined Radial and Longitudinal Parameters	0.89	76	90	0.02

Table 6.3: Area under the curve, sensitivity and specificity for individual and combined radial parameters.

When using a combination of basal and apical longitudinal diastolic strain rate the sensitivity/specificity for detecting diastolic dysfunction was 56%/82%. The sensitivity/ specificity when combining basal, mid and apical circumferential diastolic strain rate was 40%/ 85%.

Of the 10 feature tracking parameters identified above, the ROC characteristics were studied to see whether these parameters were able to distinguish between grades of severity of diastolic dysfunction. Of the 10 parameters seen which were able to predict diastolic dysfunction, none were able to produce cut off values or significant AUC from ROC curves to differentiate between grades of diastolic dysfunction.

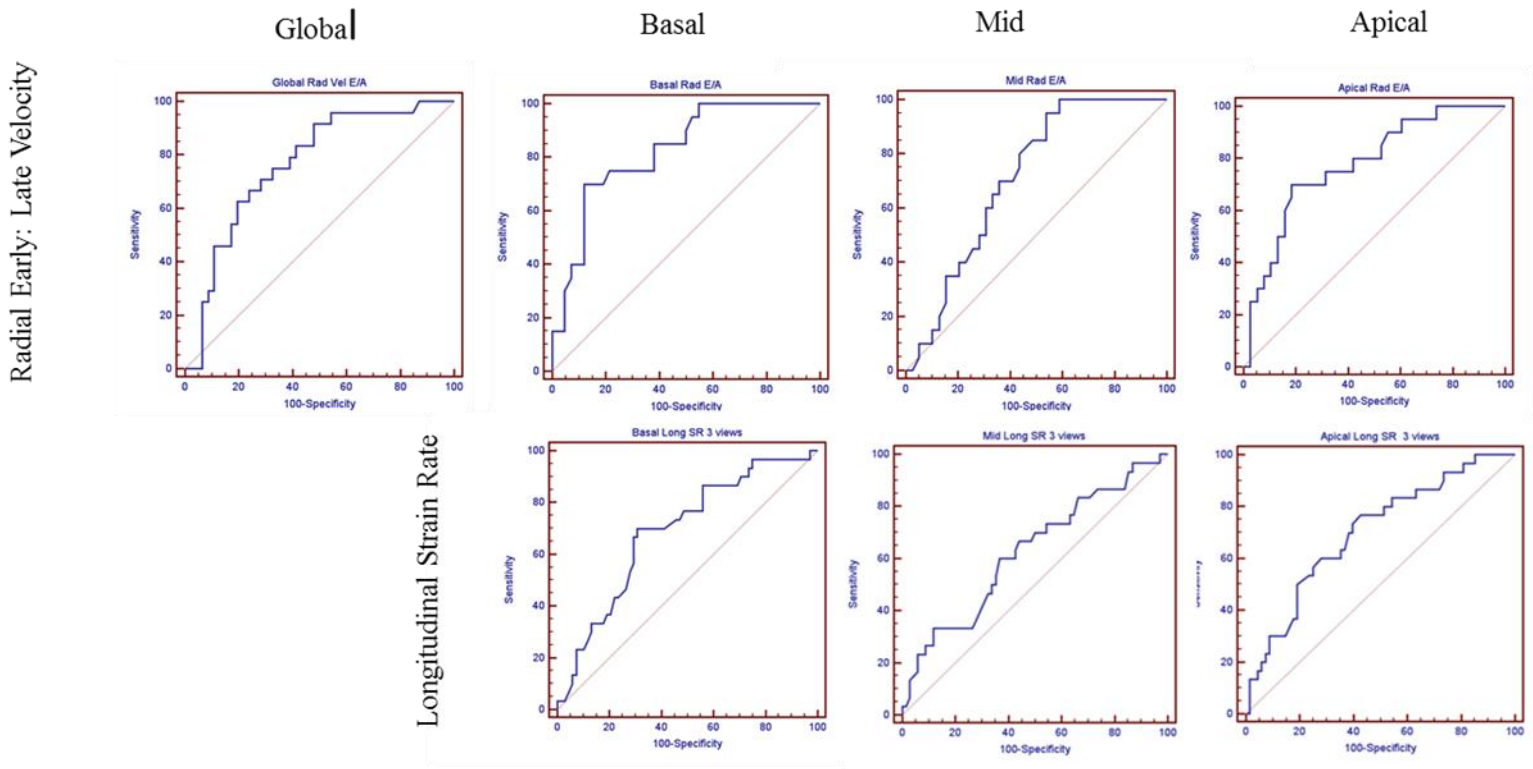

Figure 6.1: Receiver operator characteristic curves for the ability of diastolic feature tracking parameters to detect diastolic dysfunction. Top row: Radial early: late velocity; Bottom row: longitudinal strain rate

6.4.3 Feature tracking variables observer variability

The Bland Altman analysis and ICCs for inter and intra observer reproducibility are shown in Table 6.4. Levels of agreement were better for global radial early: late diastolic velocity (interobserver ICC 0.90; bias 0.07 and LOA -1.2 to 1.4) than for regional radial early: late diastolic velocity (e.g. basal radial early: late diastolic velocity interobserver ICC 0.81; bias 0.17 and LOA -2.9 to 2.6). Observer reproducibility for longitudinal strain parameters showed poorer intraclass correlations for basal (0.19) and mid regional levels than for apical diastolic longitudinal strain rate (0.61).

Table 6.4: Inter and intra observer reproducibility for diastolic feature tracking parameter

CMR diastolic parameter	Inter observer agreement				Intra observer agreement			
	Bias	LOA	ICC	95% CI for ICC	Bias	LOA	ICC	95% CI for ICC
Global radial early:late velocity	0.07	-1.6 to 1.8	0.90	0.63 to 0.97	-0.18	-1.45 to 1.08	0.88	0.57 to 0.97
Basal radial early:late velocity	-1.07	-2.93 to 2.58	0.81	0.23 to 0.95	-0.03	-3.1 to 3.04	0.77	0 to 0.94
Mid radial early:late velocity	0.14	-2.7 to 3	0.23	-2.9 to 0.82	-0.76	-3.45 to 1.96	0.70	0 to 0.92
Apical radial early:late velocity	0.24	-1.36 to 1.85	0.91	0.67 to 0.97	0.22	-2.72 to 2.72	0.76	0 to 0.93
Basal longitudinal strain rate (S^{-1})	0.02	-1.46 to 1.50	-0.02	-5.2 to 0.76	0.06	-1.2 to 1.3	0.50	-1.3 to 0.88
Mid longitudinal strain rate (S^{-1})	-0.02	-1.00 to 0.97	0.19	-3.4 to 0.81	0.13	-0.9 to 1.2	0	-3.5 to 0.75
Apical longitudinal strain rate (S^{-1})	-0.13	-1.06 to 0.79	0.61	-0.5 to 0.90	0.16	-0.4 to 0.76	0.85	0.44 to 0.96

6.4.4 Feature tracking parameters correlation with echo markers of diastolic dysfunction.

The correlation between the feature tracking parameters identified in Table 6.2 and echocardiographic indices of diastolic function (E/A; DT; E/e'; Mean E; LA volume) are shown in Table 6.5. As it can be seen Radial E:A velocities had modest but significant correlation with echocardiographic E/A ratio (r = 0.43); E/e' (r = 0.44); Mean e' (r=0.55) and LA volume (r = 0.33). No feature tracking parameters correlated with echocardiographic mitral valve inflow deceleration time.

Table 6.5: Diastolic feature tracking parameters with significant correlations with echocardiographic indices of diastolic function.

Parameter	E/A		
	R	P	95% CI for R
Global Rad E:A	0.26	0.04	0.02-0.5
Basal Rad E:A	0.38	0.004	0.12 to 0.59
Apical Rad E:A	0.43	0.001	0.17 to 0.64
	E/E'		
	R	P	95% CI for R
Global Rad E:A	-0.25	0.05	-0.48 to -0.003
Basal Rad E:A	-0.44	0.001	-0.64 to -0.19
Apical Rad E:A	-0.3	0.03	-0.54 to -0.02
Apical Long SR	0.25	0.04	0.01 to 0.46
	Mean e'		
	R	P	95% CI for R
Global Rad E:A	0.55	0.0001	0.45 to 0.78
Basal Rad E:A	0.51	0.0001	0.27 to 0.69
Mid Rad E:A	0.41	0.00002	0.16 to 0.62
Apical Rad E:A	0.44	0.00017	0.17 to 0.64
Basal Long SR	0.25	0.04	0.01 to 0.46
	LA Volume		
	R	P	95% CI for R
Basal Rad E:A	-0.33	0.03	-0.57 to -0.03

6.4.5 Variation of feature tracking parameters with age

The variation of the diastolic feature tracking parameters with age is shown in Table 6.7 Global and regional radial early: late velocities declined with increasing age.

	20-39yrs	40-59yrs	60+yrs
Global radial early:late velocity	4.28±1.77	3.06±1.78	1.82±1.69
Basal radial early:late velocity	4.37±1.45	3.77±1.41	2.98±1.09
Mid radial early:late velocity	4.29±1.42	3.95±2.24	2.87±1.44
Apical radial early:late velocity	4.05±2.38	2.84±1.89	1.69±1.92
Basal longitudinal strain rate (S^{-1})	1.15±0.51	1.11±0.42	1.03±0.38
Mid longitudinal strain rate (S^{-1})	1.05±0.43	1.16±0.37	1.01±0.37
Apical longitudinal strain rate (S^{-1})	1.03±0.35	1.07±0.40	1.07±0.48
Data presented as mean± standard deviation.			

Table 6.7: Normal mean diastolic feature tracking parameters by age group.

6.5 Discussion

This study has shown the ability of radial diastolic velocities and longitudinal strain rates to predict diastolic dysfunction with acceptable levels of sensitivity and specificity.

The ROC analysis has shown that the AUC/ sensitivity / specificity for the combined radial parameters (0.90/77%/88%) and the combination of all 6 radial and longitudinal values (0.94/76%/91%) are similar to previous studies which have assessed the ability of

echocardiographic E/e' to predict either LV filling pressure by cardiac catheterisation (0.82/70%/93%)[124] or pulmonary capillary wedge pressure (0.66/66%/50%)[125].

In this study, the combination of several feature tracking parameters predicted diastolic dysfunction with greater accuracy than when individual parameters were used. This concept of using several parameters rather than any single parameter has been shown to be beneficial also for the ability of echocardiographic indices to predict diastolic dysfunction [124].

We have also shown modest correlations between certain feature tracking parameters and echocardiographic E/e' (r=0.4), transmitral E/A ratio (r=0.4, mean e' (r = 0.5). Moderate correlations have previously been reported in studies assessing the relationship between invasive measures of diastolic function and echocardiographic E/e' (r = 0.4-0.64)[126]. In addition, we have seen found that with increasing age radial early:late velocities decline similarly to echocardiographic indices of diastolic dysfunction, table 5 [127].

The interobserver agreement in this study for feature tracking parameters was moderate, with better agreement seen for radial values than longitudinal values. Whilst no values for observer agreement for diastolic function have been reported previously using feature tracking, the poor interobserver variability of certain systolic deformation parameters has been highlighted both for feature tracking [128] and for speckle tracking echocardiography [45, 110].

In summary, our results have shown that radial diastolic early: late velocities and longitudinal diastolic strain rates are able to identify diastolic dysfunction. Despite the lower temporal resolution seen with CMR compared to tissue Doppler echocardiography, we have

seen here that sensitivity and specificity levels for the identification of diastolic dysfunction are comparable to echocardiographic tissue Doppler E/e' and demonstrates the potential for feature tracking to be used for research applications. Further assessment of diastolic function using feature tracking would be of benefit to assess its application in health and disease states although improvements in observer variability and further validation studies using a combination of multimodality imaging and invasive measures of diastolic function will be of benefit.

Chapter 7: Quantification Of Left And Right Ventricular Mass, Volumes And Ejection Fraction By Magnetic Resonance Feature Tracking: Comparison With Traditional Disc Summation Methods

7.1 Introduction

Methods to evaluate LV mass, left and right volumes and ejection fraction accurately in a reproducible manner are important as clinical and research tools. CMR has demonstrated excellent accuracy and reproducibility for the estimation of ventricular volumes and LV mass [84-85] based on the contoured disc summation method, which is widely accepted as the gold standard technique. Recently, software has been developed that can track features, such as the cavity boundary or tissue patterns, of steady state free precession (SSFP) CMR cine images [68, 76, 94], relative to a manually-identified endocardial contour. This 'feature tracking' software has introduced the possibility to evaluate myocardial systolic deformation parameters directly from cine images, in a way analogous to techniques used for speckle tracking echocardiography. As with echocardiographic myocardial deformation analysis, the software also generates estimates of ventricular mass, volumes and ejection fraction.

The aims of this chapter were:

1. To obtain measures of ventricular volumes, ejection fraction and mass using both feature tracking (CMR-FT) and contoured disc summation methods (CMR-volumetrics) from a large group of subjects with different ages and genders.

2. To determine the agreement and reproducibility of volumetric and mass analysis of both techniques.

3. To assess whether different uses of the feature tracking software could improve reproducibility.

7.2 Methods

Two hundred and forty eight healthy volunteers were recruited as described in chapter 2 (100 males, age 20-39 years; 148 females, age 20-49 years) underwent the same standardised CMR scan (Chapter 2.3.1). The CMR images (HLA view) were analysed to obtain volume, ejection fraction and mass analysis by manual contouring and feature tracking are described in Chapter 2.3.3 and 2.4.4 respectively. Ten subjects were re analysed by the initial reader and a second reader, both blinded to the original results, to assess intra and inter operator variability.

7.3 Statistical analysis

Summary variables for subject characteristics and ranges of results are presented as mean ± SD for continuous variables and as frequency for categorical variables. Variables were assessed for normal distribution using the Kolmogrov Smirnov test. Continuous variables with normal distribution were compared using the paired Student t test and using the Wilcoxon test otherwise. Pearson's correlation coefficient was used when assessing normally distributed data and Spearman for non-normally distributed data. Agreement between CMR-FT and CMR-Volumetrics results were assessed using Bland Altman [95] analysis to identify the bias and the limits of agreement with 95% confidence intervals. Observer agreement was evaluated by the intra class correlation coefficient (ICC)[108], as described in section 4.3. An ICC value of 1 indicates perfect agreement and, for example, an ICC of 0.95 indicates the balance of the variance (1 – ICC = 5%) is attributable to error; in this study due to instrumentation or operator [109]. For comparison purposes we classed ICC scores of <0.4 as poor reproducibility; 0.4-0.6 as low; 0.6-0.8 as moderate and >0.8 as good

reproducibility. All computations were performed using SPSS 18 (SPSS Inc., Chicago, IL, USA). P value less than 0.05 was considered statistically significant.

7.4 Results

7.4.1 Feasibility of feature tracking analysis

The time for feature tracking analysis (from initial contouring to obtaining the final results) was significantly shorter (84±24 seconds) compared to Argus manual contouring (429±78 seconds), $p<0.05$.

7.4.2 Baseline CMR feature tracking and CMR-volumetrics results

The baseline parameters obtained using the two analysis techniques according to gender are shown in Table 7.1. Significant differences ($p<0.05$) were seen for both techniques when comparing males with females for all parameters. In detail, for both CMR-FT and CMR-volumetrics biventricular volumes and LV mass was higher in males when compared to females whereas ejection fraction for CMR-Volumetrics and CMR-FT (corrected) was greater in females.

Table 7.1: Mean group values for the measured parameters using feature tracking and traditional CMR manual contouring grouped by gender.

	Male (n=95)		Female (n=153)	
	CMR	FT	CMR	FT
LVEF (%)	63±6	55±5	66±6	55±6
LVEF Cor (%)	63±6	61±6	66±6	63±6
LV EDV (mls)	159±25	158±27	128±23	122±23
LV ESV (mls)	58±13	73±16	44±10	59±16
LV ESV Cor (mls)	58±13	62±14	44±13	46±11
LV Mass (g)	127±21	137±24	85±20	96±23
RVEF (%)	59±6	42±17	61±6	44±16
RVEF Cor (%)	59±6	57±8	61±6	62±8
RV EDV (mls)	166±29	99±24	133±26	70±19
RV ESV (mls)	58±13	58±21	44±10	39±16
RV ESV Cor (mls)	58±13	42±12	44±10	27±10
Data presented as mean ± SD.				

7.4.3 Agreement between feature tracking and manual CMR contouring for LV mass, volumes and ejection fraction.

There was a good correlation between both techniques for the assessment of mass (r = 0.85) and left ventricular EDV (r = 0.87) (Figure 4.1A), but on average, a 10g higher mass was reported by CMR-FT and a 4mL greater end diastolic volume by CMR-volumetrics (Table 7.1 and Figure 7.1A). The limits of agreement between techniques were wide (-46g to 26g for mass, -23mL to 32mL for EDV) (Table 7.2).

Table 7.2: Bland Altman agreement between feature tracking and traditional CMR manual contouring for left ventricular parameters

	Standard Analysis Based on ED frame		Analysis Based on ES frame	
	Bias / (CI)	Limits of agreement	Bias / CI	Limits of agreement
Mass CMR vs. Mass FT (g)	-10 (-12 to -8)	-46 to 26		
EDV CMR vs. EDV FT	4 (3 to 6)	-23 to 32		
ESV CMR vs. ESV FT	-15 (-16 to -13)	-41 to 12	-2 (-3 to -1)	-19 to 14
EF CMR vs. EF FT	10 (9 to 11)	-4 to 23	3 (2 to 4)	-9 to 15
RV EDV CMR vs. RV EDV FT	64 (61 to 67)	20 to 108		
RV ESV CMR vs. RV ESV FT	18 (15 to 20)	-27 to 62	31 (28 to 34)	-11 to 73
RV EF CMR vs. EF FT	16 (14 to 19)	-16 to 48	1 (0 to 2)	-16 to 19

The correlation between techniques was not as good for ESV (r = 0.66) and particularly poor for the estimation of ejection fraction (r = 0.26). This resulted in large biases and wide limits of agreement (Table 7.2). However, estimates of ESV could be improved if the end systolic frame was used as the reference frame for the feature tracking software. With this approach the correlation improved (r = 0.81) as did the bias (from -15g to -2g) and limits of agreement (-41mL to 12mL vs. -19mL to 14mL) (Figure 4.1 B). Similarly estimation of ejection fraction improved with this approach (r = 0.48, bias 3%, limits of agreement -10% to 15%) (Figure 7.1 C).

Figure 7.1A: Correlation and Bland Altman analysis for the agreement of left ventricular mass (left) and end diastolic volume, right.

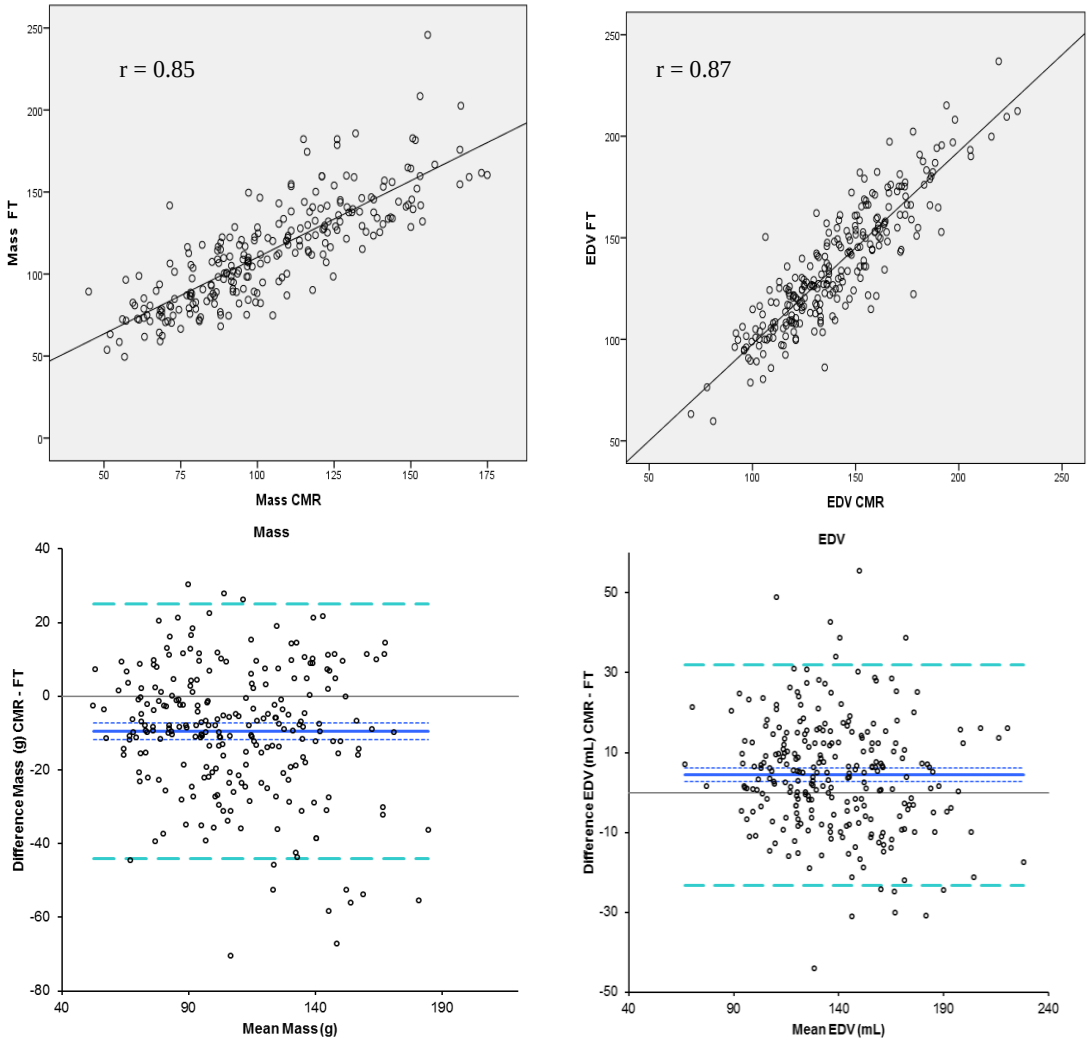

Figure 7.1B: Correlation and Bland Altman analysis for the agreement of left ventricular end systolic volume (left) and corrected end systolic volume, right.

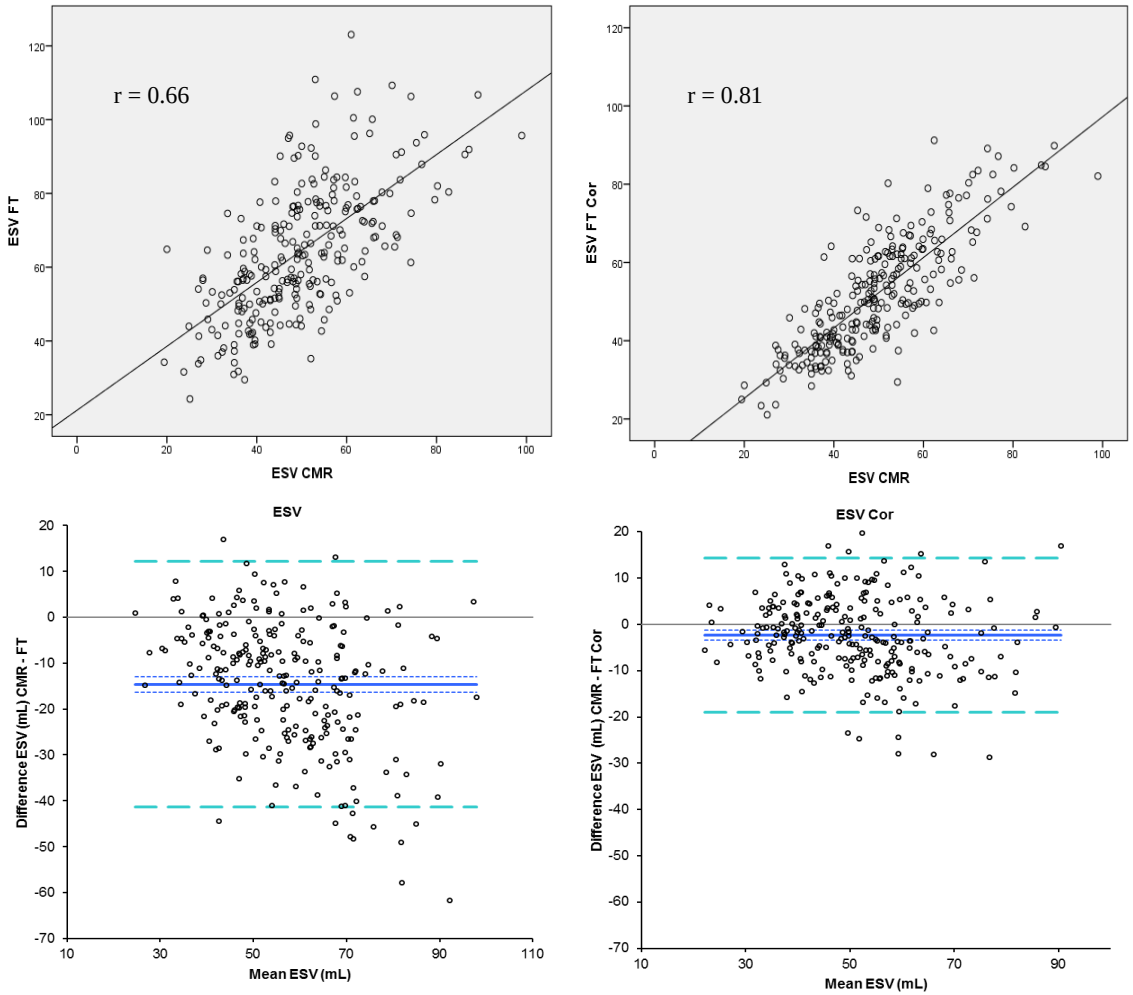

Figure 7.1C: Correlation and Bland Altman analysis for the agreement of left ventricular ejection fraction (left) and corrected ejection fraction, right.

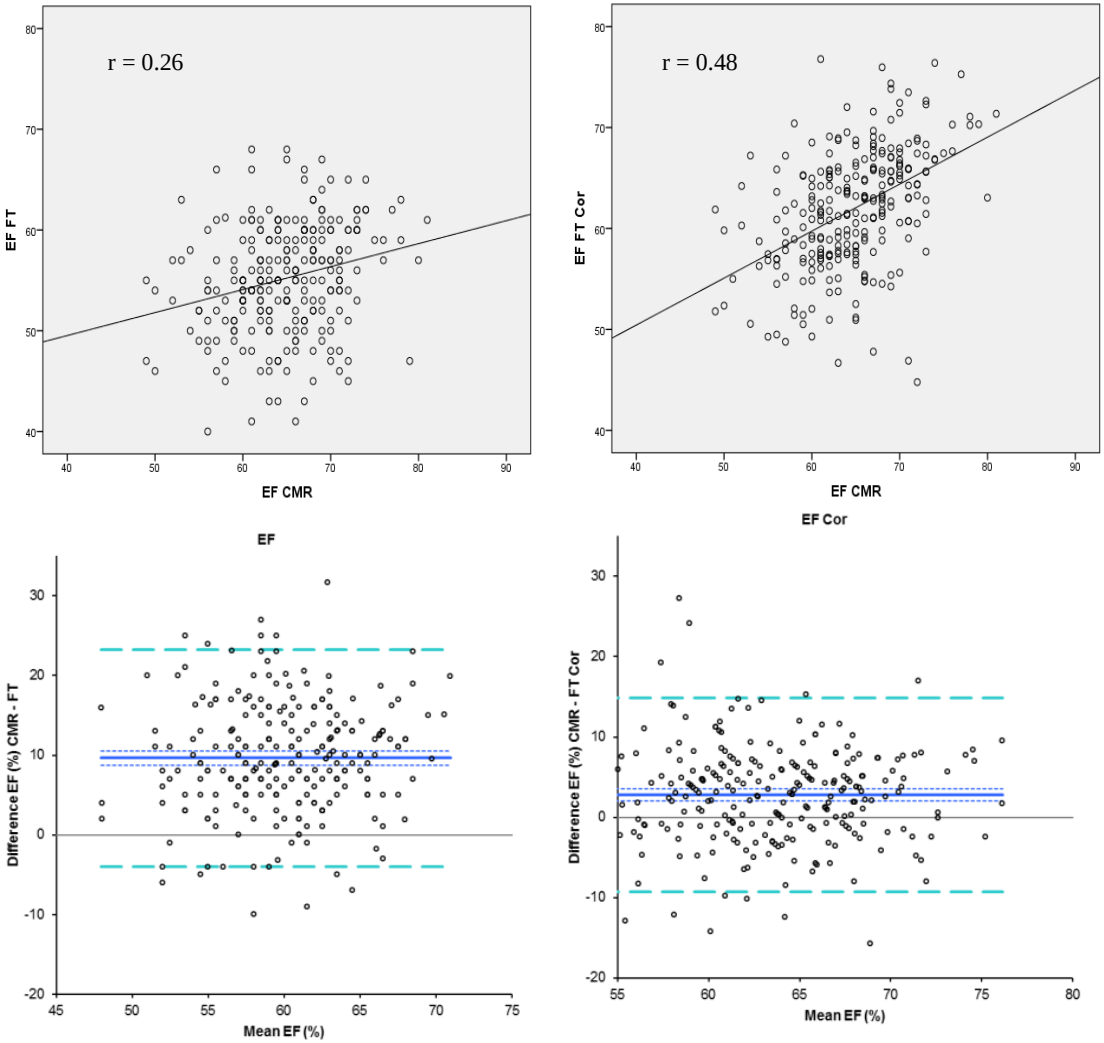

7.4.4 Agreement between feature tracking and manual CMR contouring for RV volumes and ejection fraction.

Although the correlations seen between both techniques for the assessment of right ventricular EDV was good (r = 0.72 Figure 7.2A.), the Bland Altman agreement overall was poor with a large bias (64mL) and wide limits of agreement (20mL to 108mL). This poor agreement was also seen for the assessment of right ventricular end systolic volumes (r = 0.4; bias 18mL; limits of agreement -27mL to 62mL, Figure 7.2B) as well as ejection fraction (r = 0.2; bias 16% limits of agreement -16% to 48%, Figure 7.2C), without any notable improvement when using the end systolic frame as the reference frame (to estimate ESV) for evaluation of the corrected ESV or EF.

Figure 7.2A Correlation and Bland Altman analysis for the agreement of right ventricular end diastolic volume

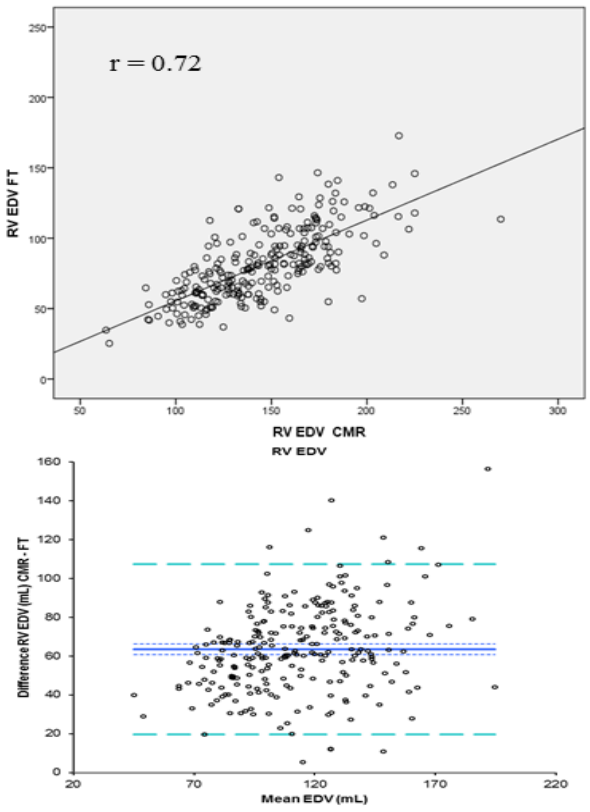

Figure 7.2B: Correlation and Bland Altman analysis for the agreement of right ventricular end systolic volume (left) and corrected end systolic volume, right.

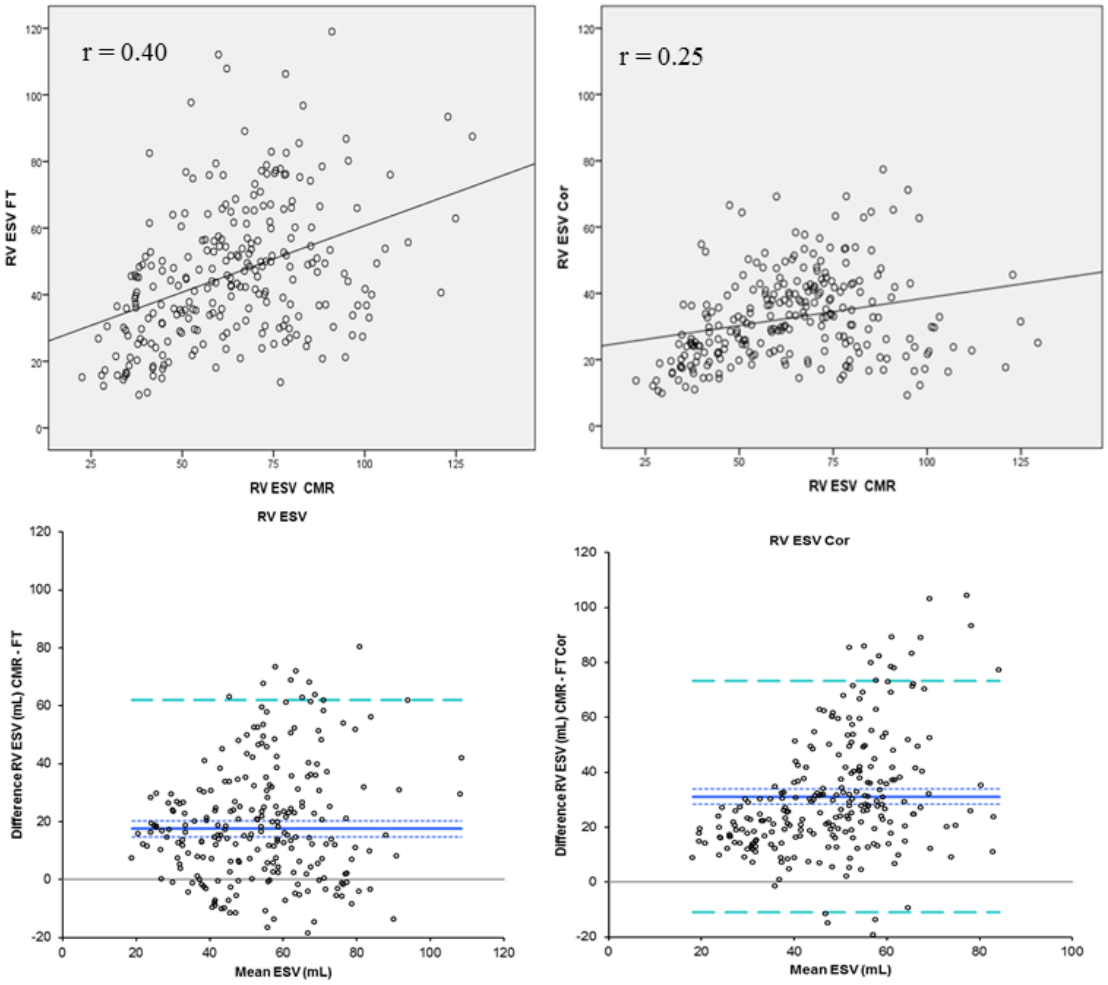

Figure 7.2C: Correlation and Bland Altman analysis for the agreement of right ventricular ejection fraction (left) and corrected ejection fraction, right.

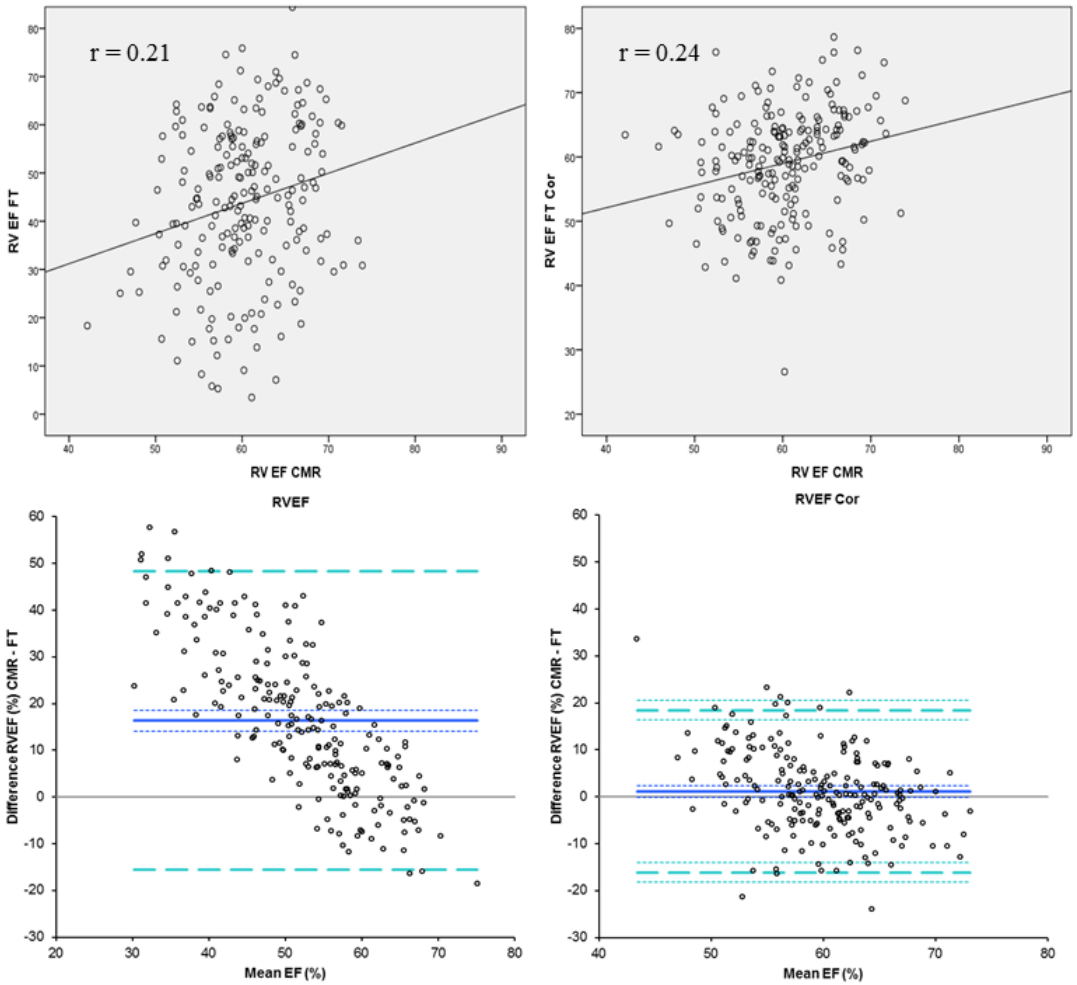

7.4.5 Inter and intra observer reproducibility

Good inter and intra observer mean ICCs were seen between both techniques (Figure 7.3) for both left and right ventricular EDV and left ventricular mass with intra-class correlation coefficients ranging from 0.81 to 0.98. Agreement was poorer for ESV (e.g. left ventricular inter observer ICC 0.45; intra observer ICC 0.94) and ejection fraction but could be improved for left ventricular measures when observer variability was based on the corrected end systolic frame (e.g. left ventricular inter observer ICC 0.65; intra observer ICC 0.94).

A

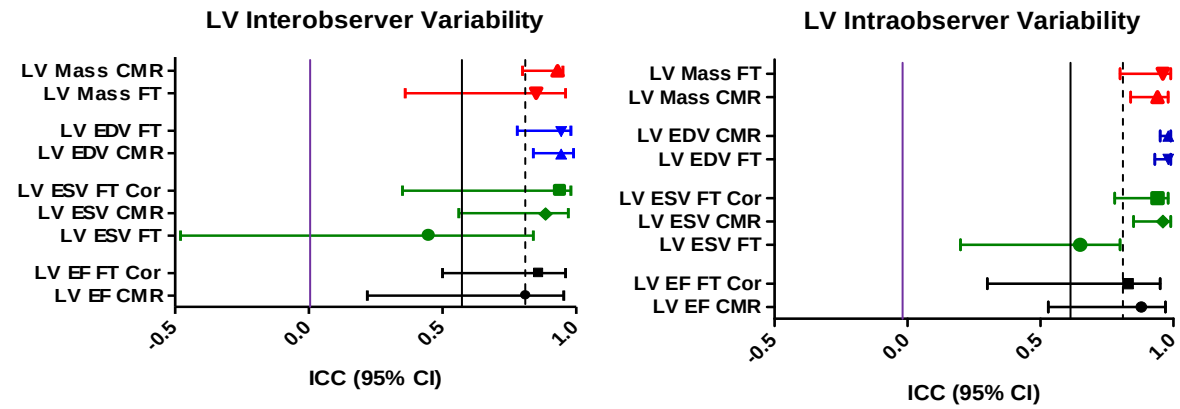

B

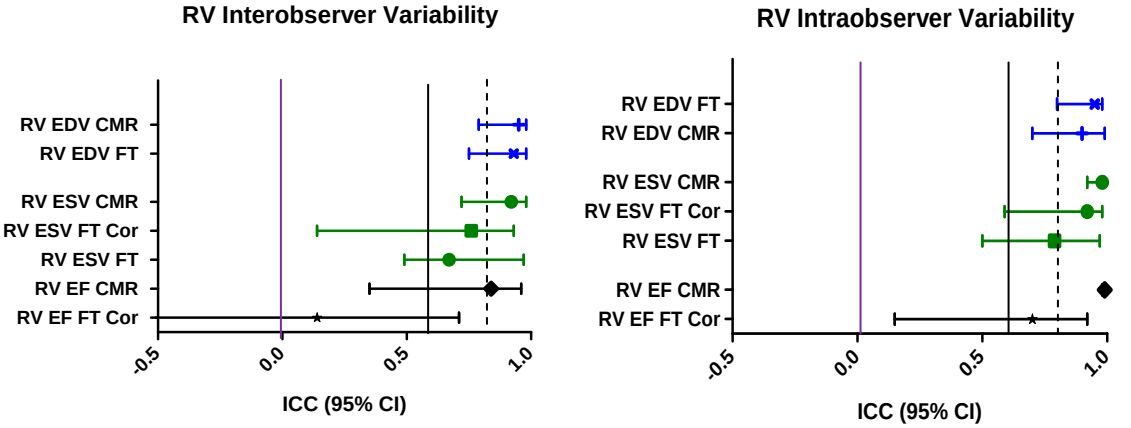

Figure 7.3: Intra class correlation coefficients for observer variability

A: Intra class correlation coefficients for left ventricular parameters - inter and intra observer agreement. Levels for an ICC of 0 shown in purple line. Levels for moderate reliability (ICC 0.6) shown as solid black line; levels for good reliability (ICC >0.8) shown as dashed black line.

B: Intra class correlation coefficients for right ventricular parameters - inter and intra observer agreement. Levels for an ICC of 0 shown in purple line. Levels for moderate reliability (ICC 0.6) shown as solid black line; levels for good reliability (ICC >0.8) shown as dashed black line.

7.5 Discussion

This study demonstrates that in this group of healthy volunteers with normal ejection fraction feature tracking cardiac magnetic resonance analysis is able to estimate ventricular mass, volumes and EF in a considerably shorter time than required for manually contoured disc summation techniques. Although correlations for measures between techniques for estimation of LV volumes and mass are good, detailed analysis demonstrates agreement between feature tracking and the gold standard disc summation method is overall modest for left ventricular parameters. In particular, estimation of left ventricular ESV and EF was poor, although we demonstrate that different applications of the software can improve the accuracy.

The agreement for left ventricular EF and LV volumes between CMR-volumetrics and CMR-FT seen here was similar to that seen between two dimensional (2D) and three dimensional (3D) echocardiography with CMR [129]. The agreement for LV mass in this study is similar to the comparison between 3D echocardiography and CMR and better than demonstrated for a comparison of 2D echocardiography with CMR [130]. The agreement for ESV is poor, likely due to the fact that the feature tracking algorithm follows similar voxels through subsequent frames around an initial contoured point rather than the actual contour detection in each slice. Consistent with this concept, using the end systolic frame as the reference image improved accuracy.

It is not surprising that the agreement between the two techniques used was poor for all RV parameters evaluated. In addition to differences in techniques, the complex geometry of the right ventricle would not have been fully incorporated when using the HLA view for the estimation for the ventricular volumes using feature tracking. This is one of the reasons

seen here for feature tracking underestimating RV volumes when compared with CMR-volumetrics.

Reproducible measurements of cardiovascular function are important for the assessment of disease and monitoring of pharmacological treatments in longitudinal follow up. Despite overall modest agreement for LV parameters and poor agreement for RV parameters between techniques, both intra and inter observer analysis with feature tracking was good for EDV, mass and ejection fraction. This suggests the feature tracking software analysis is consistent within and between observers and other factors must account for the variability in measures between techniques. Some of this variation may be because the traditional CMR disc summation approach uses short axis views for contouring and therefore fully takes account of three dimensional variation in all the walls during the cardiac cycle whereas feature tracking delineation is based on the HLA view. Furthermore, the inclusion or exclusion of papillary muscles within the left ventricular cavity also alters the volume of mass, as can the decision to include or exclude the rim of signal at the epicardial – pericardial fat interface [131].

Whilst new measurement techniques do not often have a perfect agreement with established gold standards, continuing advances in tracking of borders may further improve the accuracy of the measures seen in this study. Within multimodality imaging it has been shown that 2D based analysis gives reasonable correlation with 3D based analysis in morphologically normal hearts. However, once the hearts are deformed, 3D methods are required for accurate assessment [41]. As this study cohort comprised healthy volunteers with normal LV ejection fraction, we are unable to address the clinical value of feature tracking in hearts which are morphologically abnormal. In addition, whilst all subjects in this

study had normal ejection fraction, future investigations may be beneficial to see whether a multi plane approach using feature tracking may yield more favourable results in subjects with low ejection fraction and regional wall motion abnormality. The use of normal ranges derived using feature tracking may also be of use in the future.

In summary, CMR-FT agreement of RV volumetric parameters when compared to CMR-volumetrics is poor. For left ventricular parameters, differences exist when compared with the traditional manual contouring approach particularly with regard to ESV and EF, likely due to a combination of analysis technique and computational differences. Whilst we have shown that in normal healthy control subjects, CMR-FT is a potentially promising piece of software further work is required to improve its accuracy. Currently, CMR manual contouring following the acquisition of a whole-heart stack remains the gold standard approach for the estimation of ventricular ejection fraction, mass and volumes in both research volunteers and clinical patients.

Chapter 8: Limitations, Summary And Conclusions

8.1 Limitations

The estimation of normal values for deformation imaging using feature tracking is discussed in chapter 3. I acknowledge that the study population (n =145) were relatively young (mean age 29.7±7.6 years). Therefore, the results presented here for normal values may not be representative of older population groups.

The feature tracking software used in this work was a prototype provided by TomTec. At the onset of this work a member of the TomTec company provided support in how to process images for both researchers who's readings would be used to estimate inter and intraobserver variability. A more rigorous form of standardisation such as review of a subset of subjects to evaluate similar placement of the original contours would have been beneficial.

Inter and inter observer variability has been assessed for various deformation parameters throughout this work. There is relatively poor observer variability for a number of feature tracking parameters (e.g. global radial strain interobserver agreement has a coefficient of variation of 32.3%, Table 3.2). It is possible that the inclusion of the LVOT in the basal slice of the LV assessment may contribute to this poor observer variability.

As with any technique, the reproducibility of both the dimension and functional assessment is a vital component that should be established. This can be undertaken at a number of levels. In this work the majority of reproducibility was performed using inter and intra observer variability. However, one limitation of this work is the lack of use of the test – retest scenario. The analysis of retest variation is a component often overlooked for both CMR and echocardiographic studies although is common within clinical practice when

assessing patients over a number of years. The inclusion of this would have given a more informative picture of reproducibility.

During this work, the use of feature tracking software to estimate diastolic deformation values was evaluated (Chapter 6). Here, diastolic function was evaluated in a group of subjects with varying diastolic function. Here, diastolic function was graded according to the American and European society of echocardiography guidelines (figure 2.8) by assessing the E/A ration; deceleration time and E/e' levels. It is acknowledged that not all subjects fell neatly into either grade I, II or III diastolic function grading as in some cases parameters fell into two grading groups. In these cases then the diastolic grading was chosen depending on the grade which had the majority of parameters in agreement.

In Chapter 7, the use of feature tracking to estimate ventricular volumes and function was assessed. Here for feature tracking assessment the cine HLA image was used as opposed to the 'gold' standard of manual contouring using the disc summation approach with short axis views. Some of the variation seen is because the traditional CMR disc summation approach uses short axis views for contouring and therefore fully takes account of three dimensional variation in all the walls during the cardiac cycle whereas feature tracking delineation is based on the HLA view. In addition, as this study cohort comprised healthy volunteers with normal LV ejection fraction, we are unable to address the clinical value of feature tracking in hearts which are morphologically abnormal. In addition, whilst all subjects in this study had normal ejection fraction, future investigations may be beneficial to see whether a multi plane approach using feature tracking may yield more favourable results in subjects with low ejection fraction and regional wall motion abnormality.

8.2 Aims of original work

This work was carried out with four main aims:

1. To define normal feature tracking LV systolic deformation values and to assess their reproducibility.
2. To compare LV and RV feature tracking strain values with CMR tagging and speckle tracking echocardiography.
3. To assess the feasibility of feature tracking to measure diastolic function and to correlate this with standard echocardiographic assessment.
4. To assess the ability of feature tracking to estimate ventricular volumes, mass and ejection fraction.

In this chapter the extent to which these aims have been achieved and the implication for future research and potential for clinical use will be assessed.

8.3 Normal feature tracking systolic deformation values

This work has generated ranges for all left ventricular myocardial systolic strain parameters as well as myocardial displacement and velocities using feature tracking down to a segmental level in a large group of healthy subjects [132]. We have found that for systolic strain, circumferential strain is the most reproducible, followed by longitudinal strain with radial strain having poor reproducibility (Table8.1). Furthermore measures for global function were more reproducible than those for regional function. This is in keeping with studies which have found that segmental reproducibility is poor [70, 75]. Whilst radial strain parameters showed poor reproducibility, interestingly systolic radial velocities and displacement values shoed good agreement. This is likely as the values are calculated by the

measurement of movement of features around one radial contour (e.g. endocardial) rather than for strain and strain rate values which would use both endocardial and epicardial contours. It has also recently been shown that the assessment of strain using feature tracking is independent of field strength [133-134]. Given these findings, further development of algorithms is needed to improve reproducibility, particularly of radial strain and also at regional and segmental levels to allow this software to be used confidently by clinicians.

Table 8.1: Summary of agreement for systolic deformation feature tracking parameters.

	Parameter	Normal Value	FT Interobserver	FT Intraobserver	CMR Tagging vs. FT Agreement	
					Bias	LOA
GOOD AGREEMENT	Global Circumferential Strain	-0.21 ±0.03	4.9	2.8	-0.007	-0.06 to 0.04
	Mid Circumferential Strain	-0.18 ±0.03	4.5	6.4	0.02	0.04 to 0.07
	Global Radial Velocity (cm/s)	2.5 ±0.36	2.4	6.2		
	Basal Radial Velocity (cm/s)	2.84 ±0.53	5.2	5.1		
	Mid Radial Velocity (cm/s)	2.48 ±0.41	6.4	4.5		
	Apical Radial Velocity (cm/s)	2.19 ±0.41	6.2	7.3		
	Global Radial Displacement (mm)	5.1 ±.073	2.7	4.3		
	Basal Radial Displacement (mm)	6.02 ±1.08	7.5	4.3		
	Mid Radial Displacement (mm)	4.89 ±0.82	6.4	4.5		
	Apical Radial Displacement (mm)	4.38 ±0.82	7.5	5.7		
MODERATE AGREEMENT	Basal Circumferential Strain	-0.22 ±0.04	3.2	6	-0.05	-0.14 to 0.04
	Apical Circumferential Strain	-0.21 ±0.38	9.2	6.0	0.009	-0.05 to 0.07
	Global Circumferential Strain Rate	1.21 ±0.18	7.9	6.3	-0.21	-0.53 to 0.11
	Global Longitudinal Strain	-0.19 ±0.03	10.9	12.3	-0.01	-0.16 to 0.03
POOR AGREEMENT	Basal Circumferential Strain Rate	-1.33 ±0.28	15.9	6.3	-0.44	-1.09 to 0.21
	Mid Circumferential Strain Rate	-1.05 ±.018	6.9	18.3	-0.07	-0.42 to 0.27
	Apical Circumferential Strain Rate	-1.26 ±0.25	17.3	9.1	-0.12	-0.50 to 0.25
	Basal Longitudinal Strain	-0.21 ±0.05	10.8	17.7	-0.06	-0.19 to 0.06
	Mid Longitudinal Strain	-0.19 ±0.04	17.5	17.7	-0.05	-0.21 to 0.11
	Apical Longitudinal Strain	-0.16 ±0.05	31.3	42.7	0.04	-0.12 to 0.20
	Global Longitudinal Strain Rate	-1.08 ±0.24	16.2	16.0	-0.22	-0.82 to 0.37
	Basal Longitudinal Strain Rate	-1.21 ±0.36	34.3	19.2	0.01	-0.16 to 0.19
	Mid Longitudinall Strain Rate	-1.08 ±0.27	21.1	17.8	0.03	-0.05 to 0.12
	Apical Radial Strain Rate	-0.98 ±0.34	25.6	23.2	-0.02	-0.12 to 0.07
	Global Radial Strain	0.25 ±0.06	32.3	22.9	0.11	-0.01 to 0.23
	Basal Radial Strain	0.26 ±0.08	13.5	48.5	0.12	0.03 to 0.23
	Mid Radial Strain	0.24 ±0.08	26.3	14.8	0.12	-0.05 to 0.30
	Apical Radial Strain	0.23 ±0.09	29.1	23.9	0.08	-0.13 to 0.30
	Global Radial Strain Rate	1.25±0.4	14.9	15.6	0.26	-0.34 to 0.86
	Basal Radial Strain Rate	1.23 ±0.39	15.8	14.1	0.20	-0.71 to 1.11
	Mid Radial Strain Rate	1.25 ±0.36	27.2	11.3	0.41	-0.32 to 1.16
	Apical Radial Strain Rate	1.18 ±0.43	31.3	30.2	0.17	-0.83 to 1.16

FT observer variability are presented as COV (%). Strain values represented as a fraction written in decimal

8.4 Feature tracking assessment of LV and RV strain – comparison with CMR tagging and speckle tracking echocardiography

For the left ventricle, levels of longitudinal and circumferential strain are the most consistently measured strain parameters between modalities although currently, given the systematic biases in normal ranges with certain imaging and analysis combinations, the results presented here do not support the notion that strain values are interchangeable between different imaging modalities. Even within the same imaging modality, for serial scans care should be taken to use consistent settings and analysis tools.

For the right ventricle, strain analysis using feature tracking is possible with modest observer agreement. The development of RV specific overlays and algorithms will improve this further. As for the LV, the work in chapter 5 suggests that RV strain values are not interchangeable with consistency between imaging modalities.

8.5 Diastolic function assessment using feature tracking

A potential pit fall for any analysis tool is the ability for numerous output measurements to be produced and to then know which ones are meaningful. The results from chapter 6 have shown the potential for feature tracking to assess diastolic function and in particular identified that radial diastolic velocity and longitudinal strain rates can predict diastolic dysfunction with acceptable levels of sensitivity and specificity. In addition, in a similar fashion to echocardiographic parameters the results presented in chapter 6 show age related changes to feature tracking indices of diastolic parameters. These findings given the inferior temporal resolution of CMR compared with tissue Doppler echocardiography highlight the potential that feature tracking software has to assess diastolic dysfunction.

8.6 The assessment of ventricular volumes, mass and ejection fraction using feature tracking

Here this work has shown that currently significant improvements on feature tracking algorithms are needed to allow accurate and reproducible estimations of volumes, mass and ejection fraction before this can be used routinely with confidence. Currently, CMR manual contouring following the acquisition of a whole-heart stack remains the gold standard approach for the estimation of ventricular ejection fraction, mass and volumes in both research volunteers and patients.

8.7 Conclusions

This study has examined the feasibility and practicality of CMR feature tracking in a variety of settings and has shown that there are certain parameters which can be measured with confidence given the adequate reproducibility. However, there are some feature tracking parameters where alterations in current algorithms are necessary to improve quantification, especially at a regional and segmental level.

In the era of multi modality cardiovascular imaging we are still some way away from a universally interchangeable method of strain assessment. For cardiac magnetic resonance imaging, CMR feature tracking does not necessitate any additional image acquisition and has a significantly shorter post processing time than other CMR strain analysis methods. With progression of technology it has the potential to become the CMR preferred assessment for strain quantification.

References

1. Gopal, A.S., Z. Shen, P.M. Sapin, A.M. Keller, M.J. Schnellbaecher, D.W. Leibowitz, O.O. Akinboboye, R.A. Rodney, D.K. Blood, and D.L. King, *Assessment of Cardiac Function by Three-dimensional Echocardiography Compared With Conventional Noninvasive Methods.* Circulation, 1995. **92**(4): p. 842-853.
2. Teichholz, L.E., T. Kreulen, M.V. Herman, and R. Gorlin, *Problems in echocardiographic volume determinations: Echocardiographic-angiographic correlations in the presence or absence of asynergy.* The American Journal of Cardiology, 1976. **37**(1): p. 7-11.
3. Leeson, P., D. Augustine, A. Mitchell, and H. Becher, *Echocardiography*, in *Echocardiography*. 2012, Oxford University Press.
4. Kühl, H.P., M. Schreckenberg, D. Rulands, M. Katoh, W. Schäfer, G. Schummers, A. Bücker, P. Hanrath, and A. Franke, *High-resolution transthoracic real-time three-dimensional echocardiography: Quantitation of cardiac volumes and function using semi-automatic border detection and comparison with cardiac magnetic resonance imaging.* Journal of the American College of Cardiology, 2004. **43**(11): p. 2083-2090.
5. Nosir, Y.M., M. Lequin, J. Kasprzak, R. van Domburg, W. Vletter, J. Yao, J. Stoker, F.T. Cate, and J.T.C. Roelandt, *Measurements and day-to-day variabilities of left ventricular volumes and ejection fraction by three-dimensional echocardiography and comparison with magnetic resonance imaging.* The American Journal of Cardiology, 1998. **82**(2): p. 209-214.
6. Abraham, T.P., V.L. Dimaano, and H.-Y. Liang, *Role of Tissue Doppler and Strain Echocardiography in Current Clinical Practice.* Circulation, 2007. **116**(22): p. 2597-2609.
7. Rodriguez, L., M. Garcia, M. Ares, B.P. Griffin, S. Nakatani, and J.D. Thomas, *Assessment of mitral annular dynamics during diastole by Doppler tissue imaging: Comparison with mitral Doppler inflow in subjects without heart disease and in patients with left ventricular hypertrophy.* American Heart Journal, 1996. **131**(5): p. 982-987.
8. Nagueh, S.F., K.J. Middleton, H.A. Kopelen, W.A. Zoghbi, and M.A. Quinones, *Doppler tissue imaging: a noninvasive technique for evaluation of left ventricular relaxation and estimation of filling pressures.* Journal of the American College of Cardiology, 1997. **30**(6): p. 1527-33.
9. Lu, X., V. Nadvoretskiy, L. Bu, A. Stolpen, N. Ayres, R.H. Pignatelli, J.P. Kovalchin, M. Grenier, B. Klas, and S. Ge, *Accuracy and reproducibility of real-time three-dimensional echocardiography for assessment of right ventricular volumes and ejection fraction in children.* Journal of the American Society of Echocardiography : official publication of the American Society of Echocardiography, 2008. **21**(1): p. 84-9.
10. Niemann, P.S., L. Pinho, T. Balbach, C. Galuschky, M. Blankenhagen, M. Silberbach, C. Broberg, M. Jerosch-Herold, and D.J. Sahn, *Anatomically Oriented Right Ventricular Volume Measurements With Dynamic Three-Dimensional Echocardiography Validated by 3-Tesla Magnetic Resonance Imaging.* Journal of the American College of Cardiology, 2007. **50**(17): p. 1668-1676.
11. Gopal, A., E. Chukwu, C. Iwuchukwu, A. Katz, R. Toole, W. Schapiro, and N. Reichek, *Normal values of right ventricular size and function by real-time 3-dimensional echocardiography: comparison with cardiac magnetic resonance imaging.* J Am Soc Echocardiogr, 2007. **20**(5): p. 445-55.
12. Grapsa, J., D.P. O'Regan, H. Pavlopoulos, G. Durighel, D. Dawson, and P. Nihoyannopoulos, *Right ventricular remodelling in pulmonary arterial hypertension with three-dimensional echocardiography: comparison with cardiac magnetic resonance imaging.* European journal of echocardiography : the journal of the Working Group on Echocardiography of the European Society of Cardiology, 2010. **11**(1): p. 64-73.
13. Jenkins, C., J. Chan, K. Bricknell, M. Strudwick, and T.H. Marwick, *Reproducibility of right ventricular volumes and ejection fraction using real-time three-dimensional*

echocardiography: Comparison with cardiac mri.* CHEST Journal, 2007. **131**(6): p. 1844-1851.
14. Pavlicek, M., A. Wahl, T. Rutz, S.F. de Marchi, R. Hille, K. Wustmann, H. Steck, C. Eigenmann, M. Schwerzmann, and C. Seiler, *Right ventricular systolic function assessment: rank of echocardiographic methods vs. cardiac magnetic resonance imaging.* European Journal of Echocardiography, 2011.
15. Maceira, A.M., S.K. Prasad, M. Khan, and D.J. Pennell, *Reference right ventricular systolic and diastolic function normalized to age, gender and body surface area from steady-state free precession cardiovascular magnetic resonance.* European Heart Journal, 2006.
16. Pennell, D.J., U.P. Sechtem, C.B. Higgins, W.J. Manning, G.M. Pohost, F.E. Rademakers, A.C. van Rossum, L.J. Shaw, and E.K. Yucel, *Clinical indications for cardiovascular magnetic resonance (CMR): Consensus Panel report.* European Heart Journal, 2004. **25**(21): p. 1940-1965.
17. MØGELVANG, J., K.H. STOKHOLM, K. SAUNÄMAKI, A. REIMER, M. STUBGAARD, C. THOMSEN, P. FRITZ-HANSEN, and O. HENRIKSEN, *Assessment of left ventricular volumes by magnetic resonance in comparison with radionuclide angiography, contrast angiography and echocardiography.* European Heart Journal, 1992. **13**(12): p. 1677-1683.
18. Katz, J., J. Whang, L.M. Boxt, and R.J. Barst, *Estimation of right ventricular mass in normal subjects and in patients with primary pulmonary hypertension by nuclear magnetic resonance imaging.* Journal of the American College of Cardiology, 1993. **21**(6): p. 1475-1481.
19. Grothues, F., J.C. Moon, N.G. Bellenger, G.S. Smith, H.U. Klein, and D.J. Pennell, *Interstudy reproducibility of right ventricular volumes, function, and mass with cardiovascular magnetic resonance.* American Heart Journal, 2004. **147**(2): p. 218-223.
20. Paulus, W.J., C. Tschöpe, J.E. Sanderson, C. Rusconi, F.A. Flachskampf, F.E. Rademakers, P. Marino, O.A. Smiseth, G. De Keulenaer, A.F. Leite-Moreira, A. Borbély, I. Édes, M.L. Handoko, S. Heymans, N. Pezzali, B. Pieske, K. Dickstein, A.G. Fraser, and D.L. Brutsaert, *How to diagnose diastolic heart failure: a consensus statement on the diagnosis of heart failure with normal left ventricular ejection fraction by the Heart Failure and Echocardiography Associations of the European Society of Cardiology.* European Heart Journal, 2007. **28**(20): p. 2539-2550.
21. Halley Cm, H.P.L.K.M.K.T.J.D.J.W.A., *MOrtality rate in patients with diastolic dysfunction and normal systolic function.* Archives of Internal Medicine, 2011. **171**(12): p. 1082-1087.
22. Redfield, M.M., S.J. Jacobsen, Burnett, J.C. Jr, D.W. Mahoney, K.R. Bailey, and R.J. Rodeheffer, *Burden of systolic and diastolic ventricular dysfunction in the community: Appreciating the scope of the heart failure epidemic.* JAMA, 2003. **289**(2): p. 194-202.
23. Nagueh, S.F., C.P. Appleton, T.C. Gillebert, P.N. Marino, J.K. Oh, O.A. Smiseth, A.D. Waggoner, F.A. Flachskampf, P.A. Pellikka, and A. Evangelista, *Recommendations for the Evaluation of Left Ventricular Diastolic Function by Echocardiography.* Journal of the American Society of Echocardiography : official publication of the American Society of Echocardiography, 2009. **22**(2): p. 107-133.
24. Møller, J.E., E. Søndergaard, S.H. Poulsen, and K. Egstrup, *Pseudonormal and restrictive filling patterns predict left ventricular dilation and cardiac death after a first myocardial infarction: a serial color M-mode doppler echocardiographic study.* Journal of the American College of Cardiology, 2000. **36**(6): p. 1841-1846.
25. Nagueh, S.F., H. Sun, H.A. Kopelen, K.J. Middleton, and D.S. Khoury, *Hemodynamic determinants of the mitral annulus diastolic velocities by tissue Doppler.* Journal of the American College of Cardiology, 2001. **37**(1): p. 278-285.
26. Nagueh, S.F., C.P. Appleton, T.C. Gillebert, P.N. Marino, J.K. Oh, O.A. Smiseth, A.D. Waggoner, F.A. Flachskampf, P.A. Pellikka, and A. Evangelisa, *Recommendations for the*

Evaluation of Left Ventricular Diastolic Function by Echocardiography. European Journal of Echocardiography, 2009. **10**(2): p. 165-193.
27. Dokainish, H., W.A. Zoghbi, N.M. Lakkis, F. Al-Bakshy, M. Dhir, M.A. Quinones, and S.F. Nagueh, *Optimal Noninvasive Assessment of Left Ventricular Filling Pressures: A Comparison of Tissue Doppler Echocardiography and B-Type Natriuretic Peptide in Patients With Pulmonary Artery Catheters.* Circulation, 2004. **109**(20): p. 2432-2439.
28. Bellenger, N.G., M.I. Burgess, S.G. Ray, A. Lahiri, A.J.S. Coats, J.G.F. Cleland, and D.J. Pennell, *Comparison of left ventricular ejection fraction and volumes in heart failure by echocardiography, radionuclide ventriculography and cardiovascular magnetic resonance. Are they interchangeable?* European Heart Journal, 2000. **21**(16): p. 1387-1396.
29. Engels, G., E. Müller, K. Reynen, N. Wilke, and K. Bachmann, *Evaluation of left ventricular inflow and volume by MR.* Magnetic Resonance Imaging, 1993. **11**(7): p. 957-964.
30. Westenberg, J.M., *CMR for Assessment of Diastolic Function.* Current Cardiovascular Imaging Reports, 2011. **4**(2): p. 149-158.
31. Geyer, H., G. Caracciolo, H. Abe, S. Wilansky, S. Carerj, F. Gentile, H.J. Nesser, B. Khandheria, J. Narula, and P.P. Sengupta, *Assessment of myocardial mechanics using speckle tracking echocardiography: fundamentals and clinical applications.* Journal of the American Society of Echocardiography , 2010. **23**(4): p. 351-69
32. Leitman, M., P. Lysyansky, S. Sidenko, V. Shir, E. Peleg, M. Binenbaum, E. Kaluski, R. Krakover, and Z. Vered, *Two-dimensional strain–a novel software for real-time quantitative echocardiographic assessment of myocardial function.* Journal of the American Society of Echocardiography : official publication of the American Society of Echocardiography, 2004. **17**(10): p. 1021-1029.
33. Marwick, T.H., *Clinical applications of tissue Doppler imaging: a promise fulfilled.* Heart, 2003. **89**(12): p. 1377-1378.
34. Blessberger, H. and T. Binder, *Two dimensional speckle tracking echocardiography: basic principles.* Heart, 2010. **96**(9): p. 716-722.
35. Choi, J.-O., S.W. Cho, Y.B. Song, S.J. Cho, B.G. Song, S.-C. Lee, and S.W. Park, *Longitudinal 2D strain at rest predicts the presence of left main and three vessel coronary artery disease in patients without regional wall motion abnormality.* European Journal of Echocardiography, 2009. **10**(5): p. 695-701.
36. Hanekom, L., G.-Y. Cho, R. Leano, L. Jeffriess, and T.H. Marwick, *Comparison of two-dimensional speckle and tissue Doppler strain measurement during dobutamine stress echocardiography: an angiographic correlation.* European Heart Journal, 2007. **28**(14): p. 1765-1772.
37. Bertini, M., S.A. Mollema, V. Delgado, M.L. Antoni, A.C.T. Ng, E.R. Holman, G. Boriani, M.J. Schalij, and J.J. Bax, *Impact of Time to Reperfusion After Acute Myocardial Infarction on Myocardial Damage Assessed by Left Ventricular Longitudinal Strain.* The American Journal of Cardiology, 2009. **104**(4): p. 480-485.
38. Kim, M.-S., Y.-J. Kim, H.-K. Kim, J.-Y. Han, H.-G. Chun, H.-C. Kim, D.-W. Sohn, B.-H. Oh, and Y.-B. Park, *Evaluation of left ventricular short- and long-axis function in severe mitral regurgitation using 2-dimensional strain echocardiography.* American Heart Journal, 2009. **157**(2): p. 345-351.
39. Popovic, Z.B., D.H. Kwon, M. Mishra, A. Buakhamsri, N.L. Greenberg, M. Thamilarasan, S.D. Flamm, J.D. Thomas, H.M. Lever, and M.Y. Desai, *Association Between Regional Ventricular Function and Myocardial Fibrosis in Hypertrophic Cardiomyopathy Assessed by Speckle Tracking Echocardiography and Delayed Hyperenhancement Magnetic Resonance Imaging.* Journal of the American Society of Echocardiography, 2008. **21**(12): p. 1299-1305.
40. Mansencal, N., N. Abbou, R. Pillière, R. El Mahmoud, J.-C. Farcot, and O. Dubourg, *Usefulness of Two-Dimensional Speckle Tracking Echocardiography for Assessment of Tako-Tsubo Cardiomyopathy.* The American Journal of Cardiology, 2009. **103**(7): p. 1020-1024.

41. Nesser, H.-J., V. Mor-Avi, W. Gorissen, L. Weinert, R. Steringer-Mascherbauer, J. Niel, L. Sugeng, and R.M. Lang, *Quantification of left ventricular volumes using three-dimensional echocardiographic speckle tracking: comparison with MRI.* European Heart Journal, 2009. **30**(13): p. 1565-1573.
42. Thebault, C., E. Donal, A. Bernard, O. Moreau, F. Schnell, P. Mabo, and C. Leclercq, *Real-time three-dimensional speckle tracking echocardiography: a novel technique to quantify global left ventricular mechanical dyssynchrony.* European Journal of Echocardiography, 2011. **12**(1): p. 26-32.
43. Marwick, T.H., *Consistency of myocardial deformation imaging between vendors.* European Journal of Echocardiography, 2010. **11**(5): p. 414-416.
44. Manovel, A., D. Dawson, B. Smith, and P. Nihoyannopoulos, *Assessment of left ventricular function by different speckle-tracking software.* European Journal of Echocardiography, 2010. **11**(5): p. 417-421.
45. Gayat, E., H. Ahmad, L. Weinert, R.M. Lang, and V. Mor-Avi, *Reproducibility and Inter-Vendor Variability of Left Ventricular Deformation Measurements by Three-Dimensional Speckle-Tracking Echocardiography.* Journal of the American Society of Echocardiography : official publication of the American Society of Echocardiography, 2011. **24**(8): p. 878-885.
46. Fukuda, Y., H. Tanaka, D. Sugiyama, K. Ryo, T. Onishi, H. Fukuya, M. Nogami, Y. Ohno, N. Emoto, H. Kawai, and K. Hirata, *Utility of right ventricular free wall speckle-tracking strain for evaluation of right ventricular performance in patients with pulmonary hypertension.* Journal of the American Society of Echocardiography : official publication of the American Society of Echocardiography, 2011. **24**(10): p. 1101-8.
47. Bernard, Y., M. Morel, V. Descotes-Genon, J. Jehl, N. Meneveau, and F. Schiele, *Value of Speckle Tracking for the Assessment of Right Ventricular Function in Patients Operated on for Tetralogy of Fallot. Comparison with Magnetic Resonance Imaging.* Echocardiography, 2013: p. n/a-n/a.
48. Chow, P.C., X.C. Liang, E.W. Cheung, W.W. Lam, and Y.F. Cheung, *New two-dimensional global longitudinal strain and strain rate imaging for assessment of systemic right ventricular function.* Heart, 2008. **94**(7): p. 855-9.
49. Altekin, R.E., M.S. Karakas, A. Yanikoglu, D. Ozel, O. Ozbudak, I. Demir, and N. Deger, *Determination of right ventricular dysfunction using the speckle tracking echocardiography method in patients with obstructive sleep apnea.* Cardiology journal, 2012. **19**(2): p. 130-9.
50. Kalogeropoulos, A.P., A. Deka, W. Border, M.A. Pernetz, V.V. Georgiopoulou, J. Kiani, M. McConnell, S. Lerakis, J. Butler, R.P. Martin, and W.M. Book, *Right ventricular function with standard and speckle-tracking echocardiography and clinical events in adults with D-transposition of the great arteries post atrial switch.* Journal of the American Society of Echocardiography : official publication of the American Society of Echocardiography, 2012. **25**(3): p. 304-12.
51. Stefani, L., G. Pedrizzetti, A. De Luca, R. Mercuri, G. Innocenti, and G. Galanti, *Real-time evaluation of longitudinal peak systolic strain (speckle tracking measurement) in left and right ventricles of athletes.* Cardiovascular Ultrasound, 2009. **7**: p. 17.
52. Teske, A.J., M.G. Cox, B.W. De Boeck, P.A. Doevendans, R.N. Hauer, and M.J. Cramer, *Echocardiographic tissue deformation imaging quantifies abnormal regional right ventricular function in arrhythmogenic right ventricular dysplasia/cardiomyopathy.* Journal of the American Society of Echocardiography : official publication of the American Society of Echocardiography, 2009. **22**(8): p. 920-7.
53. Perry, R., C.G. De Pasquale, D.P. Chew, and M.X. Joseph, *Assessment of early diastolic left ventricular function by two-dimensional echocardiographic speckle tracking.* European Journal of Echocardiography, 2008. **9**(6): p. 791-795.
54. Shanks, M., R.B. Thompson, I.D. Paterson, B. Putko, A. Khan, A. Chan, H. Becher, and G.Y. Oudit, *Systolic and Diastolic Function Assessment in Fabry Disease Patients Using Speckle-*

Tracking Imaging and Comparison with Conventional Echocardiographic Measurements. Journal of the American Society of Echocardiography : official publication of the American Society of Echocardiography, 2013. **26**(12): p. 1407-1414.
55. Bansal, M., G.-Y. Cho, J. Chan, R. Leano, B.A. Haluska, and T.H. Marwick, *Feasibility and Accuracy of Different Techniques of Two-Dimensional Speckle Based Strain and Validation With Harmonic Phase Magnetic Resonance Imaging.* Journal of the American Society of Echocardiography, 2008. **21**(12): p. 1318-1325.
56. Singh, G.K., B. Cupps, M. Pasque, P.K. Woodard, M.R. Holland, and A. Ludomirsky, *Accuracy and Reproducibility of Strain by Speckle Tracking in Pediatric Subjects with Normal Heart and Single Ventricular Physiology: A Two-Dimensional Speckle-Tracking Echocardiography and Magnetic Resonance Imaging Correlative Study.* Journal of the American Society of Echocardiography : official publication of the American Society of Echocardiography, 2010. **23**(11): p. 1143-1152.
57. Ibrahim, E.-S., *Myocardial tagging by Cardiovascular Magnetic Resonance: evolution of techniques--pulse sequences, analysis algorithms, and applications.* Journal of Cardiovascular Magnetic Resonance, 2011. **13**(1): p. 36.
58. Castillo, E., N. Osman, B. Rosen, I. El-Shehaby, L. Pan, M. Jerosch-Herold, S. Lai, D. Bluemke, and J. Lima, *Quantitative assessment of regional myocardial function with MR-tagging in a multi-center study: interobserver and intraobserver agreement of fast strain analysis with Harmonic Phase (HARP) MRI.* J Cardiovasc Magn Reson, 2005. **7**: p. 783 - 91.
59. Donekal, S., B. Ambale-Venkatesh, S. Berkowitz, C. Wu, E.Y. Choi, V. Fernandes, R. Yan, A. Harouni, D. Bluemke, and J.A.C. Lima, *Inter-study reproducibility of cardiovascular magnetic resonance tagging.* Journal of Cardiovascular Magnetic Resonance, 2013. **15**(1): p. 37.
60. Altiok, E., M. Neizel, S. Tiemann, V. Krass, M. Becker, C. Zwicker, R. Koos, M. Kelm, N. Kraemer, F. Schoth, N. Marx, and R. Hoffmann, *Layer-specific analysis of myocardial deformation for assessment of infarct transmurality: comparison of strain-encoded cardiovascular magnetic resonance with 2D speckle tracking echocardiography.* European Heart Journal – Cardiovascular Imaging, 2013. **14**(6): p. 570-578.
61. Hor, K., R. Baumann, G. Pedrizzetti, G. Tonti, W. Gottliebson, M. Taylor, W. Benson, and W. Mazur, *Magnetic resonance derived myocardial strain assessment using feature tracking.* J Vis Exp, 2011. **48**: p. 2356.
62. Ceelen, F., R. Hunter, R. Boubertakh, W. Sommer, M. Armbruster, R. Schilling, and S. Petersen, *Effect of atrial fibrillation ablation on myocardial function: insights from cardiac magnetic resonance feature tracking analysis.* The international journal of cardiovascular imaging, 2013. **29**(8): p. 1807-1817.
63. Barison, A., V. Cobb, A. Hline, D. Sado, S. White, A. Flett, S. Banypersad, T. Treibel, A. Herrey, and J. Moon, *Myocardial strain in a health and disease: CMR feature tracking analysis in cardiac hypertrophy.* Journal of Cardiovascular Magnetic Resonance, 2013. **15**(Suppl 1): p. E116.
64. Stone, I., R. Boubertakh, E. Stephenson, F. Zemrak, R. Weerackody, N. Sekhri, M. Westwood, C. Davies, S. Mohiddin, and S. Petersen, *Cardiac magnetic resonance myocardial feature tracking: feasibility for use in left ventricular non-compaction.* Journal of Cardiovascular Magnetic Resonance, 2013. **15**(Suppl 1): p. E119.
65. Breuninger, K., S. Lehrke, P. Matheis, Y. Sander, R. Kammerer, L. Rust, C. Galuschky, H. Katus, G. Korosoglou, and S. Buss, *Feature tracking cardiac magnetic resonance imaging for the evaluation of myocardial strain in patients with dilated cardiomyopathy and in healthy controls.* Journal of Cardiovascular Magnetic Resonance, 2013. **15**(Suppl 1): p. P167.
66. Taylor, R.J., F. Umar, C. Meyyappan, W.E. Moody, B. Stegemann, R.P. Steeds, J.N. Townend, and F. Leyva, *Feature-tracking cardiovascular magnetic resonance as a novel technique for the assessment of mechanical dyssynchrony.* European Heart Journal, 2013. **34**(suppl 1).

67. Steinmetz, M., S.-C. Alt, S. Kutty, J. Sohns, C. Unterberg-Buchwald, T. Paul, G. Hasenfuss, J. Lotz, P. Lamata, and A. Schuster, *Quantification of intra and inter-ventricular dyssynchrony in Ebstein's anomaly using cardiovascular magnetic resonance myocardial feature tracking.* Journal of Cardiovascular Magnetic Resonance, 2014. **16**(Suppl 1): p. O108.
68. Schuster, A., S. Kutty, A. Padiyath, V. Parish, P. Gribben, D. Danford, M. Makowski, B. Bigalke, P. Beerbaum, and E. Nagel, *Cardiovascular magnetic resonance myocardial feature tracking detects quantitative wall motion during dobutamine stress.* Journal of Cardiovascular Magnetic Resonance, 2011. **13**(1): p. 58.
69. Kutty, S., S. Rangamani, J. Venkataraman, L. Li, A. Schuster, S. Fletcher, D. Danford, and P. Beerbaum, *Reduced global longitudinal and radial strain with normal left ventricular ejection fraction late after effective repair of aortic coarctation: a CMR feature tracking study.* The international journal of cardiovascular imaging, 2013. **29**(1): p. 141-150.
70. Kempny, A., R. Fernandez-Jimenez, S. Orwat, P. Schuler, A. Bunck, D. Maintz, H. Baumgartner, and G.-P. Diller, *Quantification of biventricular myocardial function using cardiac magnetic resonance feature tracking, endocardial border delineation and echocardiographic speckle tracking in patients with repaired tetralogy of fallot and healthy controls.* Journal of Cardiovascular Magnetic Resonance, 2012. **14**(1): p. 32.
71. Schmidt, R., S. Orwat, A. Kempny, P. Schuler, R. Radke, P.C. Kahr, A. Hellige, H. Baumgartner, and G.-P. Diller, *Value of Speckle-tracking Echocardiography and MRI-based Feature Tracking Analysis in Adult Patients after Fontan-type Palliation.* Congenital Heart Disease, 2014: p. n/a-n/a.
72. Morton, G., A. Schuster, R. Jogiya, S. Kutty, P. Beerbaum, and E. Nagel, *Inter-study reproducibility of cardiovascular magnetic resonance myocardial feature tracking.* J Cardiovasc Magn Reson, 2012. **14**: p. 43.
73. Lewandowski, A.J., D. Augustine, P. Lamata, E.F. Davis, M. Lazdam, J. Francis, K. McCormick, A.R. Wilkinson, A. Singhal, A. Lucas, N.P. Smith, S. Neubauer, and P. Leeson, *Preterm Heart in Adult Life: Cardiovascular Magnetic Resonance Reveals Distinct Differences in Left Ventricular Mass, Geometry, and Function.* Circulation, 2013. **127**(2): p. 197-206.
74. Lewandowski, A.J., W.M. Bradlow, D. Augustine, E.F. Davis, J. Francis, A. Singhal, A. Lucas, S. Neubauer, K. McCormick, and P. Leeson, *Right Ventricular Systolic Dysfunction in Young Adults Born Preterm.* Circulation, 2013. **128**(7): p. 713-720.
75. Wu, L., T. Germans, A. Guclu, M. Heymans, C. Allaart, and A. van Rossum, *Feature tracking compared with tissue tagging measurements of segmental strain by cardiovascular magnetic resonance.* Journal of Cardiovascular Magnetic Resonance, 2014. **16**(1): p. 10.
76. Hor, K.N., W.M. Gottliebson, C. Carson, E. Wash, J. Cnota, R. Fleck, J. Wansapura, P. Klimeczek, H.R. Al-Khalidi, E.S. Chung, D.W. Benson, and W. Mazur, *Comparison of Magnetic Resonance Feature Tracking for Strain Calculation With Harmonic Phase Imaging Analysis.* JACC: Cardiovascular Imaging, 2010. **3**(2): p. 144-151.
77. Morton, G., A. Schuster, R. Jogiya, S. Kutty, P. Beerbaum, and E. Nagel, *Inter-study reproducibility of cardiovascular magnetic resonance myocardial feature tracking.* Journal of Cardiovascular Magnetic Resonance, 2012. **14**(1): p. 43.
78. Orwat, S., A. Kempny, G.P. Diller, P. Bauerschmitz, A.C. Bunck, D. Maintz, R.M. Radke, and H. Baumgartner, *Cardiac magnetic resonance feature tracking- a novel method to assess myocardial strain: Comparison with echocardiographic speckle tracking in healthy volunteers and in patients with left ventricular hypertrophy.* Kardiologia polska, 2013.
79. Fonseca, C.G., H.C. Oxenham, B.R. Cowan, C.J. Occleshaw, and A.A. Young, *Aging alters patterns of regional nonuniformity in LV strain relaxation: a 3-D MR tissue tagging study.* American Journal of Physiology - Heart and Circulatory Physiology, 2003. **285**(2): p. H621-H630.
80. Götte, M.J.W., T. Germans, I.K. Rüssel, J.J.M. Zwanenburg, J.T. Marcus, A.C. van Rossum, and D.J. van Veldhuisen, *Myocardial Strain and Torsion Quantified by Cardiovascular Magnetic*

Resonance Tissue TaggingStudies in Normal and Impaired Left Ventricular Function. Journal of the American College of Cardiology, 2006. **48**(10): p. 2002-2011.
81. Moore, C.C., C.H. Lugo-Olivieri, E.R. McVeigh, and E.A. Zerhouni, *Three-dimensional Systolic Strain Patterns in the Normal Human Left Ventricle: Characterization with Tagged MR Imaging.* Radiology, 2000. **214**(2): p. 453-466.
82. Shehata, M.L., S. Cheng, N.F. Osman, D.A. Bluemke, and J.A. Lima, *Myocardial tissue tagging with cardiovascular magnetic resonance.* J Cardiovasc Magn Reson, 2009. **11**: p. 55.
83. Harrild, D., Y. Han, T. Geva, J. Zhou, E. Marcus, and A. Powell, *Comparison of cardiac MRI tissue tracking and myocardial tagging for assessment of regional ventricular strain.* The International Journal of Cardiovascular Imaging (formerly Cardiac Imaging): p. 1-10.
84. Ostrzega, E., J. Maddahi, H. Honma, J.V. Crues Iii, K.J. Resser, Y. Charuzi, and D.S. Berman, *Quantification of left ventricular myocardial mass in humans by nuclear magnetic resonance imaging.* American Heart Journal, 1989. **117**(2): p. 444-452.
85. Myerson, S.G., N.G. Bellenger, and D.J. Pennell, *Assessment of Left Ventricular Mass by Cardiovascular Magnetic Resonance.* Hypertension, 2002. **39**(3): p. 750-755.
86. Alfakih, K., T. Bloomer, S. Bainbridge, G. Bainbridge, J. Ridgway, G. Williams, and M. Sivananthan, *A comparison of left ventricular mass between two-dimensional echocardiography, using fundamental and tissue harmonic imaging, and cardiac MRI in patients with hypertension.* European Journal of Radiology, 2004. **52**(2): p. 103-109.
87. Young, A.A., B. Li, R.S. Kirton, and B.R. Cowan, *Generalized spatiotemporal myocardial strain analysis for DENSE and SPAMM imaging.* Magn Reson Med, 2011.
88. Lang, R.M., M. Bierig, R.B. Devereux, F.A. Flachskampf, E. Foster, P.A. Pellikka, M.H. Picard, M.J. Roman, J. Seward, J. Shanewise, S. Solomon, K.T. Spencer, M. St. John Sutton, and W. Stewart, *Recommendations for chamber quantification.* European Journal of Echocardiography, 2006. **7**(2): p. 79-108.
89. Appleton, C.P., J.L. Jensen, L.K. Hatle, and J.K. Oh, *Doppler evaluation of left and right ventricular diastolic function: A technical guide for obtaining optimal flow velocity recordings.* Journal of the American Society of Echocardiography : official publication of the American Society of Echocardiography, 1997. **10**(3): p. 271-292.
90. Waggoner, A.D. and S.M. Bierig, *Tissue Doppler imaging: A useful echocardiographic method for the cardiac sonographer to assess systolic and diastolic ventricular function.* Journal of the American Society of Echocardiography : official publication of the American Society of Echocardiography, 2001. **14**(12): p. 1143-1152.
91. Lang, R.M., M. Bierig, R.B. Devereux, F.A. Flachskampf, E. Foster, P.A. Pellikka, M.H. Picard, M.J. Roman, J. Seward, J. Shanewise, S. Solomon, K.T. Spencer, M. St John Sutton, and W. Stewart, *Recommendations for chamber quantification.* Eur J Echocardiogr, 2006. **7**(2): p. 79-108.
92. Ng, A.C.T., V. Delgado, M. Bertini, M.L. Antoni, R.J. van Bommel, E.P.M. van Rijnsoever, F. van der Kley, S.H. Ewe, T. Witkowski, D. Auger, G. Nucifora, J.D. Schuijf, D. Poldermans, D.Y. Leung, M.J. Schalij, and J.J. Bax, *Alterations in multidirectional myocardial functions in patients with aortic stenosis and preserved ejection fraction: a two-dimensional speckle tracking analysis.* European Heart Journal, 2011. **32**(12): p. 1542-1550.
93. Lewandowski, A.J., M. Lazdam, E. Davis, I. Kylintireas, J. Diesch, J. Francis, S. Neubauer, A. Singhal, A. Lucas, B. Kelly, and P. Leeson, *Short-Term Exposure to Exogenous Lipids in Premature Infants and Long-Term Changes in Aortic and Cardiac Function.* Arteriosclerosis, Thrombosis, and Vascular Biology, 2011. **31**(9): p. 2125-2135.
94. Maret, E., T. Todt, L. Brudin, E. Nylander, E. Swahn, J. Ohlsson, and J. Engvall, *Functional measurements based on feature tracking of cine magnetic resonance images identify left ventricular segments with myocardial scar.* Cardiovascular Ultrasound, 2009. **7**(1): p. 53.
95. Bland JM, A.D., *Statistical methods for assessing agreement between two methods of clinical measurement.* Lancet, 1986. **1**: p. 307-310.

96. Marwick, T.H., R.L. Leano, J. Brown, J.-P. Sun, R. Hoffmann, P. Lysyansky, M. Becker, and J.D. Thomas, *Myocardial Strain Measurement With 2-Dimensional Speckle-Tracking Echocardiography: Definition of Normal Range.* J Am Coll Cardiol Img, 2009. **2**(1): p. 80-84.
97. Saito, K., H. Okura, N. Watanabe, A. Hayashida, K. Obase, K. Imai, T. Maehama, T. Kawamoto, Y. Neishi, and K. Yoshida, *Comprehensive Evaluation of Left Ventricular Strain Using Speckle Tracking Echocardiography in Normal Adults: Comparison of Three-Dimensional and Two-Dimensional Approaches.* Journal of the American Society of Echocardiography : official publication of the American Society of Echocardiography, 2009. **22**(9): p. 1025-1030.
98. Swoboda, P., A. Larghat, J. Greenwood, and S. Plein, *Reproducibility of strain and twist measurements calculated using CSPAMM tagging.* Journal of Cardiovascular Magnetic Resonance, 2011. **13**(Suppl 1): p. P52.
99. Hor, K.N., R. Baumann, G. Pedrizzetti, G. Tonti, W.M. Gottliebson, M. Taylor, W. Benson, and W. Mazur, *Magnetic resonance derived myocardial strain assessment using feature tracking.* J Vis Exp, 2011(48).
100. Simonetti, O.P. and S.V. Raman, *Straining to Justify Strain Measurement.* J Am Coll Cardiol Img, 2010. **3**(2): p. 152-154.
101. Moore, C.C., C.H. Lugo-Olivieri, E.R. McVeigh, and E.A. Zerhouni, *Three-dimensional Systolic Strain Patterns in the Normal Human Left Ventricle: Characterization with Tagged MR Imaging1.* Radiology, 2000. **214**(2): p. 453-466.
102. Föll, D., B. Jung, E. Schilli, F. Staehle, A. Geibel, J. Hennig, C. Bode, and M. Markl, *Magnetic Resonance Tissue Phase Mapping of Myocardial Motion / CLINICAL PERSPECTIVE.* Circulation: Cardiovascular Imaging, 2010. **3**(1): p. 54-64.
103. Young, A., H. Imai, C. Chang, and L. Axel, *Two-dimensional left ventricular deformation during systole using magnetic resonance imaging with spatial modulation of magnetization [published erratum appears in Circulation 1994 Sep;90(3):1584].* Circulation, 1994. **89**(2): p. 740-752.
104. Lawton, J., B. Cupps, A. Knutsen, N. Ma, B. Brady, L. Reynolds, and M. Pasque, *Magnetic resonance imaging detects significant sex differences in human myocardial strain.* BioMedical Engineering OnLine, 2011. **10**(1): p. 76.
105. Hurlburt, H.M., Aurigemma, G.P., Hill, J.C., Narayanan, A., Gaasch, W.H., Tighe, D.A., *Direct Ultrasound Measurement of Longitudinal, Circumferential, and Radial Strain Using 2-Dimensional Strain Imaging in Normal Adults.* Echocardiography, 2007. **24**(7): p. 723-731.
106. Edvardsen, T., B.L. Gerber, J. Garot, D.A. Bluemke, J.A.C. Lima, and O.A. Smiseth, *Quantitative Assessment of Intrinsic Regional Myocardial Deformation by Doppler Strain Rate Echocardiography in Humans.* Circulation, 2002. **106**(1): p. 50-56.
107. Petersen, S.E., F. Wiesmann, L.E. Hudsmith, M.D. Robson, J.M. Francis, J.B. Selvanayagam, S. Neubauer, and K.M. Channon, *Functional and structural vascular remodeling in elite rowers assessed by cardiovascular magnetic resonance.* J Am Coll Cardiol, 2006. **48**(4): p. 790-7.
108. Bland, J.M. and D.G. Altman, *Statistics Notes: Measurement error and correlation coefficients.* BMJ, 1996. **313**(7048): p. 41-42.
109. Weir, J., *Quantifying test-retest reliability using the intraclass correlation coefficient and the SEM.* Journal of Strangth and Conditioning Research, 2005. **19**(1): p. 231-240.
110. Seo, Y., T. Ishizu, Y. Enomoto, H. Sugimori, M. Yamamoto, T. Machino, R. Kawamura, and K. Aonuma, *Validation of 3-Dimensional Speckle Tracking Imaging to Quantify Regional Myocardial Deformation / CLINICAL PERSPECTIVE.* Circulation: Cardiovascular Imaging, 2009. **2**(6): p. 451-459.
111. Kuznetsova, T., L. Herbots, T. Richart, J. D'hooge, L. Thijs, R.H. Fagard, M.-C. Herregods, and J.A. Staessen, *Left ventricular strain and strain rate in a general population.* European Heart Journal, 2008. **29**(16): p. 2014-2023.
112. Dalen, H., A. Thorstensen, S.A. Aase, C.B. Ingul, H. Torp, L.J. Vatten, and A. Stoylen, *Segmental and global longitudinal strain and strain rate based on echocardiography of 1266*

healthy individuals: the HUNT study in Norway. European Journal of Echocardiography, 2010. **11**(2): p. 176-183.
113. Meris, A., F. Faletra, C. Conca, C. Klersy, F. Regoli, J. Klimusina, M. Penco, E. Pasotti, G.B. Pedrazzini, T. Moccetti, and A. Auricchio, *Timing and Magnitude of Regional Right Ventricular Function: A Speckle Tracking-Derived Strain Study of Normal Subjects and Patients with Right Ventricular Dysfunction.* Journal of the American Society of Echocardiography : official publication of the American Society of Echocardiography, 2010. **23**(8): p. 823-831.
114. Fukuda, Y., H. Tanaka, D. Sugiyama, K. Ryo, T. Onishi, H. Fukuya, M. Nogami, Y. Ohno, N. Emoto, H. Kawai, and K.-i. Hirata, *Utility of Right Ventricular Free Wall Speckle-Tracking Strain for Evaluation of Right Ventricular Performance in Patients with Pulmonary Hypertension.* Journal of the American Society of Echocardiography : official publication of the American Society of Echocardiography, 2011.
115. Taylor, M.D., K.N. Hor, W. Mazur, D.W. Benson, and W.M. Gottliebson, *Right ventricular strain in patients with tetralogy of Fallot.* Journal of Cardiovascular Magnetic Resonance, 2011. **13**(Suppl 1): p. P204.
116. Lu, J.C., M. Ghadimi Mahani, P.P. Agarwal, T.B. Cotts, and A.L. Dorfman, *Usefulness of Right Ventricular Free Wall Strain to Predict Quality of Life in "Repaired" Tetralogy of Fallot.* The American Journal of Cardiology, 2013. **111**(11): p. 1644-1649.
117. Leong, D.P., S. Grover, P. Molaee, A. Chakrabarty, M. Shirazi, Y.H. Cheng, A. Penhall, R. Perry, H. Greville, M.X. Joseph, and J.B. Selvanayagam, *Nonvolumetric Echocardiographic Indices of Right Ventricular Systolic Function: Validation with Cardiovascular Magnetic Resonance and Relationship with Functional Capacity.* Echocardiography, 2011: p. no-no.
118. Redfield Mm, J.S.J.B.J.J.C.M.D.W.B.K.R.R.R.J., *Burden of systolic and diastolic ventricular dysfunction in the community: Appreciating the scope of the heart failure epidemic.* JAMA: The Journal of the American Medical Association, 2003. **289**(2): p. 194-202.
119. Bella, J.N., V. Palmieri, M.J. Roman, J.E. Liu, T.K. Welty, E.T. Lee, R.R. Fabsitz, B.V. Howard, and R.B. Devereux, *Mitral Ratio of Peak Early to Late Diastolic Filling Velocity as a Predictor of Mortality in Middle-Aged and Elderly Adults.* Circulation, 2002. **105**(16): p. 1928-1933.
120. Kasner, M., D. Westermann, P. Steendijk, R. Gaub, U. Wilkenshoff, K. Weitmann, W. Hoffmann, W. Poller, H.-P. Schultheiss, M. Pauschinger, and C. Tschöpe, *Utility of Doppler Echocardiography and Tissue Doppler Imaging in the Estimation of Diastolic Function in Heart Failure With Normal Ejection Fraction.* Circulation, 2007. **116**(6): p. 637-647.
121. Dokainish, H., J.S. Nguyen, J. Bobek, R. Goswami, and N.M. Lakkis, *Assessment of the American Society of Echocardiography-European Association of Echocardiography guidelines for diastolic function in patients with depressed ejection fraction: an echocardiographic and invasive haemodynamic study.* European Journal of Echocardiography, 2011.
122. *CMR imaging for diastolic hemodynamic assessment fantasy or reality?* JACC Cardiovasc Imaging., 2012. **5**(1): p. 25-7.
123. Kutty, S., S. Rangamani, J. Venkataraman, L. Li, A. Schuster, S. Fletcher, D. Danford, and P. Beerbaum, *Reduced global longitudinal and radial strain with normal left ventricular ejection fraction late after effective repair of aortic coarctation - a CMR feature tracking study.* Journal of Cardiovascular Magnetic Resonance, 2012. **14**(0): p. 1-2.
124. Dokainish, H., J.S. Nguyen, R. Sengupta, M. Pillai, M. Alam, J. Bobek, and N. Lakkis, *Do Additional Echocardiographic Variables Increase the Accuracy of E/e' for Predicting Left Ventricular Filling Pressure in Normal Ejection Fraction? An Echocardiographic and Invasive Hemodynamic Study.* Journal of the American Society of Echocardiography : official publication of the American Society of Echocardiography, 2010. **23**(2): p. 156-161.
125. Mullens, W., A.G. Borowski, R.J. Curtin, J.D. Thomas, and W.H. Tang, *Tissue Doppler Imaging in the Estimation of Intracardiac Filling Pressure in Decompensated Patients With Advanced Systolic Heart Failure.* Circulation, 2009. **119**(1): p. 62-70.

126. Ommen, S.R., R.A. Nishimura, C.P. Appleton, F.A. Miller, J.K. Oh, M.M. Redfield, and A.J. Tajik, *Clinical Utility of Doppler Echocardiography and Tissue Doppler Imaging in the Estimation of Left Ventricular Filling Pressures : A Comparative Simultaneous Doppler-Catheterization Study.* Circulation, 2000. **102**(15): p. 1788-1794.
127. Klein, A.L., D.J. Burstow, A.J. Tajik, P.K. Zachariah, K.R. Bailey, and J.B. Seward, *Effects of age on left ventricular dimensions and filling dynamics in 117 normal persons.* Mayo Clinic proceedings. Mayo Clinic, 1994. **69**(3): p. 212-224.
128. *Inter-study reproducibility of cardiovascular magnetic resonance myocardial feature tracking.* J Cardiovasc Magn Reson., 2012. **14**(1): p. 43.
129. Nishikage, T., H. Nakai, V. Mor-Avi, R.M. Lang, I.S. Salgo, S.H. Settlemier, S. Husson, and M. Takeuchi, *Quantitative assessment of left ventricular volume and ejection fraction using two-dimensional speckle tracking echocardiography.* European Journal of Echocardiography, 2009. **10**(1): p. 82-88.
130. Mor-Avi, V., L. Sugeng, L. Weinert, P. MacEneaney, E.G. Caiani, R. Koch, I.S. Salgo, and R.M. Lang, *Fast Measurement of Left Ventricular Mass With Real-Time Three-Dimensional Echocardiography.* Circulation, 2004. **110**(13): p. 1814-1818.
131. Steen, H., K. Nasir, E. Flynn, I. El-Shehaby, S. Lai, H. Katus, D. Bluemcke, and J. Lima, *Is Magnetic Resonance Imaging the 'Reference Standard' for Cardiac Functional Assessment? Factors Influencing Measurement of Left Ventricular Mass and Volumes.* Clinical Research in Cardiology, 2007. **96**(10): p. 743-751.
132. Augustine, D., A. Lewandowski, M. Lazdam, A. Rai, J. Francis, S. Myerson, A. Noble, H. Becher, S. Neubauer, S. Petersen, and P. Leeson, *Global and regional left ventricular myocardial deformation measures by magnetic resonance feature tracking in healthy volunteers: comparison with tagging and relevance of gender.* J Cardiovasc Magn Reson, 2013. **15**: p. 8.
133. Schuster, A., G. Morton, S.T. Hussain, R. Jogiya, S. Kutty, K.N. Asrress, M.R. Makowski, B. Bigalke, D. Perera, P. Beerbaum, and E. Nagel, *The intra-observer reproducibility of cardiovascular magnetic resonance myocardial feature tracking strain assessment is independent of field strength.* European Journal of Radiology, 2013. **82**(2): p. 296-301.
134. Singh, A., C. Steadman, J. Khan, S. Nazir, P. Kanagala, and G. McCann, *Inter-study reproducibility of circumferential strain and strain rates at 1.5T and 3T: a comparison of tagging and feature tracking.* Journal of Cardiovascular Magnetic Resonance, 2014. **16**(Suppl 1): p. P354.